MSc Thesis Report

‘A heat-transfer based method for slip-joint contact area measurement’

R.G. Atkinson

19-02-2018

TU Delft

The Slip-joint Connection

'A heat-transfer based method for slip-joint contact area measurement'

by

R.G. Atkinson

in partial fulfilment of the requirements for the degree of

Master of Science

at the Delft University of Technology,
to be defended publicly on Monday February 19, 2018 at 2:00 PM.

Student Number:	4513568	
Thesis committee:	Prof. Dr. A. Metrikine	TU Delft, Chairman
	Ir. J.S. Hoving,	TU Delft, Daily Supervisor
	Ir. T.P.J. Kamphuis,	DOT B.V., Daily Supervisor

This thesis is confidential and cannot be made public until February 19, 2023.

TU Delft

Preface

This thesis covers the past nine months of work in developing and testing a method for the evaluation of slip-joint contact area. This has been an excellent learning experience for me, with an interesting combination of theoretical and hands-on experimental work. Working up close with a full scale wind turbine for the first time has been a great experience and a fitting way to finish my degree in Offshore Engineering.

This project would not have progressed so well without the help and support of those around me, who all have my sincere gratitude. Firstly, this project would never have gotten off the ground without Jan van der Tempel providing the opportunity, for which I am very thankful. Secondly, I would like to thank Thijs Kamphuis for his input and guidance, as well as the rest of the committee, Andrei Metrikine and Jeroen Hoving for helping to focus the direction of the project. I would also like to thank everyone else at DOT who offered advice during the project, including the guys in the Schiehal for being extremely helpful and accommodating in carrying out the experiments.

I would like to thank my fiancée, Jen, who has been very patient and supportive throughout my whole MSc degree and especially so during the busier periods of this project. Finally, to my friends from Offshore, it has been great and I can't imagine a better group of people to have shared the last two years with.

R.G.Atkinson
Delft, February 2018

Abstract

The Delft Offshore Turbine (DOT) concept is focused on the development of a new offshore wind turbine including, amongst other innovations, a slip-joint that connects the turbine tower and monopile foundation. The slip-joint is a mechanical, friction-based connection that provides many advantages over a bolted or grouted connection, such as the ability to support high loads, reduced maintenance costs and rapid installation. However, for the slip-joint to be accurately designed and to have its performance guaranteed, it is necessary to know the contact behaviour within the slip-joint post-installation.

Heat transfer has been selected as the optimal measurement basis over magnetic, electrical and other techniques, as heat transfer through the slip-joint wall is correlated with both contact pressure and air gap size (in non-contact regions). Therefore, a continuous, active heating thermographic point measurement method has been developed to measure the contact pressure and contact gaps in the slip-joint connection. In practice, this involves the use of an induction heater to heat one side of the slip-joint while, on the other side, a thermal camera measures the heat transfer through the slip-joint wall. This method was tested on a sample slip-joint from a decommissioned onshore wind turbine.

Prior to full scale testing, the method has been validated through comparison with a finite element model of heat transfer between parallel plates. This comparison shows that the method is sensitive to variations in contact and pressure, especially in regions where contact pressure is close to zero. Additional small-scale experiments were conducted with two 8mm steel plates separated by a known gap. These experiments demonstrated the sensitivity of the method to gap size variations of less than 0.1mm and indicate the ability of the measurement setup to resolve gap sizes greater than 1mm in the sample slip-joint. Finally, single-ply validation testing shows the precision of the measurement method to be ±13% (at 90% confidence interval).

Following validation, the method was used to measure the contact distribution across 207 grid points on the sample slip-joint. The results show thin (0.3-1m), longitudinal low-pressure regions extending from the top and bottom of the joint towards the centre. Physical verification with feeler gauges indicates that 34% of the joint is not in contact (with 95% confidence interval of [22% 51%]). Feeler gauge testing also shows that the correlation between heat measurements and actual gap size is in agreement in both full-scale and small-scale validation measurements. Finally, feeler gauge measurements show there is a ±13% error in the thermal measurements.

The results show that the thermographic method for slip-joint contact area measurement is suitable to resolve pressure and gap size variations in the slip-joint. Additionally, the measurement results show that it is necessary for engineers to consider up to 50% non-contact during the design process

and joint contact should be assessed in all slip-joints post-installation. Finally, future development of the method through the use of more sensitive equipment and performing additional single-ply measurements to establish a clearer error estimate is recommended. This should be augmented by a comparison to residual stress measurements using the Magnetic Barkhausen Noise (MBN) method, as well as acoustic resonance stiffness measurements, to verify contact results and examine the cause of such contact variations in a sample joint.

Contents

Figures

Tables

1 Introduction

1.1 General

In 2016 wind energy surpassed coal as the second largest source of power generation in Europe (behind gas), with 12.5GW installed and grid connected. Of this, 1.6GW was from offshore wind turbines, bringing the total capacity of offshore wind to 12.5GW in Europe. In addition, 11 offshore wind projects, worth a combined €18.2bn passed critical financial milestones for new projects, a 39% increase on 2015. Together, the above statistics indicate a strong future for the offshore wind industry in Europe with continued growth through 2017 and beyond [1, 2].

Turbines installed offshore bare many similarities to onshore turbines but are generally significantly larger, both in terms of hub height and blade length. This is typically due to the higher cost efficiency of larger turbines and to minimal restrictions on the increased noise caused by longer blades. Another major difference in offshore turbines is the need for a foundation structure between the seabed and the base of the wind turbine tower. Previously a variety of designs have been used for this support structure including gravity- base (concrete) foundations, jacket (truss) structures and steel tripod structures, however monopiles have emerged as a clear industry favourite. Of existing offshore structures, over 80% are now using monopile foundations; with this portion increasing as most new installations turn to monopiles.

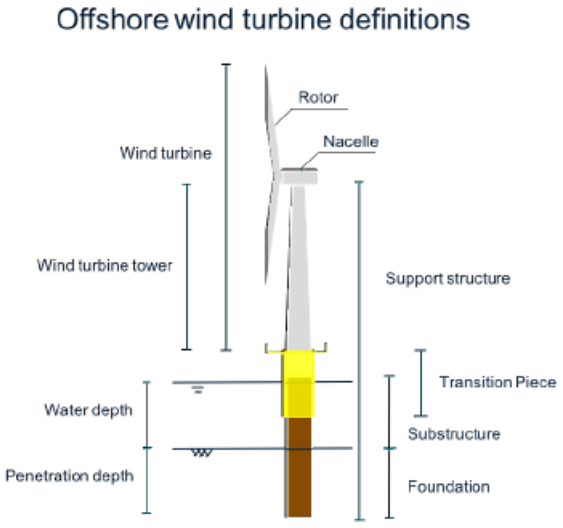

Figure 1 - Offshore wind turbine components

Despite their popularity, a number of engineering issues remain unresolved with the monopile support structure. The foremost of these issues is the optimal way to connect the monopile to the wind turbine tower. The industry standard currently involves the use of a transition piece which is lowered over the monopile and connected via grouting and shear-keys. This presents a number of unresolved questions, such as the integrity of the grout over the lifetime of the turbine [3] and the ability of bolts to withstand the environmental loads, especially with rapidly increasing turbine size. The 'slip-joint' is therefore offered as an alternative to the current connection options and is currently being developed by Delft Offshore Turbine (DOT) B.V. for use in their offshore projects.

1.2 Delft Offshore Turbine

DOT is a start-up company focussed on the development of an innovative wind turbine based around the concept of a hydraulic drive train. Typical offshore wind turbines utilise a standard mechanical drive train, directly powering a high-speed generator within the nacelle of the turbine. This process requires the use of a (typically) heavy generator and gearbox assembly, which increases the mass and complexity of the nacelle assembly. The added weight and complexity of a standard nacelle not only affects the loads on the support structure but also increases the number of components that may require costly offshore maintenance. Furthermore, the generation of electricity by each individual turbine necessitates the laying of many large copper cables offshore to direct power back to a sub-station.

The DOT concept attempts to solve these issues by utilising each turbine to pump a hydraulic fluid (seawater in this case) back to a centralised hydro-generator. The high torque generated by each turbine allows the use of high torque, low RPM pumps directly coupled to the low speed shaft of the nacelle. This eliminates a great deal of weight from the nacelle and also allows more efficient electricity generation, through the use of a single Pelton turbine, rather than many smaller generators. This concept is illustrated in Figure 2 and Figure 3.

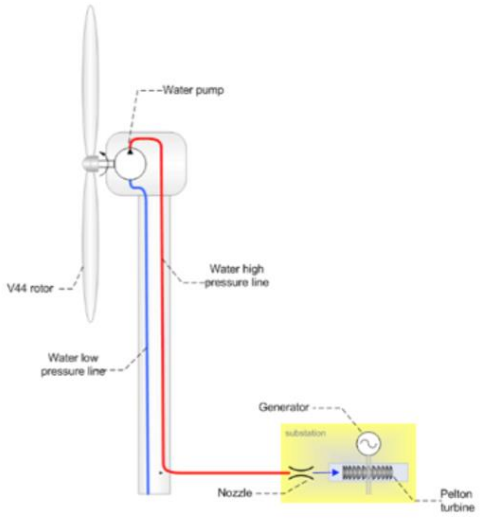

Figure 2 - DOT offshore wind turbine concept

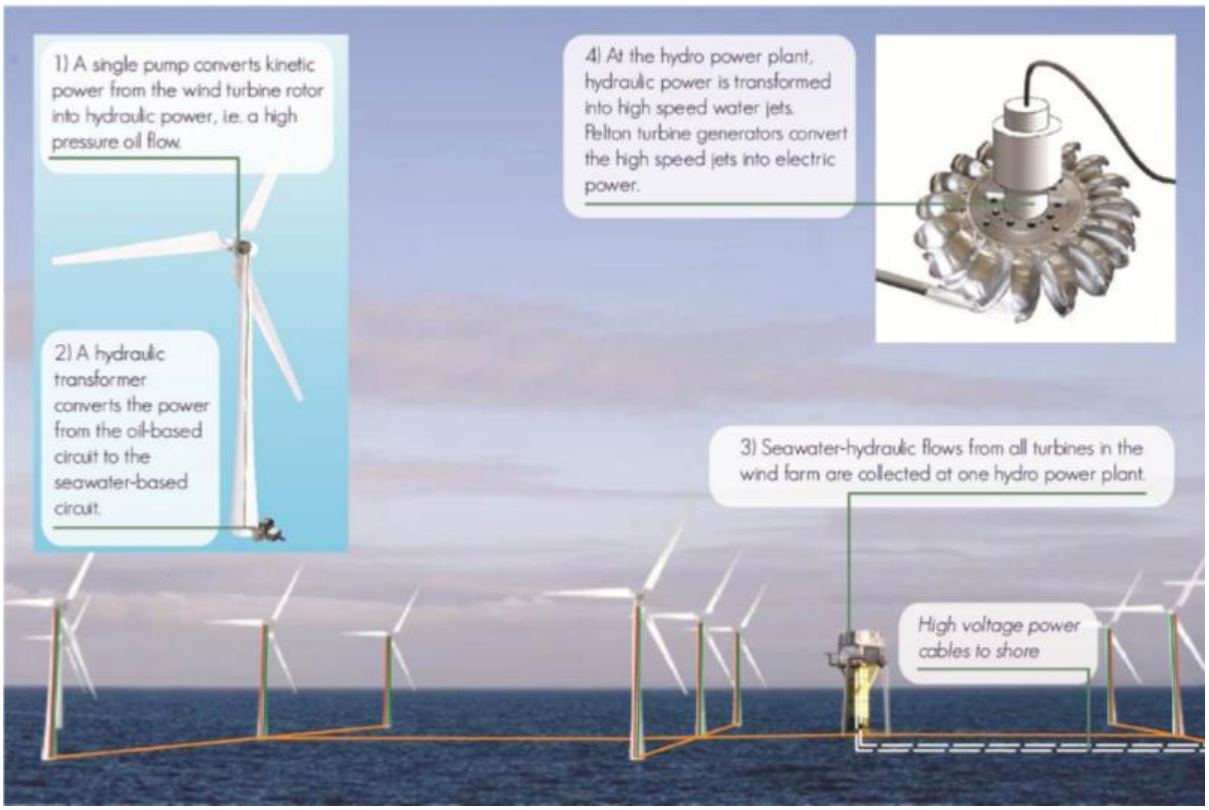

Figure 3 - DOT offshore turbine concept

Apart from this, the positive effect of generating electricity at one central location reduces the number of generators and subsea power cables throughout the wind farm, also cutting down on the installation and material (copper) costs. Although the efficiency per turbine is somewhat reduced due to the hydraulic drive train, the overall cost per kWh can be drastically reduced with an estimated magnitude of 30% to 50% [4].

1.3 The Slip Joint

The slip-joint, as noted above, is an alternative method of connecting the wind turbine to the support structure. The primary working principle of the joint is somewhat similar to stacking plastic cups inside each other. The upper section of the joint is of slightly larger diameter than the lower portion of the joint, allowing it to slide over the top (Figure 4). Due to the cone angle of the two pieces the strength of the connection increases as the top section slides further over the bottom piece, eventually reaching a final setting point.

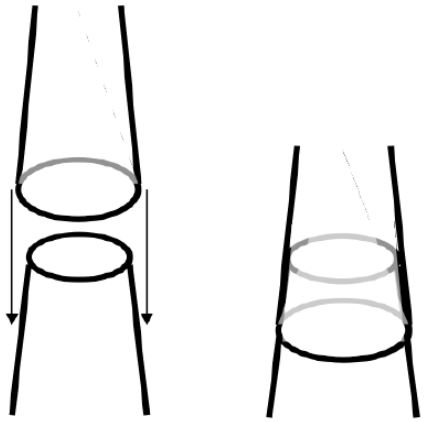

Figure 4 - The slip-joint concept

This idea was originally used by the Dutch company WindMaster in the design of the 'Duinvogel' single turbine demonstration project at Scheveningen. The Duinvogel was installed in 1995 and continued operating until 2014, with some upgrades taking place in 2010. However, WindMaster ceased operating in 1998, shortly after the Duinvogel was installed, which effectively stopped further investigation into the slip joint design. In 2003 the idea was onceagain picked up by the founder of DOT B.V. as a method of decreasing installation time in offshore turbines and potentially reducing steel costs by effectively eliminating the transition piece.

Figure 5 - Duinvogel slip-joint in-situ

Following the decommissioning of the Duinvogel, a DOWEC report found that the slip joint would be suitable for offshore use [5]. Furthermore, investigation of the slip joint from the decommissioned Duinvogel tower found no structural reliability issues. Such encouraging developments, along with the issues found with current connections pave the wave for further investigation into slip-joint design and the use of the slip-joint in the tower-monopile connection of offshore turbines.

However, there are still a number of design issues that have to be addressed for the connection. These include the settling behaviour of the joint, the limit and fatigue strength of the joint when subject to offshore environmental loads and the stress distribution within the slip joint. The stress distribution in the joint is related to the force transfer mechanisms and affects the design strength of

the joint. Therefore the goal of this thesis is to investigate contact area within the slip joint in order to provide more insight into load paths and potential dynamic response of the joint.

1.4 Research Objectives

In order to effectively address the project goal of developing a method for assessing slip-joint contact area, the research space has been summarised in six research questions.

1. *How can the slip-joint contact area be validated/measured?*

This research question is intended to cover the assessment of existing methods for use in this context as well as investigation into any new methods. A final method should be selected and justification provided as to its suitability to the task at hand.

2. *What is an appropriate measurement procedure utilising the selected method(s)?*

This research question covers the development and justification of a specific measurement process, including experimental equipment and setup once an appropriate technique has been selected.

3. *What are the sensitivities of the proposed method(s)?*

This research question covers the validation of the accuracy and precision of the developed measurement process. This includes quantitative evaluation of the measurement sensitivity, resolution and factors that may affect measurement results.

4. *What is the contact/pressure distribution of the test slip-joint?*

This objective addresses the results of measurements of the sample slip-joint. Notable features of the contact/pressure distribution should be identified to allow comparison with other slip-joints or alternative measurement methods.

5. *What are the potential causes of the observed results and what are the implications of these results?*

This covers the investigation of possible causes of the observed contact/pressure distribution, how this distribution may vary in other joints and the implication of such a distribution. The identification of causes of such a distribution may also allow recommendation of contact optimisation measures.

6. *How can the selected method(s) be improved?*

The ultimate research objective in this field is the development of a thorough understanding of slip-joint mechanics and a fast, accurate and reliable method for verifying contact/pressure post-

installation. Improvements to the current method towards the achievement of this goal should therefore be proposed.

1.5 Scope Exclusions

The research is focussed on the initial development of a test method and is therefore focussed on method selection, performance and any results obtained. The following items are therefore excluded from the scope of the project;

- Full development and/or use of more than a single test method for slip-joint assessment,
- Development of a complete test procedure for offshore/commercial use,
- Development of a test apparatus/equipment for offshore/commercial use,
- Mechanical modelling of the slip-joint, either for comparison with or based on measurement results,
- Design recommendations for the slip-joint based on contact/pressure results.

1.6 Research Approach

In order to adequately answer the proposed research questions, the following research approach was utilised. Initially, a literature review was conducted to analyse the non-destructive testing methods available and assess their applicability to slip-joint measurement. Following this a test method was selected and specific measurement technique developed for the sample slip-joint available. This method was supported by the results of three validation procedures, as well as a limited initial run of measurements.

Following development and validation procedures the sample slip-joint was prepared and measured using the developed method. The results of this measurement campaign are analysed with respect to distribution features and percentage, as well as causes and implications of such a pressure/contact distribution. Finally, ways for improving the current method and alternative methods that may provide further insight have been examined. Based on this investigation, recommendations are made on ways to improve the accuracy of the method and potential developments of the method for offshore commercial use.

1.7 Thesis Structure

The structure of the thesis largely follows the research approach, with the research questions answered sequentially across 7 chapters. The layout and topic of these chapters is as follows;

1.7.1 Chapter 1 - Introduction

The introduction presents the research topic, the rationale for the project and provides an outline of the key aspects of the topic.

1.7.2 Chapter 2 – Background

1. *How can the slip-joint contact area be validated/measured?*

Chapter two provides the fundamental basis for subsequent chapters, outlining key concepts of the slip-joint and non-destructive testing. This chapter answers research question 1 by establishing the available test methods, how thermal measurements work and why a heat-based method is the best option for the slip joint.

1.7.3 Chapter 3 – Experimental Method

2. *What is an appropriate measurement procedure utilising the selected method(s)?*

Chapter 3 addresses the second research question, focussing on the measurement equipment, setup and processing for testing of the sample slip-joint.

1.7.4 Chapter 4 - Validation

3. *What are the sensitivities of the proposed method(s)?*

Chapter four outlines the validation procedures utilised to determine the accuracy of the method and determine its applicability for use with the slip-joint. It further outlines sensitivities of the method with regard to both accuracy/precision, as well as parameters which may affect the results.

1.7.5 Chapter 5 - Results

4. *What is the contact/pressure distribution of the test slip-joint?*

Chapter five presents the results of the initial round of slip-joint testing, the full measurement of the slip-joint and subsequent feeler gauge testing. Qualitative results, with respect to the observed features of the pressure/contact distribution, as well as quantitative results, with respect to the contact percentage, are presented.

1.7.6 Chapter 6 - Discussion

5. *What are the potential causes of the observed results and what are the implications of these results?*

6. *How can the selected method(s) be improved?*

Chapter 6 addresses the causes and implications of the results, as well as discussing how more accurate results could be obtained in a more rapid manner.

1.7.7 Chapter 7 – Conclusion

Chapter seven provides a summary of the key conclusions of the report with regards to both the measurement method itself and the measured pressure/contact distribution in the sample slip-joint. Recommendations are also made in this chapter with regards to improvement of the speed and accuracy of the method, as well as future measurement techniques that could provide useful comparative data.

2 Background

2.1 Slip Joint Mechanics

In order to understand the effect of contact variations on the operation of the slip-joint, one must understand the force transfer mechanisms within the joint. A complete description is provided in [6], although a short summary is provided here for reference. The slip-joint connect is subject to a static vertical load, as well as a dynamic overturning moment and shear forces, arising from gravity and environmental loads respectively.

The vertical static load is resisted through both joint elasticity and friction factors with friction forming the majority of the load bearing mechanism (~70-80%)[6]. The elastic proportion of the reaction force is taken up through a hoop stress in both the inner and outer cone. The hoop stress due to the static vertical load is then inversely proportional to wall thickness, overlap length, cone angle and friction coefficient. According to [6] the bending moment can be decomposed into a pair of horizontally acting distributed loads, or alternatively a coupled pair of vertical point loads. Since the sum of vertical and horizontal loads is zero in both cases, the moment can theoretically be represented in either way, with the main difference being that a horizontal force representation excludes the effects of friction forces in the joint. It is noted that in reality the force transfer likely occurs through a combined mechanism [6].

Considering that the environmental overturning moment is typically far greater than the axial loads in a typical wind turbine, we may consider the effect of sub-optimal contact on the hoop stress due to an overturning moment. If the overturning moment is represented as horizontal loads then the hoop stress is inversely proportional to wall thickness and overlap length squared. Conversely, if the moment is represented as a coupled vertical load then the hoop stress is inversely proportional to wall thickness, overlap length, diameter and the tangent of the cone angle plus the friction coefficient. If a factor is introduced to compensate for a reduction in contact area, we can see that in both cases the hoop stress is inversely proportional to the contact percentage. Therefore, for example, if only 50% of the joint is in contact the hoop stress could double. This will affect the joint design due to variation in the predicted fatigue life and ultimate strength, although the impact is likely highly dependent on the location of non-contact regions. For a further explanation of slip-joint mechanics see [5] and [6].

2.2 Available Measurement Methods

A number of measurement methods have been compared to determine the most appropriate method for investigating contact area in the slip-joint connection. A brief summary of all relevant methods is presented below, with all destructive test methods eliminated from contention. A heat-transfer based method was selected as the optimal method and is therefore presented last in the list along with more detailed background information.

It should be noted that the referenced studies focus primarily on detection of a defect within solid or bonded composites, which clearly differs from gap size detection in steel slip-joints. However, one may envisage the slip-joint as two laminated sheets of steel with a delamination 'defect' of varying magnitude between the outer and inner layers. The challenge is then, not to determine the presence of the 'defect' (since it exists everywhere in the joint), but rather to determine its magnitude (the size of the air gap). The reason that a 'defect' is considered to be present everywhere (even in contacting regions), is that even in contact regions the material properties of the slip-joint are not continuous across the contact region. Noting this, we may analyse measurement techniques made for composites by considering the interface between the two layers of the slip joint as one continuous delamination defect of varying magnitude.

2.2.1 Model Updating

Model updating is the process of updating a model (in this case structural) to better describe an object based on some real life data from the object. In the case of the slip joint, one would make a simplified model of the turbine tower (including the slip joint), then after measuring certain values from an installed wind turbine (with slip joint), the results from the model and real life may be compared. An optimisation method of choice is then used to minimise the cost function, which is an application specific algorithm developed to describe the 'error' of the model [7]. The cost function is sometimes applied in the form of a 'sensitivity matrix' (based on eigenvalues and eigenvectors), which is then compared with the 'error' of the model [8].

The benefits of this method in the case of the wind turbine tower are that the measured parameters could be chosen to be reasonably easy to measure and non-destructive. For example, the operational mode shapes of the tower could be measured and then compared to the model in order to update it. However, in order for this method to work properly, the initial model must (be assumed to) accurately represent the parameters of the design not under investigation. Ideally, any tower property not fully known should be included in the cost function; however including too many variables can decrease the accuracy of the cost function in what is known as 'overfitting'. Therefore, the tower itself would have to be accurately modelled leaving only slip joint variables to investigate. These variables would then have to be chosen so as to accurately model the structural properties of the joint, also ensuring minimal collinearity to avoid further errors [8]. In this case, vibration measurements from a real turbine tower (with slip joint) were available; however the difficulty in modelling the structure with minimal (or well-founded) assumptions makes this method impractical.

2.2.2 Magnetic Field Measurements

There are many different measurement methods based on magnetic field variation currently in use in industry. They can broadly be categorised into those using oscillating magnetic fields and those using stationary fields. In the present application there is an inherent disadvantage to using oscillating fields as the penetration depth of the magnetic field scales with the oscillation frequency. The field strength in the measurement material decreases exponentially with depth, therefore a standard penetration depth has been defined to facilitate comparative measurements. This standard penetration depth is also known as the skin depth and is the point at which eddy currents in the material will be 37% of the surface current density. The skin depth can be calculated as below, (note that it is inversely proportional to the root of the angular field frequency).

$$\delta = \sqrt{\frac{2\pi}{\sigma \mu_r \omega}}$$

Where;

ω = angular frequency of magnetic field
σ = electrical conductivity of medium
μ_r = magnetic permeability of medium

(Typical skin depth values for carbon steel (1040) are <10mm)[9]

The use of stationary magnetic fields is however a more promising field. Park et al. [10] have investigated the effect of multiple 6mm steel plates on the (stationary) field of a large electromagnet, in an effort to easily and remotely quantify how many stacked plates are picked up by the electromagnet at any one time. It could be envisaged that this application is not too dissimilar to determining the gap size between two thicker steel plates (as the size of this gap would also affect the field in the electromagnet. However as shown in the figure below, in Park (et al.)'s testing the difference in sensor output when adding additional steel plate is in the order of 2-5%. It is evident that a system where there is always two steel 'plates' and they are moving slightly further apart from each other would produce a significantly lower sensor response.

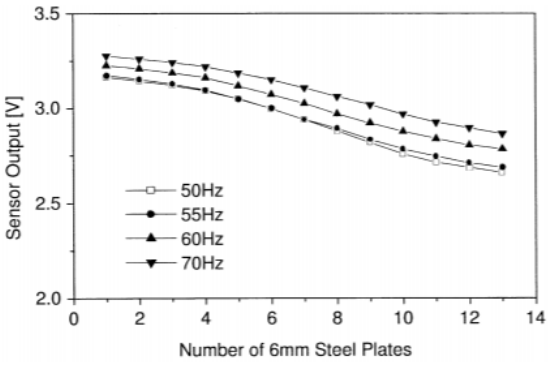

Figure 6 - Magnetic detection of layered steel plates

A similar issue has been found with most magnetic field measurement techniques, in that, extremely precise and well calibrated sensor equipment would be required. For this reason and due to the lack

of experience of the author in this field, another measurement technique has been chosen. Nevertheless this is an avenue that warrants future exploration.

2.2.3 Ultrasound

Ultrasonic measurements may be used to detect minute flaws in solid bodies. The measurement device works by emitting a small ultrasonic pulse from the sensor head into the target material. The pulse then travels through the body and is reflected by any defects back towards the sensor head. The propagation time of the ultrasonic wave may then be used to calculate the distance travelled and hence the thickness of the material. This is illustrated in Figure 7.

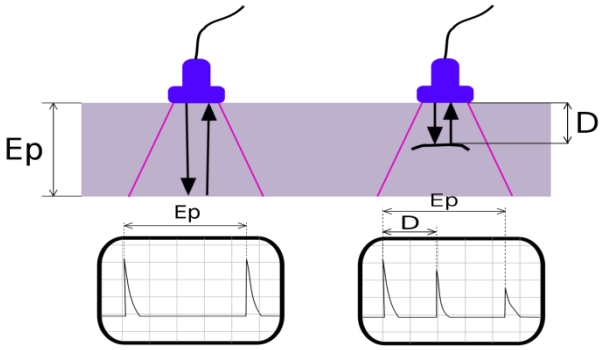

Figure 7 - Ultrasound Measurement Principle

The benefits of this method are that it can pick up very small flaws in the material, only requires access to one side of the material and is a relatively simple and quick measurement to perform. All of these benefits would make it appropriate for use offshore, therefore this method has been previously tested with the DOT500 onshore installation [11]. The results of such tests found that the near entirety of the sound wave is reflected back at the posterior wall of the first 'layer' of the slip joint. This is as one may expect, as a sudden change in the density of the propagation medium always causes a large amount of reflection. In practical terms, this means that minimal ultrasonic energy travels across the gap between the two plates (even when there is contact), and even less is returned to the sensor for evaluation of gap size. The wave transmission across the gap between the two plates could be improved with the application of an interstitial substance denser than air, however filling the entire slip joint cavity with grease or water provides its own significant challenges. Therefore it was concluded that this method is not appropriate for the application at hand.

2.2.4 Eddy Current

Eddy current testing is very similar to active magnetic field test methods noted previously. The key difference being that in eddy current testing the applied magnetic field is generated by means of an inductance circuit, whereas in an active magnetic field setup, it is usually generated by a directly oscillating magnet. In practice this difference is inconsequential and eddy current testing is far more widely used because of the practically of utilising an inductance circuit to generate a response in the

test material. However, eddy current testing suffers from the same issues related to the maximum effective penetration of the test field.

Despite the drawbacks, it is possible to detect the size of an air gap between two plates, as shown by Huang and Wu [12]. However, the error increases from <10% with an air gap of 0.5mm to over 100% with an air gap of <0.1mm, which is a region of interest in the present application. Additionally, these results are obtained using a 4mm upper layer of aluminium and <2mm thick lower layer of aluminium, which is has notably higher eddy current penetration than carbon steel. Furthermore, experimental results thus far are limited to layer thicknesses significantly less than those in the slip-joint, adding another barrier to the practical application of this method. Nevertheless it is the opinion of the author that this method warrants further investigation by individuals experienced in the matter, as it may be possible to measure gap size if a very powerful emitter and very sensitive receiver were combined appropriately.

2.2.5 X-Ray / Gamma Ray

X-ray and Gamma ray scanning techniques are widely used for mass scanning of cargo containers and luggage, as well as near surface scanning for micro cracks and stress concentrations in manufactured parts. The latter application is not of particular interest as the penetration depth is extremely low (<1mm steel), however the penetration depth in the former applications is very high (up to 30cm steel). The method is based on the placed of an X-ray or Gamma ray emitter on one side of the test subject and a detector on the far side. Typically in cargo applications the emitter is in a strip shape on one side of the container. The detector therefore only detects a cross-section of the test body at any one point in time, although it may generate a 2D image as the subject moves slowly past the emitter.

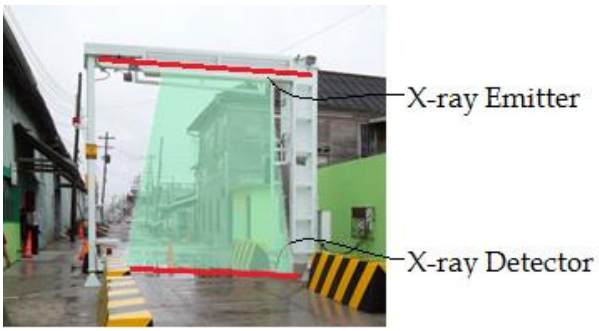

Figure 8 - X-ray scanner set-up [13]

The benefit of this technique is that slip-joints consisting large wall thickness sections could be easily penetrated, however such x-ray or gamma ray systems are large and would be difficult to utilise offshore. Furthermore, there is difficulty in accurately isolating the gap between the two walls of the slip-joint for measurement given that the measurement is planar. It may be possible observe the gap between the two slip-joint layers by passing the joint longitudinally through an x-ray container scanner. However this orientation would only give information about the gap size in a line along the outer left and right edges of the joint as those would be the only areas where the measurement plane would be perpendicular to the direction of radiation propagation (see Figure 9). Therefore the

slip joint (or measurement device) would have to be repeatedly realigned and re-measured to cover the whole joint.

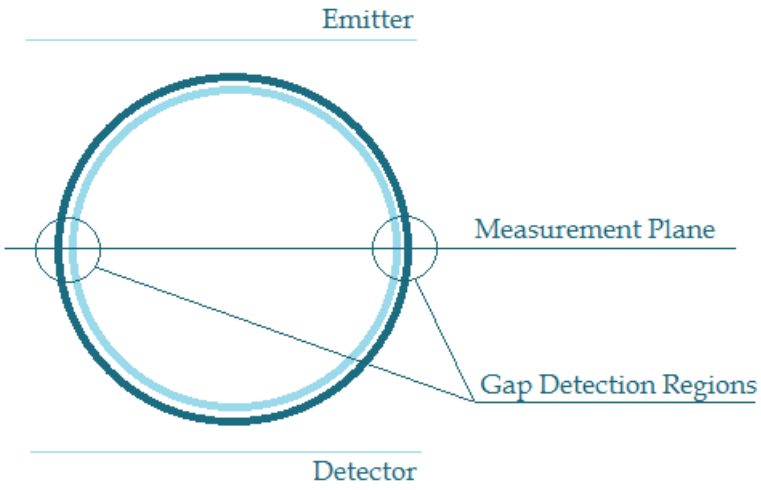

Figure 9 - Measurement locations using x-ray scanning

There exist further issues with this method, such as access to the measurement equipment and the low resolution of the measurement device [14]. Therefore, this method was deemed not suitable for the current application and has not been investigated further.

2.2.6 Acoustic Resonance

Acoustic resonance techniques rely on the evaluation of localised resonance modes of the structure. The theory indicates that a structure with a local defect such as a void or delamination (in composite structures) would experience a localised decrease in stiffness and therefore experience a shift in (local) modal frequencies when excited [15]. This test method is colloquially known as the coin-tap method, as traditionally a coin was used to tap different areas of the structure and the audible response frequency was noted to determine if there was a defect. Note that this is fundamentally different to the method of testing railway wheels by tapping, as in the latter case the global vibration modes are excited (and measured). In the railway wheel case it is therefore possible to determine that the wheel is defective (from a variation in global vibration modes), but not possible to easily determine the location of the defect.

The coin-tap method has been studied most extensively for application to composites in the aerospace industry [16, 17] although further research has been completed recently for use in wind turbine blades and alternate industries [18, 19]. Despite further research into the method, to date, all studies focus on the application of the method to composite materials, with the aim of detecting flaws such as voids and delamination. Noting this, the system at hand does share underlying characteristics with composite materials, as both exhibit local variations in stiffness due to sub-surface structural 'defects'.

Upon initial investigations of the coin-tap method by Cawley [15] it was postulated that the lower localised stiffness in defective regions would influence the magnitude and duration of the force imparted by the impact device. This was subsequently tested by Cawley and others [16, 17, 19] and confirmed to be true within certain boundaries. As [16] note, the impact force is typically modelled as a half sine wave, although in reality the curve is asymmetric due to non-linearities introduced by non-rigid body behaviour and a coupling between energy dispersion and impact force magnitude. Despite this, based on the half-sinusoidal approximation of the impact, instrumented hammers have been developed by Mitsui [20] and Boeing [17], both relying fully on the impact force time series to characterise any local defects. Latter research has focussed on the measurement and analysis of sound waves related to the surface impact [18, 21], while [16] looked at a correlation between the results of the two measurement methods, comparing their ability to detect repaired patches and supported vs unsupported conditions in a composite aircraft skin material. Wu's results showed that a combined approach is most beneficial, however the accuracy and resolution of the method in detecting small defects still requires significant improvement. For this reason this method was not appropriate for initial analysis of the slip joint, although it may provide value when used in conjunction with other methods. The possibility and details of the latter is discussed in section 6.3.3.

2.2.7 Other Methods

2.2.7.1 Water Pressure/Flow

It has been suggested by some interest parties that a water pressure of flow resistance based method may work to quantify contact area. A number of methods have been envisaged that draw on this basis, although all have significant flaws. The first example of such a method is a flow resistance test where water in pump into one end of the slip joint (between the two layers) and the flow rate is measured at the other end of the joint. The obvious downside of this method is that it is heavily influenced by the shape of contact regions and if one such region were to encircle the entire joint, no water would be able to flow through the joint, therefore providing no information about contact regions. A second water based method would involve standing the joint upright and sealing the bottom of the joint (between the two layers) and then filling up the joint with water. This would give information as to the rough volume of the voids in the joint, however it is also heavily influenced by the geometry of contact regions. For example the method would not be able to distinguish the difference between a contact region encircling a non-contact region and a region of full contact. Finally, all conceivable water based methods would only provide a global contact 'percentage' at best and have therefore not been considered for further investigation.

2.2.7.2 Neutron Techniques [22]

Neutrons have a high penetrating power and thus have benefits in characterising defects in thick sections or materials that otherwise resist alternative defect detection techniques. Neutrons exhibit strong preferential absorption by hydrogen atoms, which make them ideal for identifying moisture ingress. However, the absorption rate of carbon is similar to that of oxygen and nitrogen [22] (with Iron only slightly lower)[23], which makes adds significant challenges in determining the presence of a void between two slip-joint layers. In practice the void would appear very similar to an increase in

steel thickness and therefore, for small gaps, there would be no way to determine if the variation was in material thickness or gap size. It may improve this method if all voids in the slip-joint were filled with water, however this would only aid in regions where the water was able to penetrate. Furthermore, this method can provide almost no information about pressure distribution in contact regions, therefore it was not considered for further analysis.

2.2.7.3 Microwave and Terahertz Techniques

Microwave and Terahertz techniques operate on the principle of supplying a short pulses of energy to the test material (in either transmission or reflection mode) and measuring the output. The high frequency of the source (300MHz-4THz) allows the ability to resolve smaller defects than ultrasound techniques. Additionally terahertz techniques have shown the ability to avoid the defect 'shadowing' that ultrasound suffers from where the entire signal is reflected by the first defect reached. However, both microwave and terahertz spectroscopy techniques suffer from the major disadvantage of strong attenuation in metallic subjects, specifically subject with good electrical conductivity. Therefore, while this method has shown promise in the analysis of composite materials it is not appropriate for the application at hand.

2.3 Heat-Based Methods

Before examining the specifics of heat based methods, it should be noted that such a method has been selected for primary investigation of the slip joint. For this reason, greater detail (compared to previous methods) is presented on the theory, present literature and specific application of this method in the following sections. A final note on nomenclature; planar conduction within the plates of the slip-joint (ie. perpendicular to the normal axis of the plate) is referred to as diffusion to differentiate it from heat conduction along an axis normal to the slip-joint surface. Despite this, the underlying heat transfer mechanism is the same in both cases (only directions differs).

The primary heat based inspection method investigated to date is known as 'Transient Thermography' and was originally investigated by the National Non-Destructive Testing Centre (Hardwell, UK)[24, 25]. Transient thermography techniques are based on the measurement of the response of the test subject to a rapid pulse of heat at one of its external surfaces. A very short burst of heat is applied to the surface causing the surface to rapidly increase in temperature. As the heat source fades, the surface will begin to drop in temperature as the heat propagates through the material like a wavefront. If there is a defect (such as a void) within the material then it will restrict the passage of the heat wavefront through the material. The presence of this defect can then be detected due to two resulting phenomena; the heated surface will remain hot in the vicinity of the defect (known as reflection mode measurement) and the far surface will not heat up as much in the location of the defect (known as transmission mode measurement). These two measurement modes are shown in Figure 10.

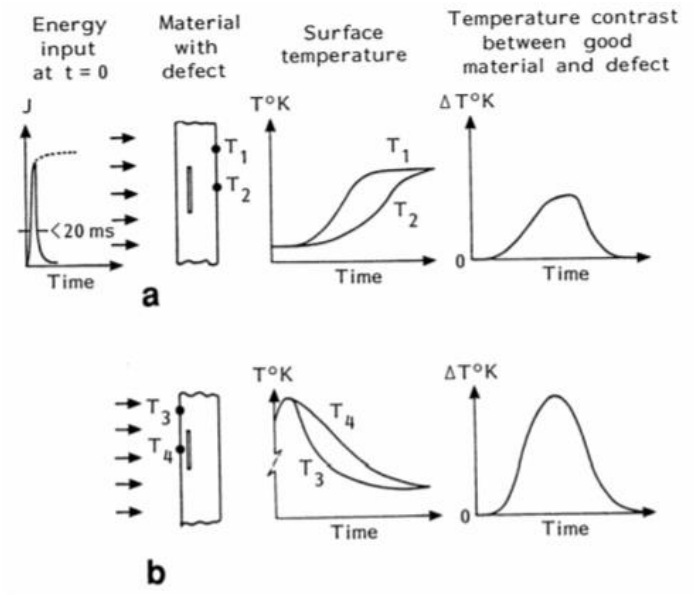

Figure 10 - Heat propagation through defective samples [26]

In either case the temperature rise on the input surface is a function of the energy in the heating pulse and the duration of the pulse. The resulting change variation in the temperature field around a defect is then a function of the size of the defect (both in diameter and depth) and the depth of the defect within the material. With a short energy pulse (in the order of 10-50ms), the presence of a defect can often be detected within a few seconds (and often a few milliseconds), depending on the geometry of the defect and material properties [27, 28]. Note that much of the present work [24, 28, 29] is focussed on the inspection of composite materials and/or materials with small and/or shallow defects. Adding to the challenges of this method, [29] found that the sensitivity of transient thermography methods is most readily summarised as a function of the defect diameter/depth ratio. It was found that while the ratio did not increase linearly with depth (providing increased sensitivity with depth), the overall minimum detectable defect size did increase. This calls into question the efficacy of the method in detecting small differences in gap size in the slip joint, although Cawley et al [26] note that results can be improved if the energy transmitted to the material is increased.

Considering the application at hand, a number of potential issues arise with this technique. Firstly, the method assumes that the heating source is large enough to heat an area significantly greater than the assumed size of any defect. Clearly in the case of the slip joint where the 'defect' covers the entire joint, this is not possible. It is therefore necessary to consider the areas of the slip joint that are in contact as a control region, with which other areas of the slip joint may be compared. In this way, the slip-joint may be analysed similarly to Cawley's scenario of a defect within a material sample [26]. Figure 11 illustrates this concept, although it omits the fact that in latter case there will be no thermal contact resistance between the upper and lower halves of the material sample. This omission is intentional, as the addition of thermal contact resistance (in the case of the slip-joint only serves to decrease the relative 'size' of the defect (air gap) and therefore necessitate a more effective detection technique.

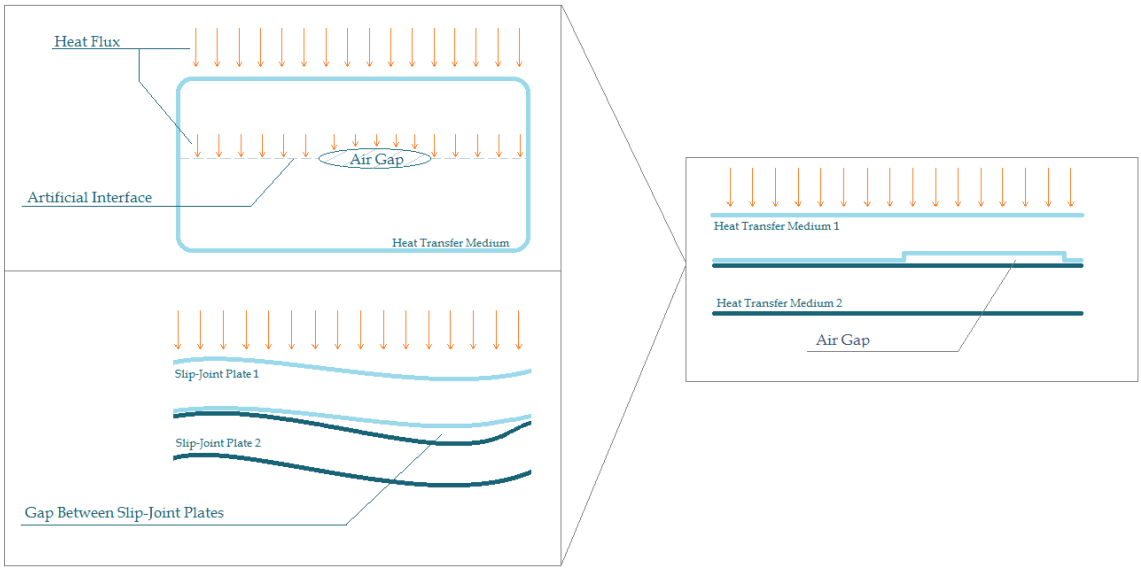

Figure 11 - Comparison of gaps in the Slip-Joint with defects in a solid material

2.3.1 Reflection Mode vs Transmission Mode

A second issue in the application of transient thermography is the selection of reflection or transmission mode measurements (see Figure 10). In reflection mode a single layer of the slip joint is heated and then subsequently measured for temperature variation. Regions with high contact between the two layers would then cool more quickly as there is lower resistance to the passage of the heat wavefront. Conversely, in areas with a large gap between the two plates, the energy would remain in the initial plate and the temperature would decrease at a slower rate. Reflection mode therefore requires the chosen surface to be heated to a significantly high temperature so as to measure the difference in heat dissipation. Furthermore, this mode requires a certain uniformity and repeatability in the heating method, as any significant variations between regions of the joint would affect the subsequent temperature measurements.

In transmission mode the chosen surface of the body is heated and the surface on the opposite side of the body is measured as the heat front propagates through the body. Regions with high contact would through have high heat flux across the slip-joint interface and regions with a large gap would have a lower heat flux resulting in 'cold' spots. Due to the natural diffusion of the heat wave within the initial layer of the slip-joint and especially across the plate interface, the far side temperature measurements are far less sensitive to localised variations in the heat source intensity. However, this diffusion also means that the method loses resolution in identifying smaller defects (interpreted in the present case as super-localised variations in gap size). The impact of this limitation should be limited, as it is assumed that the variation in interface pressure/gap size in the joint is gradual and high resolution is not a strictly necessary measurement outcome.

2.3.2 Thermal Resistance Theory

To better understand heat-based measure methods it is necessary to understand the physics of the heat transfer process and the factors influencing heat propagation. To achieve this we must separate

the two different heat conduction schemes found with the slip joint; those where an air gap is present and those where there is contact between the two layers (as per Figure 11). In this way we can determine what kind of heat transfer properties both contacting and non-contacting regions may have, what factors affect these properties and therefore how we can differentiate between the two regions using a heat based method.

2.3.2.1 Heat Transfer Between Closely Spaced Plates

In the case of no contact between the two cones of the slip joint, the localised region of occurrence may be treated as if it were two discrete plates separated by a thin layer of air. This problem has been studied extensively in the context of double-pane windows and closely-space heat exchanger fins [30] and is essentially a problem of simple series heat transfer, as Figure 12 shows.

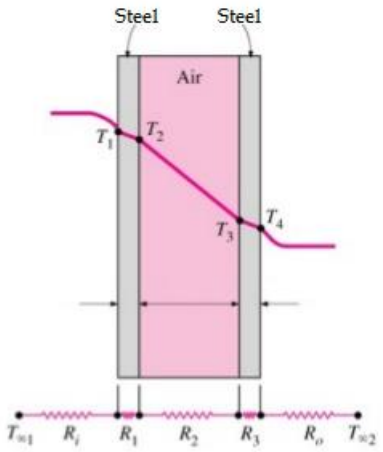

Figure 12 - Temperature profile across steel plates with an air gap. T1-T4 represent temps, Ri,Ro and R1-R3 represent thermal resistances. (not to scale) [31]

The initial element in the resistance series is related to the transfer of heat to the first steel plate. This may be from a specific heat source or just from the atmosphere, however all physical testing has been conducted under consistent indoor conditions, thus atmospheric heat transfer may be neglected. Additional thermal resistance at T_1 is specific to the heat source used to heat the first steel layer and will therefore be touched on later when heat sources are discussed. The next resistances (R1 and R3) are related to the two steel plates. The thermal resistance of the steel plate can be calculated as;

$$R_{steel} = \frac{\Delta x}{k}$$

Where;

R = Thermal Resistance [$m^2 \cdot K/W$]
Δx = Thickness of steel plate [m]
k = Thermal conductivity of mild steel [~44W/m $\cdot$ K @20°C]

In reality this resistance increases with temperature, as the steel expands with temperature (creating a larger Δx) and the thermal conductivity of steel decreases (approximately) linearly with temperature. The next resistance in the system is the resistance of the air layer. This can be

calculated in the same manner as the steel, only substituting the thermal conductivity coefficient of air (~0.024W/m · K). Clearly, given the much lower thermal conductivity of air, one would expect a much higher resistance here than in the steel layers (given similar thicknesses). However, in some cases the lower heat conductivity of the air is mitigated by the addition of convective or radiative heat transfer in the air layer. It may be possible to omit these heat transfer modes on the basis that they are negligibly small; however this assumption must be investigated.

The Nusselt number (Nu) is explicitly defined to quantify the difference in magnitude of convective and conductive heat transfer. The lower limit of the Nusselt number is 1, as the numerator is the combined convective and conductive heat transfer, while the denominator is the purely conductive heat transfer [30]. The Nusselt number varies for different geometries (such as vertically parallel plates or horizontal parallel plates), but in the most basic case;

$$Nu = C(Gr_L \Pr)^n = C(Ra_L)^n$$

$$\text{Rayleigh Number (Ra)} = Gr_L \Pr = \frac{g\beta(T_s - T_\infty)L_c^3}{\vartheta^2} Pr = \frac{g\beta(T_s - T_\infty)L_c^3}{\vartheta\alpha}$$

$$\Pr = \frac{\nu}{\alpha} = \frac{\text{viscous diffusion rate}}{\text{thermal diffusion rate}} = \frac{\mu/\rho}{k/(c_p\rho)} = \frac{c_p\mu}{k}$$

Where;

g = gravitational acceleration, m/s²
β = coefficient of volume expansion, 1/K ($\beta = 1/T$ for ideal gases)
T_s = temperature of the surface, °C
T_∞ = temperature of the fluid sufficiently far from the surface, °C
L_c = characteristic length of the geometry, m
ν = kinematic viscosity of the fluid, m²/s

C = Experimental Coefficient
n = Experimental Exponent

In order to determine the role of convection heat transfer one must assume theoretical 'test conditions' for the slip-joint. The maximum convective action will occur when there is a maximum temperature difference between the two steel plates; therefore a high temperature heating scenario is used, where one layer of the joint has already been heating for some time. It is assumed for this calculation that the max temperature differential inside the air gap will generally be less than 70°C (ie. if T_2 (Figure 12) is 90°C internally and T_3/T_4 (Figure 12) has heated to 20°C). Furthermore it is assumed that the gap between the two plates is a localised defect of roughly 1m diameter. These assumptions are based on physical observations of the author during initial testing. The size of the air gap is not specified here as it will be investigated below. Various authors have conducted experimental work to quantify the coefficients in the above Nusselt equation, which presents the following possible relations for a closed cavity with one heated wall (note: S = L_c = gap size [m]);

Equation	Limits	Value (S = 0.1m)	Value (S = 0.05m)	Value (S = 0.01m)	Source
$Nu = 1$	Ra<2x10^3 Pr = any, H/S = any				
$Nu = 0.197 Ra_S^{0.25} \left(\frac{H}{S}\right)^{-\frac{1}{9}}$	2x10^3<Ra<2x10^5 , 0.5<Pr<2, 11<H/S<42;	10.1	4.7	1	[32]
$Nu = 0.073 Ra_S^{0.333} \left(\frac{H}{S}\right)^{-\frac{1}{9}}$	2x10^5<Ra<2x10^7, 0.5<Pr<2, 11<H/S<42;				
$Nu = 0.42 Ra_S^{0.25} Pr^{0.0012} \left(\frac{H}{S}\right)^{-0.3}$	10^4<Ra<10^7, 1<Pr<2x10^4, 10<H/S<40;	11.9*	5.8*	1.1*	[33]
$Nu = 0.22 \left(\frac{H}{S}\right)^{-0.25} \left(\frac{Pr * Ra_s}{0.2 + Pr}\right)^{0.28}$	Ra<10^{10}, Pr<10, 2<H/S<10;	10.0	4.7	1*	[34]

Table 1 - Nusselt Number in slip-joint gaps

(Asterisk indicates that the equation limits are not met. These values have been individually checked to ensure that the breach does not significantly affect the end result.)

As seen in Table 1, the Nusselt number rapidly approaches 1 for gaps between the two pieces of the slip joint of less than 1cm. Visual inspection of the joint and gap size around the end of the joint indicates that the expected gap size is significantly less than this limit and convective heat transfer may therefore be neglected.

In order to quantify the effect of radiation we may consider the relative magnitudes of steady state radiative heat flux and conductive heat flux as applied to the example case used above;

Relevant Equation [W/m^2]	Value (S = 0.01m)[W]	Value (S = 0.001m)[W]	Value (S = 0.0005m)[W]	Source
$q" = -k\nabla T = -k\frac{dT}{dx}$	168	1680	3360	[30]
$q" = \frac{5.67x10^{-8}(T_H^4 - T_C^4)}{\frac{1}{\varepsilon_1} + \frac{1}{\varepsilon_2} - 1}$	377.7	377.7	377.7	[30]

Table 2 - Radiation vs conduction heat transfer in slip-joint gaps

As illustrated in Table 2, radiation plays a significant role in the heat transfer between the slip joint walls, although this diminishes as the air gap between the walls declines. It should also be noted that the table above is for a case when one wall of the slip joint has reached a high temperature and therefore radiation heat transfer is at a peak. In the initial and mid stages of heating conduction will be far more dominant. However, despite this, radiative heat transfer may not be neglected and

should be included in series with conductive heat transfer across the air gap. In Figure 12, R_2 is then equal to the parallel conduction and radiation resistances in air.

2.3.2.2 Heat Transfer Between Plates in Contact

Heat transfer between contacting materials falls broadly under the field of Thermal Contact Resistance (TCR), which seeks to identify the mechanisms and rates of heat transfer in such situations. When two surfaces contact each other, they may seem to be fully in contact on a macroscopic level, yet they will always be separated to some degree by their surface roughness asperities (see Figure 13). Therefore, there inevitably exists an increased resistance to heat transfer across such a boundary when compared to a perfectly bonded block of material.

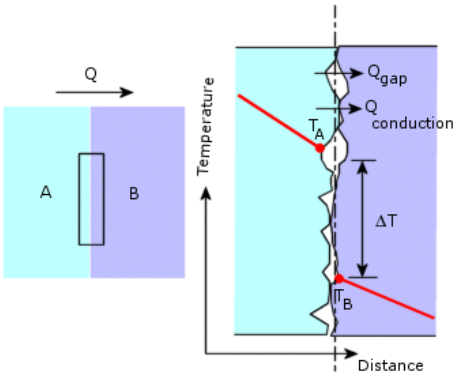

Figure 13 – Thermal Contact Resistance [35]

The heat transfer mechanisms pertinent to TCR are conduction and radiation, as the gap sizes are too small for significant free convection (see Table 1). The specific transfer modes are; conduction across contacting surface asperities, conduction across the small air gaps in the joint and radiation across the air gaps in joint. Therefore any parameter that may influence any of these conduction modes can influence the TCR of a joint. The properties influencing the joint can generally be divided into three categories [36], as per Figure 14.

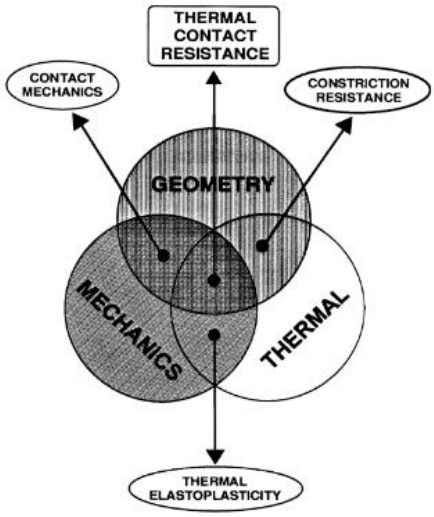

Figure 14 - Factors influencing thermal contact resistance

Following the model of Figure 14, some of the significant properties influencing a TCR problem include;

Geometry	Mechanics	Thermal
Surface Roughness (Both Parts)	Contact Pressure	Temperature Difference
Contact area size	Material Surface Hardness	Thermal Boundary Conditions
Contact area flatness	Interstitial Material Properties	Material Thermal Properties
	Material Stress State	

Table 3 - Factors influencing slip-joint thermal contact resistance

Of the above properties, the most pertinent to the slip-joint problem is the contact pressure between the two surfaces. This is the case because most of the other parameters may be assumed to be constant across the slip-joint area. Clearly, contact area size will vary over the slip-joint, however with localised measurement techniques; it can be assumed that the size of the test area is uniform across all measurements. Assuming other parameters remain constant (or controlled) between measurements, the TCR is then a function of the contact pressure [37].

$$Contact\ Force\ (F) = PA_{apparent} = H_C A_{real}$$

$$\therefore \frac{A_r}{A_a} = \frac{P}{H_c}$$

Based on the thermal-plastic deformation model of [37], the thermal contact conductance (h_c) is then;

$$h_c = \frac{2nak_s}{\varphi(\epsilon)}$$

Where the effective thermal conductivity (k_s) is;

$$k_s = \frac{2k_1k_2}{k_1 + k_2}$$

The thermal constriction parameter (φ) (for isothermal contact regions) is given by;

$$\varphi(\epsilon) = (1-\epsilon)^{1.5}, \qquad for\ 0 < \epsilon < 0.3$$

Where;

$$\epsilon = \sqrt{\frac{A_r}{A_a}}$$

The parameters *n* and *a* are based on the relative mean separation between the two contact surfaces and their equations may be found at [37]. Without the need to inspect these equations it is clear from the above that an increase in contact pressure will increase the actual area of contact (for a given apparent contact area and microhardness). This is because of plastic deformation of the surface asperities which decreases the mean distance between two surfaces, increases metal-metal contact area and increases the interstitial gas pressure. Due to the multiple actions in play here the specific relationship between contact pressure and thermal contact conductance/resistance is hard

to measure outside of laboratory conditions and is very material specific. Figure 15, gives some experimental values for TCR of Aluminium 2024-T4 and serves to outline some key features of this relationship. Namely, the TCR is non-linearly dependent on contact pressure, there is strong variation based on surface roughness and that TCR is asymptotic in the upper limit of contact pressure.

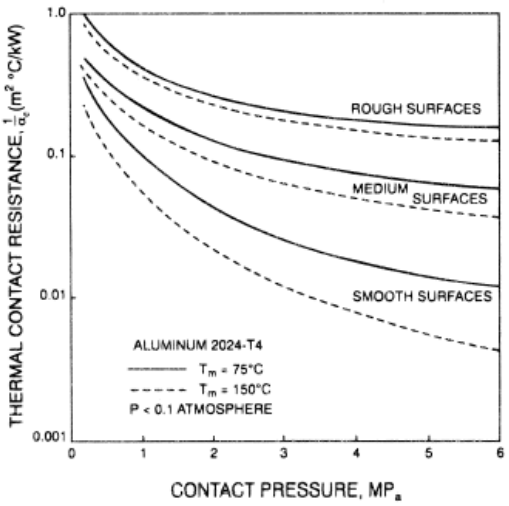

Figure 15 – Thermal contact resistance vs contact pressure [38]

Figure 16 provides similar (but non-normalised) curves for a variety of materials, including steel, which is more pertinent to the slip-joint. Note that this figure provides contact conductance instead of resistance and the contact pressure is given in log scale. An item of note on this figure is the difference between stainless steel samples and those coated with aluminium. Firstly, it can be seen that aluminium TCR has a much greater dependence on the contact pressure than standard stainless steel. It is also apparent that coated steel with a softer (or highly thermally conductive) substance, such as aluminium can potentially increase thermal conductance. This indicates that the paint coating on the slip joint (typically polyurethane and/or epoxy based), may increase the TCR due to its low thermal conductivity, however this may be minimally offset by an increased real contact area due to the lower hardness of the paint.

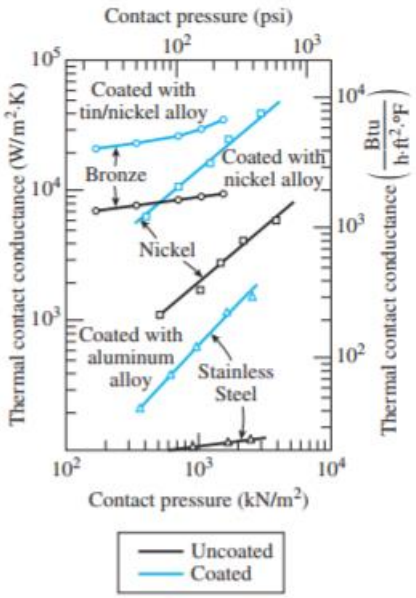

Figure 16 - Thermal recontact conductance curves for assorted materials [39]

In summary of TCR theory, we can see from both Figure 15 and Figure 16 that TCR increases rapidly as contact pressure approaches zero. This indicates that areas of the slip joint with some contact (no matter the pressure) will always have higher thermal conductance than areas with an air gap. As such, when applying heat to the one side of the slip-joint, one would expect 'cold spots' to show on the other side of the joint in areas where there is a gap in the joint. The relative 'magnitude' of the cold spots will vary with gap size, while the heat transfer in contacting regions will similarly vary with pressure, though to a lesser degree.

2.3.3 Equipment for Thermal Testing

Heat based measurement methods unanimously require the application of heat to the material, most commonly in a single or in multiple pulses [22, 40]. The application of a short single burst allows the heat to travel as a wavefront and thus the time required for the heat wavefront to reach the receiving sensor may be measured. This allows the interested party to ignore effects after this point that may be cause by indirect transfer of heat from source to sensor.

Similar methods are used in both the detection of defects with transient thermography and the determination of thermal contact resistant in laboratory conditions. Attempts in both fields generally apply a very small amount of energy to a small, well defined sample contained within a low temperature environment. This allows heat losses through convection and radiation to be minimised allowing the relevant properties to be more accurately measured. In this case the heat may be applied with either ultrasonic, x-ray or laser pulses and the results are typically measured with thermocouples.

Issues arise with this method in the case of the slip-joint, as neither the external temperature nor test boundary conditions may be easily controlled. Additionally, the thickness of the slip joint materials is significantly greater than that of typical test materials (in the order of 10x) and the

potential gap size is far greater than the induced defects in typical transient thermography tests [28]. These differences mean that diffusion within the joint plays a significant role and a very small heat pulse may never reach the other side of the slip joint with a detectable magnitude. Conversely, if the slip-joint is heated for a very long time, a greater percentage of heat may transfer between the layers of the slip-joint at regions outside the intended measurement region, interfering with the localised nature of the measurement (see Figure 17). Therefore it is necessary to heat the slip-joint as rapidly as possible to minimise diffusion and avoid non-localised heating, however a significant total amount of heat must also be transferred to the heating location to ensure that there is a notable increase in temperature on the opposite side of the joint. Note that as the joint is painted, the surface temperature should not exceed ~150°C (423K)[41] to avoid damaging the paint. This means that an increase in heating time rather than an increase in heating rate is preferable if there is a need to transfer more energy to the slip-joint.

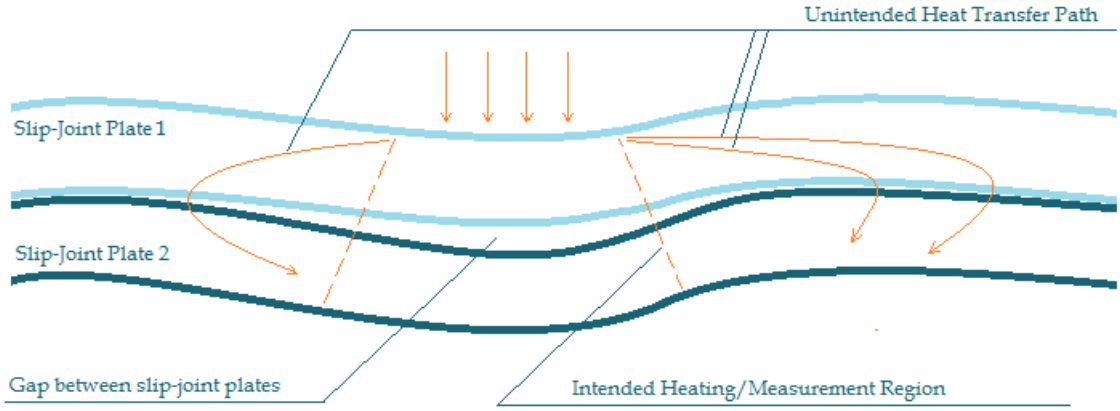

Figure 17 - Heat transfer path across slip-joint layers

2.3.3.1 Heating Equipment

Considering that the goals of the heating equipment have been established above, the heating equipment options may be examined. In this manner a suitability analysis has been performed with the results noted in Table 4. A plus indicates that the heating method performs favourably in a certain category; a circle indicates that the method performs adequately and a negative sign indicates poor performance. The principles of each method and further considerations are explained below the table.

	Heating Method						
	Laser	X-ray/Flash Tube	Induction Coil	Silicone Resistor Mat	Ceramic Resistor Mat	Direct Flame	Convection
Heating Speed	+	o	o	-	-	o	-
Set-up Speed	-	o	+	+	+	+	o
Accessibility	-	o	+	o	o	+	o
Cost	-	-	+	o	o	+	+
Reliability	+	+	+	o	o	-	-
Repeatability	+	+	o	o	-	-	-
Heat Rate Control	+	o	o	-	-	-	-

Heating Uniformity	-	o	o	+	o	-	-
Specialist Knowledge	o	o	+	+	+	+	+
Total:	0	1	5	1	-1	0	-3

Table 4 - Heating equipment comparison

2.3.3.1.1 Laser Heating

Laser heating is a surface heating method primarily used in manufacturing for heating components where very localised heating is desired. The heat input can be very accurately controlled by varying the wavelength and exposure time of the laser. The spatial accuracy, fast heating and heat control of this method are advantageous, however laser machines have difficulty heating areas larger than $1cm^2$, therefore the use in the slip-joint is limited. Additionally, rapid heating of only the outer surface of the joint rapidly increases the temperature in this region, leading to greater heat lost to the atmosphere (rather than propagating through the joint).

2.3.3.1.2 X-ray/Flash Tube Heating

X-ray and flash tube heating both involve the application of a high voltage applied across an anode and cathode contained in a glass tube. The slight difference in these two methods is that x-ray tubes have an internal vacuum and produce x-rays due to electron collision with the anode. Alternatively, in flash tubes radiation is produced due to electron collision with an inert gas contained in the glass tube. X-ray tubes produce radiation of greater energy and thus greater heating potential; however both function on the same principle of electromagnetic waves heating the slip-joint surface. The benefit of such methods is that a well-controlled amount of heat, with reasonable spatial uniformity can be quickly directed at the joint. Halogen lamps are also fast to setup, however they typically have a low efficiency which can be further impact by windy conditions.

2.3.3.1.3 Ceramic Heat Mat

Ceramic heating mats are one of many forms of flexible resistance heaters. Ceramic heaters typically consist of a resistance element embedded in a ceramic form which acts as a diffuser to more evenly conduct the generated heat. Flexible ceramic heat mats are made from many individual ceramic elements which are mechanically connected to form a flexible mat. This gives the advantage that the mat can curve around the surface of the slip joint, however due to the resistive heating mechanism, heating power is proportional to the ceramic temperature which may lead to paint damage at high power. Additionally attaching the ceramic mat to the slip joint could be challenging, as contact pressure need to be uniform for uniform heating.

2.3.3.1.4 Silicone Heat Mat

Silicone heating mats are essentially very similar to ceramic heating mats except that the resistive element is embedded in a silicone layer instead of ceramic pieces. This gives the advantage of added

flexibility and the ability to apply adhesive to the mat to allow easy application. However, being a resistance based heater silicone mats still suffer from low power output (to avoid damaging paint) and (purchasing) accessibility is also an issue.

2.3.3.1.5 Flame-based Heating

Direct flame heating is very common form of heating where steel products are involved. Typically monopiles and large pipes are heating with custom flame heaters prior to and post welding to limit residual stresses. Despite being a rapid heating method with easy accessibility, this cannot be used for the simple reason that the paint on the joint will almost certainly be damaged.

2.3.3.1.6 Convection-based Heating

There are a number of forms of convection heater, however the basic principle is that a fluid (or gas) is heated by (typically) a resistance heating element, after which the fluid flows past the target surface and transfers heat to it. This can be achieved using both water and air as the working fluid, although the simplest example in this case is the hair dryer. An industrial convection heater, similar to a large hair dryer, could heat the slip-joint rapidly, whilst also being very portable and easy to operate. However, heating would be difficult to confine to a small space and a frame would be required to hold the heater at a constant distance and angle.

2.3.3.1.7 Induction

Induction heating works by generating a high-frequency oscillating electric current in an induction coil. This oscillating current creates an oscillating magnetic field around the coil which penetrates the target material, generating eddy currents which cause joule heating. Small induction units can be handheld, with induction coils of any diameter to suit the application. Additionally, the power can be easily varied and the heat is generated directly in the upper few mm of the material, allowing the induction coil to remain cool. Given that an induction heater is already available in the DOT workshop, as well as the above reasons, induction heating has been selected the method of choice for this experiment.

The heater available is the iDuctor 1200w handheld induction heater with flexible induction cables. The longest of these cables was coiled into a pancake coil and fixed in place with silicone tape to minimise (non-inductive) heat transfer between the coil and the joint surface (as shown in Figure 18). The coil was also placed in a wooden frame which separates the unit from the heating surface by a fixed distance, leading to more consistent heating. The frame also allows the installation of small magnets (seen in Figure 18), which help to easily secure the coil to the slip-joint wall.

Figure 18 - (a) Heating coil in frame, (b) Induction unit with unwrapped coil

The induction coil in use operates at 30kHz (on maximum power setting) with a working voltage of 5.5v. The coil itself consists of 6 complete loops (in the current setup) of Litz wire of an unknown number of strands and strand thickness. The coil is 115mm in diameter and 0.8mm in thickness (including the fibre sheath around the cable and the 0.5mm thick silicone tape).

2.3.3.2 Data Acquisition Equipment

Following the decision to utilise a thermographic measurement technique, it is necessary to select a method with which to measure changes in temperature at the measurement surface. The following three measurement devices are commonly used devices that were considered for this application.

2.3.3.2.1 Thermocouple

Typical type K thermocouples are a relatively cheap spot measurement device consisting of two wires bonded together at a measurement tip. Due to the different metals used in the wire to and from the tip, a voltage is generated in the thermocouple circuit dependent on the tip temperature, allowing thermal measurements. While, high accuracy can be achieved with thermocouples, the accuracy is strongly dependent on the bond between the thermocouple and the measurement surface, making changes in measurement location time consuming. Additionally, due to the exposed wires near the measurement location, thermocouples are subject to influence from electro-magnetic fields (such as from induction heaters). In the slip-joint this should mostly not be a problem as the steel should block the radiation, however if there is a hole through the steel near the measurement location, some radiation could still get through the joint and influence readings. To combat this, electromagnetically shielded thermocouples have been invented; however these are quite expensive and suffer from the same difficulty in changing location as regular thermocouples.

2.3.3.2.2 Infrared Sensor

To combat the need to attach a measurement device to the measurement surface an infrared sensor may be used. Infrared sensors, also known as infrared pyrometers, have a very small silicone sensor which detects incoming radiation, which can be used to assess the target temperature using Planck's Law of black body radiation. Infrared sensors use optics in front of the sensor to try and focus on a single point, although in reality the device focuses in a cone, such that the target point area varies with the distance between the IR sensor and the target. The advantages of this sensor are that they are inexpensive and are immune to electromagnetic fields, because the device can simply be held outside of the field domain. However, the accuracy of IR devices is typically less than that of thermocouples and the sensor only measures a single spot, which therefore requires advanced knowledge of exactly which location needs to be measured.

2.3.3.2.3 Thermal Camera

Thermal cameras use the same technology as infrared thermal sensors, except that the silicone sensor is comprised of a large number of individual bays. This allows the temperature to be differentiated in across the measurement field and therefore a thermal image can be created. Due to this similarity, thermal cameras can also avoid the influence of electromagnetic fields and can change measurement locations quickly and easily. However, the greatest benefit of a thermal camera in this application is that it can measure the temperature across a large location at once. This useful when measuring the slip-joint because it is very difficult to exactly align the heating unit on the inside of the joint and the sensor on the outside of the joint prior to measurement. Therefore, measuring a large area means that the region being heated will always be recorded regardless of slight misalignments.

For these reasons the FLIR One Pro thermal camera has been selected for use in measurement of the sample slip-joint. The FLIR One Pro (Figure 19) is a thermal camera that utilises a smartphone to display and store the thermal images captured. The device has a 160x120 pixel sensor, -20°C-400°C measurement range, ±3°C (or 5%) accuracy and 150mK thermal resolution. While the resolution and accuracy are certainly not the highest available in thermal cameras, the preliminary nature of the measurements and limited funding make such a camera the best choice. Additionally, the camera has an external micro-USB port allowing active charging while in operation to extend the battery life from 1hour to 2+hours.

Figure 19 - FLIR One Pro Thermal Camera

2.3.4 Conclusion

A thermographic (heat-based) method is optimal for measuring the slip-joint because it can resolve both pressure and gap size differences in thick steel sections. Other methods such as magnetic field attenuation eddy current or acoustic resonance methods are less applicable, but may be used at a later point to compare with thermal measurements and validate the thermographic results.

Continuous active heating, with measurements in the transmission mode should be used for ease of measurement and to ensure a measureable quantity of heat energy is transferred through the joint. To this end, an induction heater is the best heating option due to its high power output, heating control and ease of use. To this end an iDuctor 1200w unit has been selected and an induction coil and frame prepared for use.

The induction heater best combined with a thermal camera for heat measurement, as thermal cameras can measure a large area at once, do not have to be attached to the measurement surface and are insensitive to electromagnetic radiation near the measurement surface. For this reason a FLIR One Pro thermal camera was selected for use.

3 Experimental Method

3.1 Slip Joint Geometry

The thermographic method selected for slip-joint measurement will be tested on a sample slip-joint taken from the decommissioned 'Duinvogel' onshore wind turbine, previously located at Scheveningen, North Holland. This slip-joint is pictured in-situ in Figure 5, which shows the position of this slip-joint in the middle of the turbine tower, compared to the envisaged offshore use of the slip-joint to connect the monopile and turbine tower. The slip-joint section (seen in Figure 20) was removed from the Duinvogel tower with the use of plasma cutters after the turbine was decommissioned, allowing the joint section to be transported to the DOT warehouse. In order to increase safety during transport the top of the inner cone was tack welded to the inside of the outer cone at 30 points. This stops relative movement between the cones which has the benefit of keeping the gap and pressure distribution in the joint as close as possible to the operational state.

Figure 20 - Duinvogel Slip-Joint

In order to facilitate easier inspection, the joint has been placed horizontally and elevated off the ground with two beam supports. The exact location of the supports and dimensions of the joint are shown in Figure 21. In order to further facilitate the measurement campaign, scaffolding was erected on either side and above the joint, to allow easier access to higher regions of the joint. Finally, for later clarity, the two ends of the sample slip-joint are not overlapping and are therefore referred to as single-ply regions, as opposed to the two-ply region at the centre of the joint.

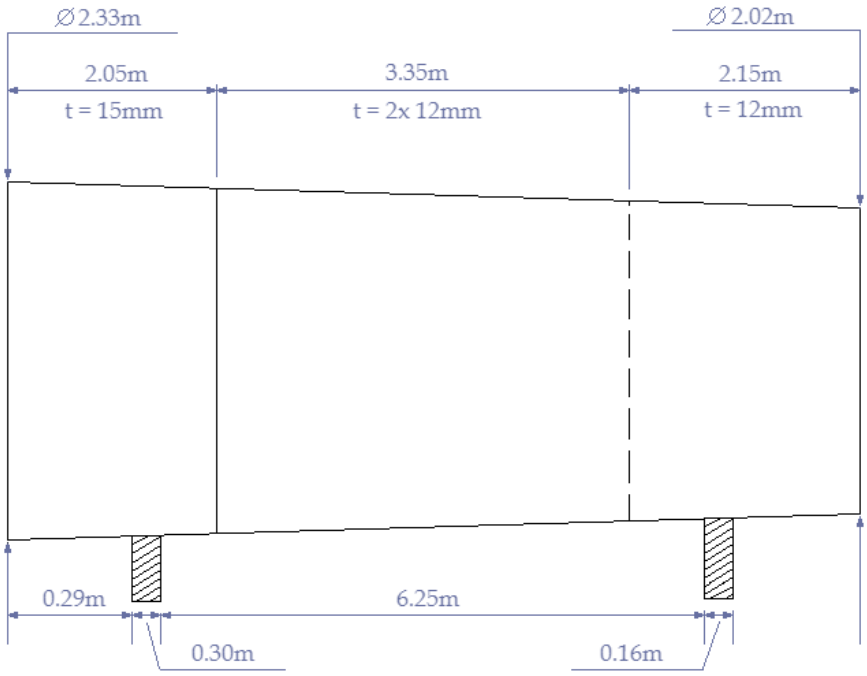

Figure 21 - Slip-joint dimensions and support locations (not to scale)

Given the age of the joint and the previous commercial use, the joint had to undergo preparatory measures prior to any testing. Inner secondary steel such as handrails, a platform and ladder sections were cut away to allow ease of movement and easier heater placement. The attachment points to the inner wall of the slip joint were not 100% removed, so placement of the heater was still obstructed in cases where the measurement point was extremely close to the attachment. Following this, the joint was cleaned, both inside and outside, with a high pressure water gun to remove built up dirt.

3.2 Measurement Process

The measurement process outlined in chapter 2 is applicable to both single-ply and two-ply regions of the joint. It is a single point measurement process, therefore a grid of the measurement surface must be built up and results interpolated between measurement points. Once a single point has been selected for measurement, the following process is used to collect the data (see Figure 22 for setup diagram);

1. The thermal camera is calibrated against an infrared spot thermometer, and then set to manual calibration mode to avoid any auto-recalibration. Two images of the measurement point are then taken, one from inside the joint and one from outside to provide a reference

for the temperature prior to heating. The thermal images should be shot in landscape orientation, keeping the image sensor parallel to the measurement surface and holding the camera such that the field of view is approximately 40cm in width at the measurement surface. Keeping these parameters constant provides enough thermal resolution (0.63mm per pixel), while also covering the majority of the heated region.

2. The induction heater coil is magnetically secured against the measurement location on the inside cone of the slip joint. Care should be taken to ensure that the centre of the coil is directly over the measurement point and that the coil itself is not in physical contact with the slip-joint wall.
3. A single thermal image is taken of an arbitrary object at the same time the heater coil is started. This image will act as a reference point for the measurement start time, as all thermal images are time-stamped. A stopwatch should also be started at this time to allow appropriate timing of thermal images. Starting the stopwatch at precisely the same time as the heater is not necessary as the thermal image time stamp is used as the governing time signature.
4. The user may then leave the heater in place (turned on), and proceed to the measurement location on the outside of the slip-joint to record thermal measurements. Images may begin to be taken of the measurement region as soon as possible (preferably within 30s of starting heating). The stopwatch may be utilised to time the taking of images to approximately 5 second intervals. This time interval is to reduce the total number of images, which extends camera battery life and lowers data storage/transfer requirements.
5. After 150s of heating the test engineer should take one last thermal image and then proceed to turn off and remove the induction coil from the slip-joint.
6. The coil should be allowed to cool to within 2°C of its starting temperature (~10 minutes) before moving to the next location and beginning from step one. Based on infrared spot measurements the induction coil heats by ~30°C during measurement, therefore cooling within 2°C of its starting temperature allows a 6.7% deviation between the first and subsequent measurements. Considering the most significant heat transfer between the induction coil and the slip-joint is through joule heating this variation is negligible.

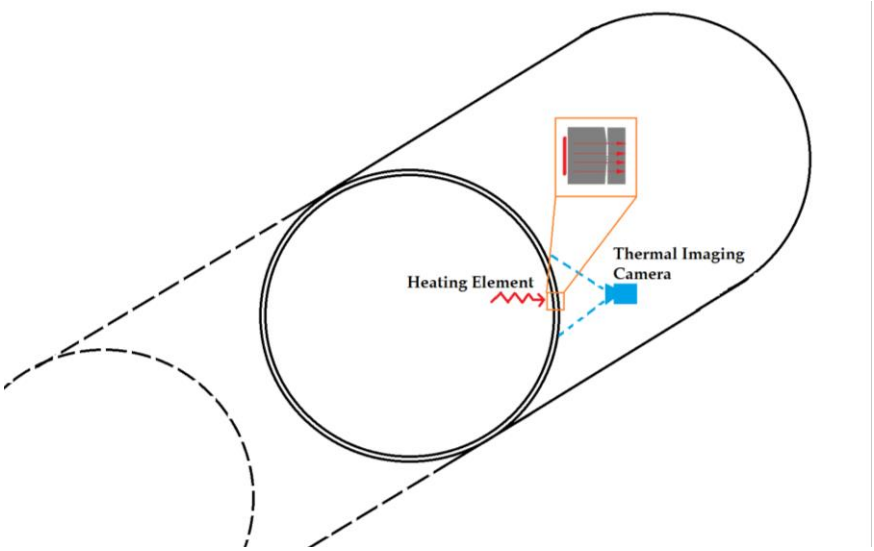

Figure 22 - Measurement set-up

3.3 Measurement Locations

3.3.1 Initial Measurement Locations

The initial two-ply measurements were conducted in two 'rings' around the slip joint, shown in red in Figure 23. Based on the latter use of 9 rings to cover the entire slip-joint, the left-hand red ring in Figure 23 is named ring 2 and the right-hand red ring is named ring 8. Considering the joint in Figure 23 is lying horizontal, the solid black ring to the left of ring 2 indicates the bottom of the outer cone of the joint, while the dotted line to the right of ring 8 is the top of the inner cone. Therefore, the left hand side of Figure 23 may be referred to as the bottom of the slip-joint and the right-hand side as the top.

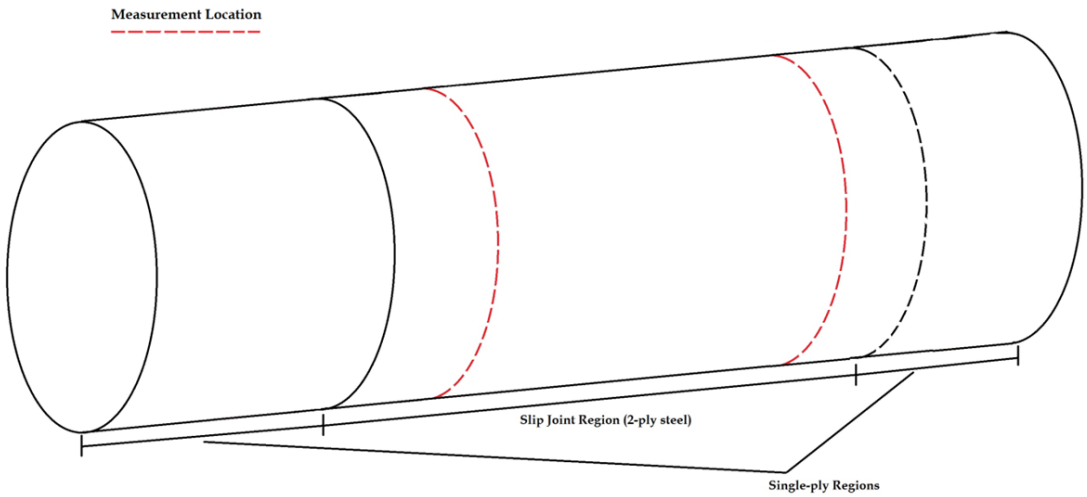

Figure 23 - Measurement Locations

Each ring consists of 23 evenly spaced points around the circumference of the joint, as shown in Figure 24. Figure 24 depicts only the two-ply region of Figure 23, oriented such that the bottom of the slip-joint is along the x axis. Ring 2 is therefore the bottom row of points in Figure 24 and ring 8 is the top row of points. Each of these points is evenly spaced at approximately 30cm apart on the joint, although this distance varies slightly per ring due to the cone angle of the tower. The points indicated in red in Figure 24 were not measured because, at this point in the project, they were too close to the ground to access. Finally, in Figure 24 and subsequent figures point 14 is taken as the 0° mark. All point 14's are located in the 3 O'clock position when looking through the sample slip-joint from the 'top' of the joint. Looking at the joint from the same position, point numbers are ascending in a clockwise direction.

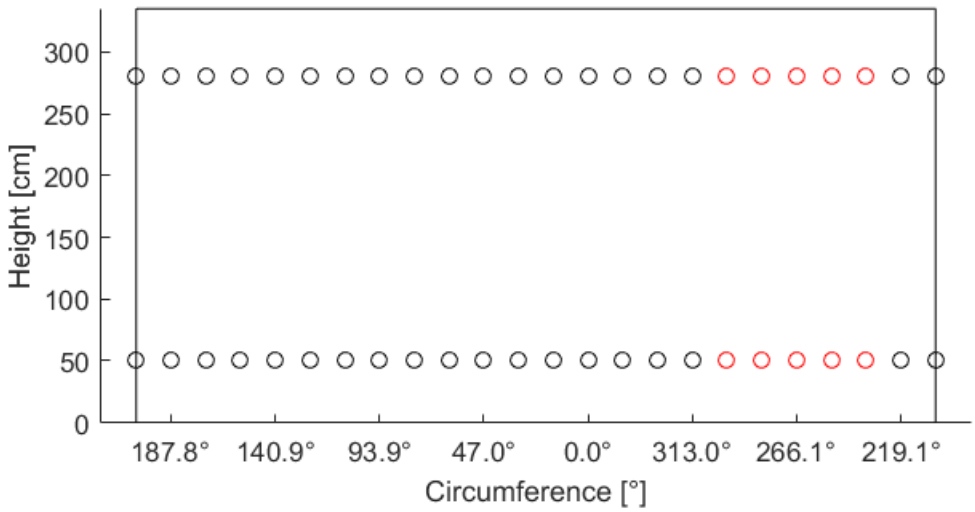

Figure 24 - Initial two-ply measurement lcoations

3.3.2 Full joint Measurement Locations

In order to measure the entire slip-joint, the two-ply region of the joint has been divided into 9 rings. The two rings from initial testing remain, while 7 additional rings of 23 points have been added. The rings are numbered 1 through 9, with 1 being the lowest ring in the joint. The points are numbered 1 through 23, with all point 1's along the left edge of Figure 25. Every point in the grid therefore has a unique 'ring point' identifier, for example, '1_12' or '4_22'. While the points in each ring are evenly distributed, the rings themselves are not evenly spaced. This may be seen in Figure 25 and was deliberately implemented to avoid physical obstacles to measurements. Despite this, six points (shown below in red) were unable to be measured due to secondary steel blocking access to the heating location.

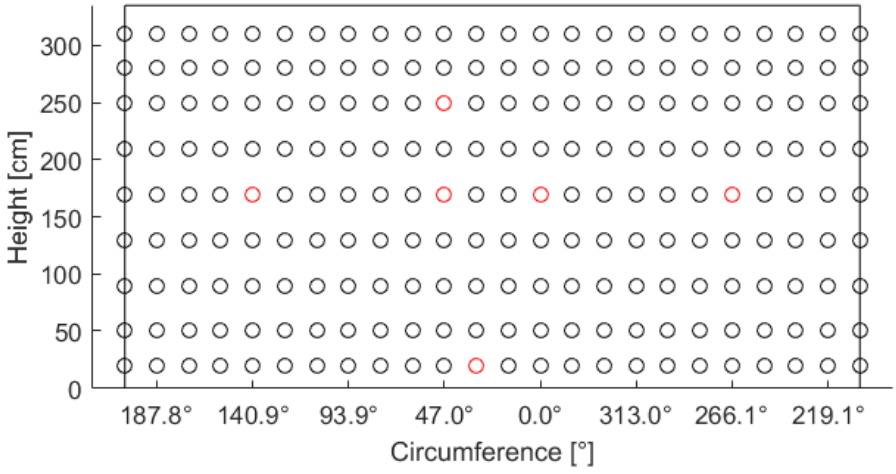

Figure 25 - Full joint measurement locations

It should be noted that the spatial density of the full joint measurement grid was determined from further initial testing which demonstrated that the low pressure regions around 240° and 350° extended several meters up the joint. Therefore, it was surmised that a ring spacing of 30-40cm

should accurately capture the low pressure regions. Clearly a higher density grid would provide more information on the boundaries of distinct low-pressure regions, however the measurement time cost must be taken into consideration.

3.4 Data Processing

Once a series of thermal images for a measurement location has been captured following the procedure in section 3.2 the images must be processed into a form that represents the thermal resistance (or conductivity) at that location. The processing is conducted in MATLAB r2015 with the aid of EXIFTOOL (a metadata analysis tool)[42], using the following process;

1. The thermal images from the measurement process are initially stored on the attached mobile phone and need to be transferred to a computer for analysis. Following this transfer the images are catalogued by measurement location.
2. Following the collation of the thermal image JPEGs, the temperature data has to be extracted from the metadata of the files. This is achieved by passing the files from MATLAB to EXIFTOOL which outputs chosen metadata fields from each thermal JPEG image to a .CSV file. The metadata includes an array of Hexadecimal values representing the irradiance values in the image which are converted to 16bit analog-digital signal values and saved as a .PNG file. Also extracted from the JPEG metadata are a number of constants required to convert the analog-digital signal values to an actual temperature. The filename of the thermal JPEG is also parsed to extract the timestamp of each image for later use.
3. The analog-digital signal counts represent a linear transform of the total collected radiation at the sensor, which is the sum of the radiation emitted from the measurement surface, radiation reflected from the surface and radiation directly from the atmosphere. In order to calculate the object temperature the latter two terms must be removed. Ignoring atmospheric radiation due to its small effect, we can say;

$$S_{measured} = \varepsilon S_{object} + (1-\varepsilon) S_{reflected}$$
$$S_{object} = \frac{S_{measured} - (1-\varepsilon) S_{reflected}}{\varepsilon}$$

Where;

$$S_{object} = Object\ A/D\ count\ [-]$$
$$S_{reflected} = Reflected\ \ A/D\ count\ [-]$$
$$S_{measured} = Total\ measured\ \ A/D\ count\ [-]$$
$$\varepsilon = Object\ emmissivity\ [-]$$

In order to convert irradiance to temperature we must first convert A/D counts to irradiance;

$$I = R_2\left(S_{object} + Offset\right)$$

Where;

$$I = Object\ irradiance\ [\frac{W}{m^3.steradian}]$$

$$R_2 = \frac{c^2}{\lambda^5} = Camera\ Constant$$

$$Offset = Camera\ Calibration\ Constant$$

Then using Planck's Law [43] ([44];

$$e^{\frac{h*c}{k*\lambda*T}} - 1 = \frac{2 * h\frac{c^2}{\lambda^5}}{I}$$

$$T(Kelvin) = \frac{h * c}{k * \lambda}\ln(\frac{2 * h\frac{c^2}{\lambda^5}}{I}) + 1$$

Where;

$$Planck's\ Constant\ (h) = 6.626x10^{-34}\ [J.s]$$

$$Boltzman's\ Constant\ (k) = 1.3807x10^{-23}[J/deg]$$

$$Speed\ of\ light\ (c) = 2.9979x10^{8}\ [m/s]$$

$$T = Object\ Temerature\ [Kelvin]$$

$$\lambda = Peak\ Spectral\ Wavelength\ (Camera\ Constant)\ [m]$$

4. Once the temperature at each pixel has been calculated using the above formulas, the resulting temperature array is saved and the same process is completed for each image in the series of thermal images for the current location.
5. From these temperature arrays the maximum temperature in any one array is extracted, representing the maximum temperature on the measurement surface at each measurement time. The maximum temperatures are then stored in a separate array along with the time of occurrence and X and Y pixel location. It has been suggested that measuring a large rectangle of the measurement surface and then 'stitching' all these thermal images together may be an effective way to measure the entire joint faster and without the need to interpolate between points. However, this method will not work because the lateral heat diffusion is uneven across the measurement surface, therefore even if pressure or gap size is even across the measurement surface, temperature results will vary. A model could be applied to the temperature results to correct for the diffusion, however the model would be quite complex (both time and space dependent), and provides an unnecessary increase in detail over spot measurements.
6. The temperature gradient in a 10pixel radius around the maximum temperature is checked to confirm that the maximum temperature is not an anomaly such as a hot pixel or scratch in the measurement surface.
7. Finally, an array of maximum temperature vs time has been obtain for the measurement location the gradient of this curve is checked again for outliers using the Mean Absolute Deviation (MAD) method, with a cut-off factor of 2[45]. Following this the mean temperature gradient is estimated at the current location after eliminating outlier gradients (such as a sudden jump in temperature). In this way, locations can be compared where the starting or final temperatures differ, or if the measurement time differs per location. The mean temperature gradient of the maximum temperature at the measurement location can

be seen as an representation of the thermal conductance of the slip joint at that location, as the temperature rise in a body is linearly proportional to the heat input.

8. Once the mean temperature gradient (°C/s) has been established at the present point, the measurement process can be applied to all other necessary points. The temperatures in between then must be interpolated using any selected method.

3.4.1 Additional Notes

There are a number of additional considerations and assumptions with regard to this measurement process which are outlined below;

- Temperature data obtained using the aforementioned equations has been compared to temperature data in FLIR proprietary software and found to match within 0.01°C. This validates the assumption that atmospheric radiation can be ignored (as it is included in FLIR software calculations).
- It has been suggested that 'stitching' all the thermal images of various locations together may be an effective way to measure the entire joint faster and without the need to interpolate between points. However, this method is not suitable because the lateral heat diffusion is uneven across the measurement surface (within each thermal image). Therefore even if pressure or gap size is even across the measurement surface, temperature results will vary due to diffusion. A model could be applied to the temperature results to correct for the diffusion, however the model would be quite complex (both time and space dependent), and provides an unnecessary increase in detail over spot measurements.
- Due to the technique of drawing the hottest point from each thermal image, the location of the hottest pixel may change over time with respect to the physical measurement surface. Some shifting of the hottest point is expected, due to uneven heating, camera insensitivity and movement of the camera between photos, therefore if (alternatively) the temperature of a single pixel was tracked, significant errors would be introduced.
- Furthermore, taking the temperature gradient of the hottest point over time allows thermal images to be taken at less precise time intervals, because individual thermal images are then not compared between locations.

The measurement process is summarised in Figure 26.

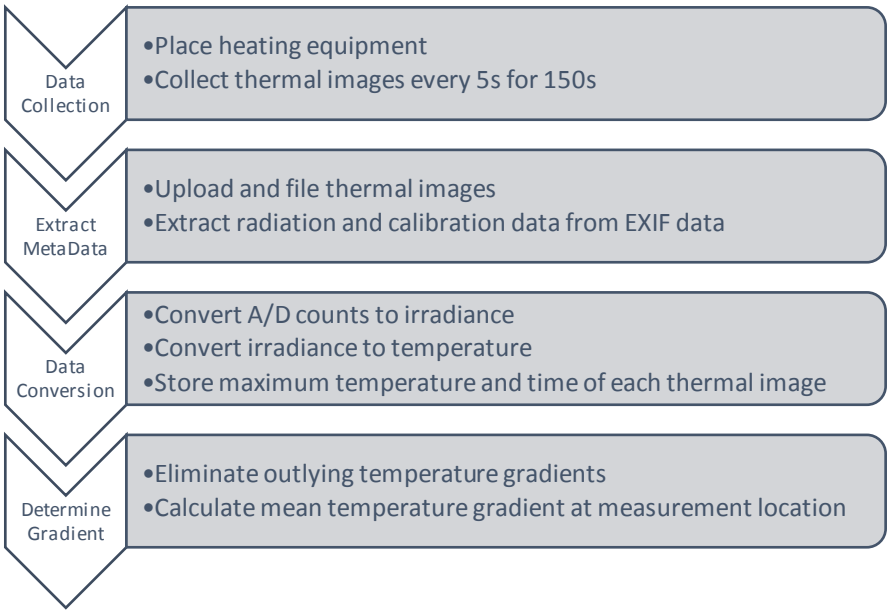

Figure 26 - Measurement process summary

3.5 Experimental Process Overview

The preceding sections describe the measurement technique for an individual location and the two-ply locations to be measured; however such measurements are part of an overarching experimental process involving many different measurements. Figure 27 shows the full overview of the experimental components of the project, including validation, preliminary and final full-scale measurements.

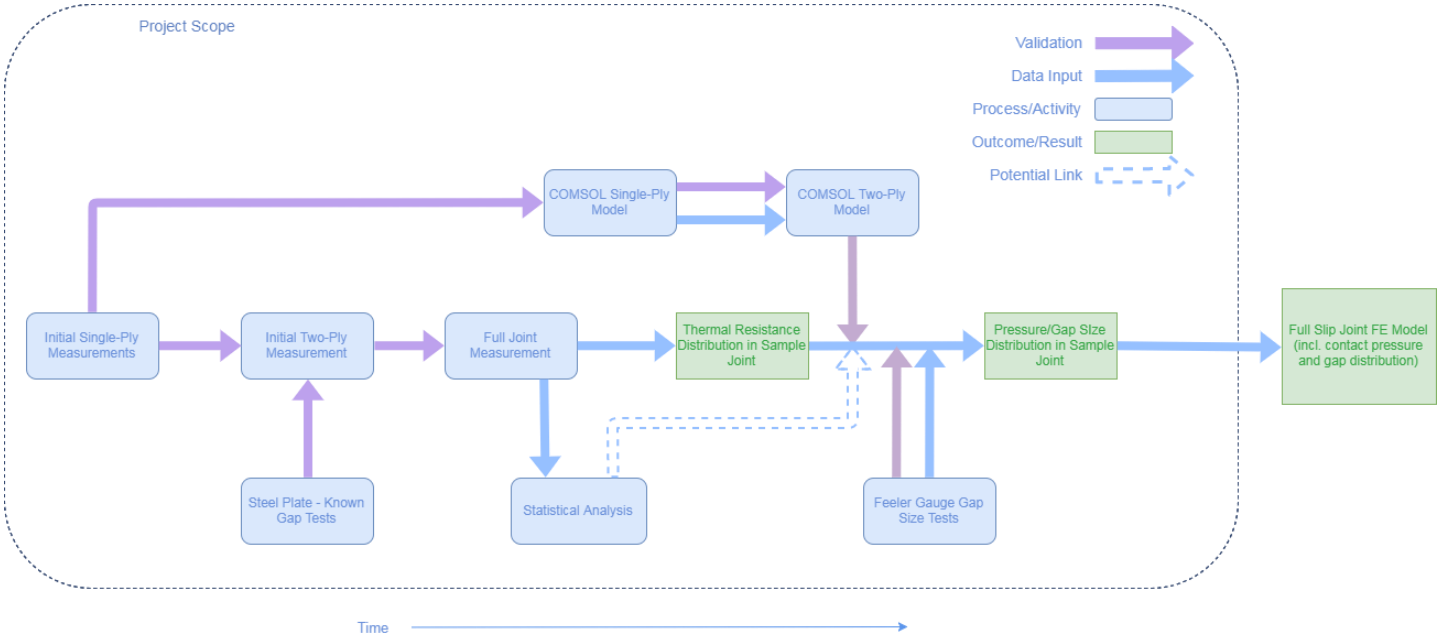

Figure 27 - Project experimental overview

3.5.1 Experimental Aims

A full description of all test procedures, including goals and conclusions is provided in the subsequent two chapters, however for clarity, a small description and the initial experimental aims are given below.

3.5.1.1 Single-Ply Testing

As noted previously, the sections at the top and bottom of the slip-joint are single-layer (non-overlapping. Measurements to various points in this region aim to provide the following information;

- An estimate of the variation in measurement values by location. The variation in material properties across the single-ply regions should be minimal; therefore variation in measurement values is a good estimate of the precision of the method.
- An estimate of the maximum possible heating time, while keeping the temperature under 150°C (to avoid paint damage).
- Determine the rate of heat diffusion within the slip-joint (to determine how much heat will 'spread' to adjacent measurement points).
- Provide an initial idea of measurement sensitivity, by analysing the ability to resolve 12mm vs 15mm single ply regions.

3.5.1.2 Small-scale Experiment

The heating process has been replicated in small-scale with two 8x100x500mm steel plates, separated by a known thickness. This experiment has the following aims;

- Establish the nature of the correlation between gap size and heat transfer (ie. correlation strength, function type).
- Determine how large of an air gap the measurement method can feasibly detect
- Determine how sensitive the measurement method is to changes in gap size, specifically when the gap size is near zero.
- Determine approximately how long the joint must be heated in order to resolve large gap sizes (ie. points with maximum thermal resistance).

3.5.1.3 COMSOL Finite Element Modelling

A simplified finite element of the slip-joint walls has been made in COMSOL multiphysics software to simulate the heating process. A single plate model is used to calibrate the finite element induction heater, before a second plate is introduced and different contact pressures/gaps are investigated. The aims of this process are;

- Investigate and confirm the correlation between contact pressure and heat transfer/temperature gradient
- Investigate and confirm the correlation between gap size and heat transfer/temperature gradient

3.5.1.4 Initial Two-ply Testing

Initial two-ply testing was limited to two rings around the slip-joint to gather preliminary information. These measurements aim to provide the following information;

- An estimate of the speed of the measurement process including setup and measurement.
- An idea of practical constraints such as, how to most effectively mount the heating coil and accessibility issues with the highest and lowest regions of the joint.
- Provide initial information on the degree of pressure/gap size variation within the joint and therefore the expected variation in temperature results.
- Provide a basis for comparison with later measurements (to establish measurement precision)

3.5.1.5 Full-Scale Testing

Full scale testing refers to the testing of all 207 grid points (9 rings x 23 points) marked out across the overlapping region of the slip-joint. These measurements (shown in Figure 25) form the primary source of information about the pressure/contact distribution in the sample slip-joint and are a strong indicator of the efficacy of the method. The experimental aims are as follows;

- Determine the thermal resistance/conductance of points across the entire slip-joint
- Therefore, provide information on the pressure/gap size distribution within the joint
- Provide information about the precision and accuracy of the method (based on comparison with other measurements)

3.5.1.6 Feeler Gauge Testing

Feeler gauge testing involves the use of thin metal strips of known thickness to check the actual gap size at various points on the slip-joint. In order to access the gap between plates, 12 holes were drilled through the joint at selected locations. Feeler gauge testing has the following aims;

- Determine the error in thermal measurements
- Determine a quantitative correlation between thermal measurements and gap size
- From the above correlation, identify the percentage of the joint in contact and the potential uncertainty in this value.

4 Verification and Validation

4.1 (Small-Scale) Plate Measurements

4.1.1 Purpose and Setup

One difficulty in validating the slip-joint measurement process is in confirming that a measureable relationship between heat-transfer and gap size exists not only in theory. To this end two sample steel plates of 8mm in thickness were used to simulate the walls of the slip joint, with feeler gauge plates of known thickness used to separate the plates. The simplified nature of this test allows several unknown variables to be eliminated, such as variation in material thickness (across different locations in the slip-joint) and variation in paint thickness (because the sample plates are not painted). Given the simplicity, this test may be used to accurately compare heat transfer rate to a known gap sizes. It may also be used to provide additional information on the expected temperature in the joint during heating, so that damage to the slip joint paint may be avoided.

The experimental setup can be seen in Figure 28, with the plates arranged in a vertical orientation. The plates themselves are mild steel of 8x100x500mm and are clamped together 50mm in from each end, leaving 400mm free space for heating. The plates were separated by feeler gauge plates of known thickness placed in the clamped region near the top and bottom of the two steel plates. The feeler gauge plates are cut in a 'U' shape, which means that they provide separation along the top/bottom edge of the steel plates and running 10cm along the sides of the steel plates. This shape of the feeler plates means that the feeler plates are as far away as possible from the heating zone and conduction through the feeler plate rather than across the air gap can be kept to a minimum. The heat is applied to the plate by the same induction heating coil used to heat the slip-joint, which was attached to the steel plates with tape (as it was not magnetised at this point). The induction coil was separated from the plates by wooden spacer blocks at the top and bottom to avoid direct contact between the coil and the surface. Finally, the temperature of the measurement surface was measured with a thermal camera to assess the heat transmission across the joint.

Figure 28 - Test plate set-up with induction coil attached

4.1.2 Results

The heat transfer across the joint was assessed for six different gap sizes; 0mm, 0.05mm, 0.2mm, 0.4mm, 0.7mm and 1mm. The temperature recorded at 30 second intervals at the hottest point on the measurement surface is shown in Figure 29. This figure shows a slightly convex heating profile, which is expected in plates with an air gap, as confirmed in section 4.3. This plot also indicates a temperature rise of more than 15 degrees in the measurement region when the plates were separated by a 1mm gap. This gives confidence that applying a similar amount of heat for a similar duration will allow large gap sizes in the slip-joint to be resolved. While the sample steel plates are thinner than in the slip joint, at 1mm gap size, the conductive resistance of the air gap is over 100 times greater than the steel; therefore an increase in steel thickness is not particularly consequential to the overall thermal resistance (and heat transfer).

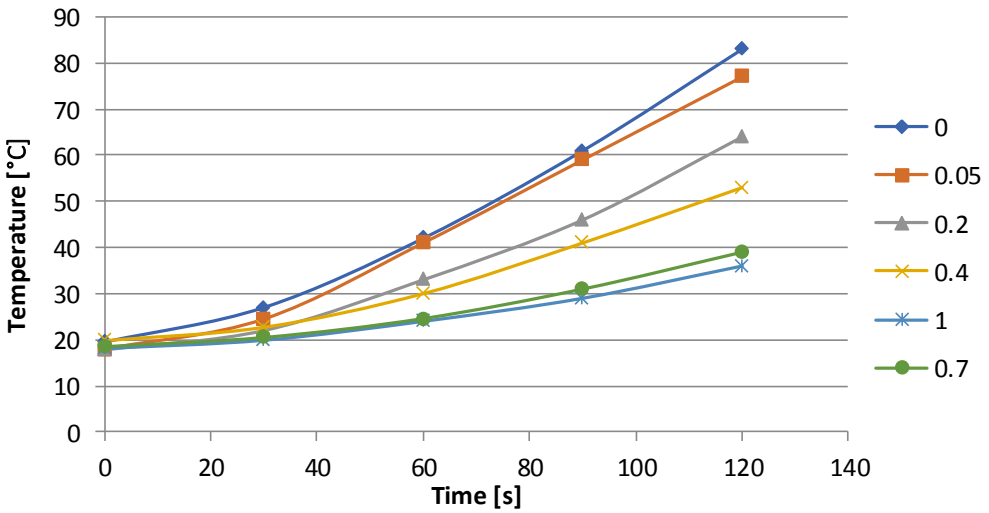

Figure 29 - Temperature vs time for varying plate separation

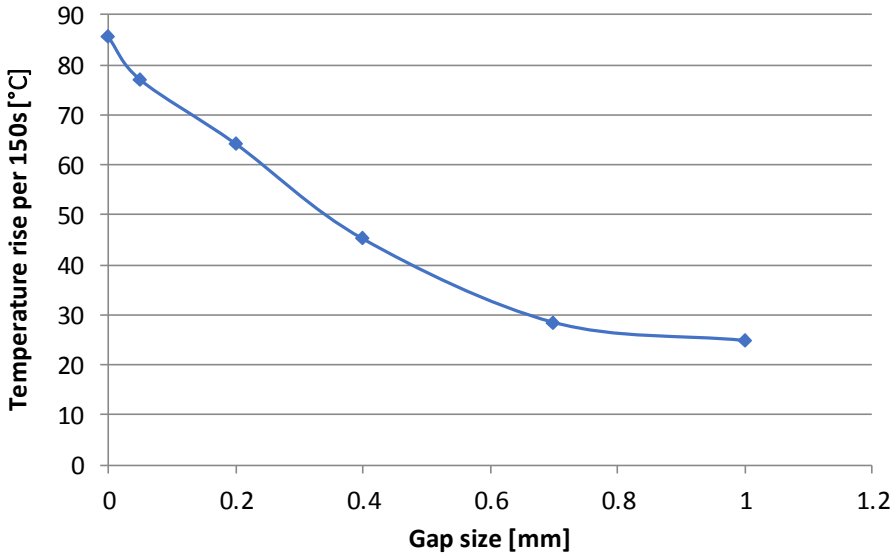

Figure 30 - Heat transfer vs gap size, for test plates

Figure 30 shows a plot of the temperature rise on the measurement surface vs known gap size. The temperature rise is taken from a projected 150s measurement period to allow better comparison with the 150s measurement time for the actual slip-joint. The key take-away from this plot is that heat transfer is not linearly correlated with gap size. Instead, a known increment in gap size will have a greater effect on thermal measurements if the initial gap size is small, than if the initial gap size were large. The effect of this is that variations in gap size in the slip-joint for locations with a small gap size may be more easily resolved than variations in gap size in large gap regions. This behaviour is not in line with a simple heat conduction model of the heat transfer between plates, as conduction resistance should be linear with gap size. The shape of the curve could then be alternatively explained by a relative increase in either convection or radiation heat transfer at large gap sizes. Considering the magnitude of the gap size, Table 1 indicates that convection is likely negligible which leaves radiation heat transfer as the cause of the non-linearity. This is in line with theoretical expectations, as an increase in conductive resistance leads to less heat transfer across the air gap which in turns leads to the first place getting hotter and the second plate heat less. Since radiation is proportional to the difference between the surface temperatures to the fourth power, this change in temperature leads to a significant increase in radiation heat transfer, which is unaffected by the gap size.

4.1.3 Conclusion

This test fulfilled its gaols of providing a clear indication of the relationship between gap size and heat transfer. It is clear that at large gap sizes, radiation becomes the governing heat transfer mechanism and causes a non-linear relationship between heat transfer and gap size. This implies that the heat transfer method is less suitable to measuring areas of the slip-joint with large gaps, than smaller gaps. It also implies that the normalised results of heat transfer measurements of the slip-joint cannot be directly taken as an indication of gap size and must first be passed through a transfer function to convert heat transfer to gap size.

The second conclusion of this validation test is that the heat transfer of the slip-joint is easily determinable with a measurement time of 120s, using the current heater setup, even with gap sizes up to 1mm. While single-ply testing results can supply the maximum test time, this validation test provides evidence that differences in gap size can be identified even at very low measurement durations (<100s).

4.2 Single-Ply Measurements

4.2.1 Purpose and Setup

The slip-joint sample used for measurements has regions above and below the 'overlap region' where the turbine tower consists of a single layer of steel and is therefore termed as a 'single-ply' region (whereas the overlapping region is termed 'two-ply'). In the single-ply region below the slip-joint the wall thickness is 15mm, while in the region above the slip-joint the wall thickness is 12mm. Measuring these regions allows errors in the heating method to be estimated by carrying out 'control' measurements on the two single-ply regions. When the second layer of the slip-joint is eliminated from the measurement, several unknown variables can be ignored, such as the gap size/contact pressure. Figure 31 below illustrates this simplification, and demonstrates that the primary variables contributing to the temperature at T2 (in the single-ply case) are; convection and radiation cooling at T2, conduction heat transfer rate through the steel and radiation heat losses at the source side (T1). If many single-ply measurements are taken under similar conditions then the variability of the temperature at T2 can provide some information about the variability of the aforementioned contributing factors.

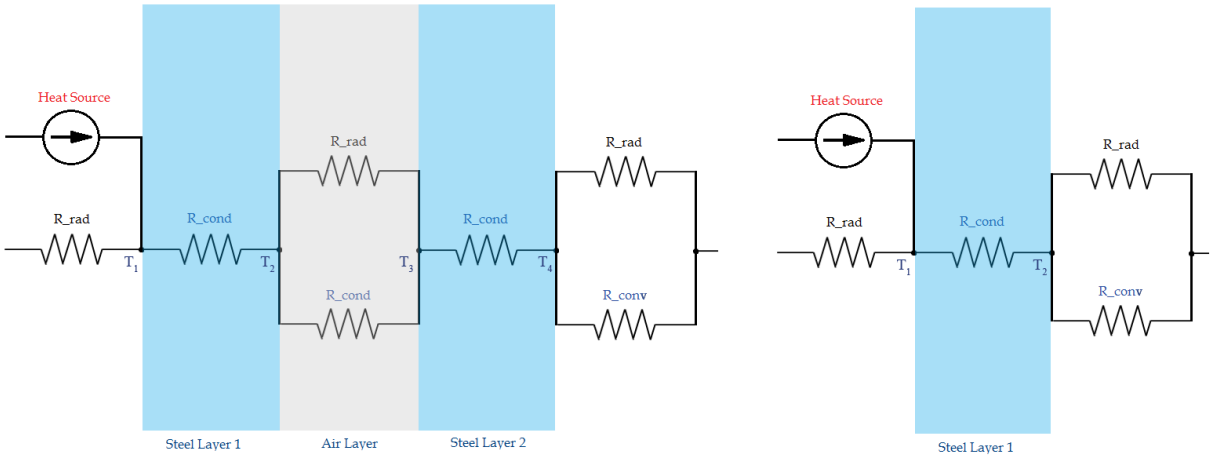

Figure 31 - (Left) Thermal resistance diagram for two-ply regions. (Right) Thermal resistance diagram for single-ply regions.

If many measurements are taken and the temperature is measured directly at T2 with a thermal camera, then variations in the temperature at T2 may be primarily attributed to variations in the heat source and conduction resistance in the steel. The conduction resistance in the steel plate is a function of the thermal conductivity of the steel and the thickness of the steel, therefore variation in T2 may indicate variation in one of these properties. These properties cannot be measured directly in order to quantify individual uncertainty values for every property; however the single ply

measurements provide a good estimate of the group variation of these properties and their expected variation in two-ply tests.

With this in mind, 26 single-ply locations were tested, 11 of which were in the 15mm region and 15 of which were on 12mm steel. One location from both the 12mm and 15mm regions were re-tested to provide some information about the consistency of the heating method. Ideally, a single spot would be re-tested many times under a large range of conditions to give the most information about the reliability of the heating method, as measuring a single spot allows the assumption of consistent plate thickness and plate thermal conductivity between measurements. Another benefit of multiple measurements in the same spot is that the deduced variation in the heat source can be subtracted from general variation across all single-ply tests to reveal the variation in results due to other factors, such as steel or paint thickness. However, given time constraints, after a limited number of initial single-ply measurements, alternative validation techniques were pursued instead. Following the completion of the measurements on the two-ply region the heating equipment malfunctioned, eliminating the possibility of further single ply measurements.

4.2.2 Results

The results of single-ply tests are presented in Figure 32, showing the heating rates in both 12mm and 15mm regions. This graph presents the mean gradient of the temperature vs time at point T2 (as per Figure 12). The starting temperature for all points is located at 12°C to facilitate easier visual comparison.

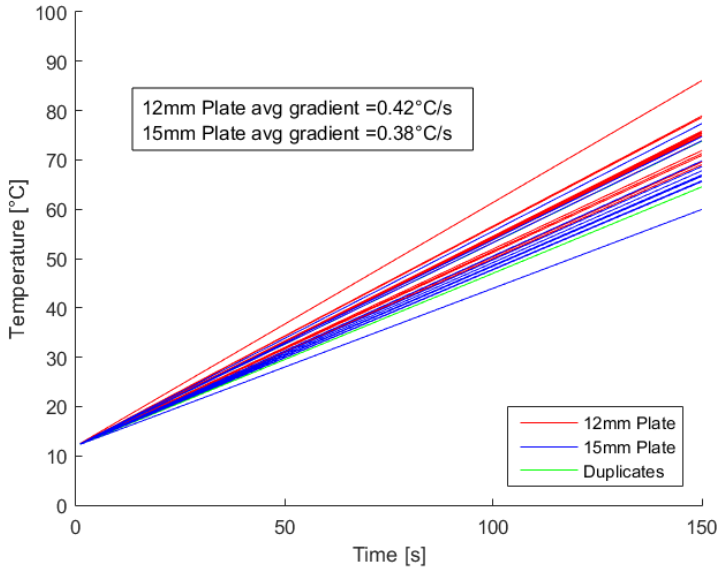

Figure 32 - Linearised single-ply measurement results

From these results it is evident that there is significant variation in either the heating source or the material properties between these measurements. The mean heating rate in the 12mm plate is 0.42°C/s with a standard deviation of 0.033°C/s. The mean heating rate in the 15mm plate is 0.38°C/s with a standard deviation of 0.029°C/s. This makes the 90% confidence interval for the 12mm plate [0.366,0.474]°C/s. Comparatively, the 90% confidence interval for the 15mm plate is [0.333 0.427]°C/s. For clarity, during a 150s measurement period, this translates to a ΔT of [54.90 - 71.10]°C for the 12mm plate and [49.95 - 64.05]°C for the 15mm plate. It is evident that there is

significant variation in these values, in the order of ±13% (at 90% C.I.) for the 12mm plate. Note that the above estimation assumes that the data is normally distributed, which is a reasonable assumption for data with a random error component.

In the absence of further information about the single-ply distribution it must be assumed that the measurements in the two-ply region share the same variability present in the single-ply region. Analysis of the 12mm and 15mm duplicate measurements shows variations of 3.87% and 6.20% respectively indicating that a sizeable portion of the variation in the single-ply measurements may be caused by variation in the heat source rather than the steel conductance or thickness. However, like with the single-ply measurements themselves, the sample size is too small to draw firm conclusions.

Single-ply measurements also provide qualitative information about the heating time scale limitations for two-ply measurements. As seen in the previous section, measurement times above 100s provide enough heat to easily cross large gaps and identify variations in gap size. However, single-ply measurements indicate that measurement times should be kept below 180s to avoid damaging any paint (at 150°C). This time length provides a significant safety margin to allow for delays in turning off the heater, natural variation in heat transfer across the joint or lower quality in the paint.

Finally, these results confirm that heating is quite localised, which allows local heat transfer to be measured without unintentionally heating the entire slip-joint. This can be seen in Figure 33a, where the photo area is roughly 30cm wide (shown by the markings every 5cm across the centre of the image). Figure 33b shows the evolution of temperature in a line across the middle of the measurement region over time. In this way, each contour on the plot shows the temperature across the middle of the measurement region at a different point in time. This shows quantitatively that even after ~150s of heating, there is minimal heat diffusion within the plate, with only a ~5°C temperature rise at 15cm from the measurement centre after 150s. Therefore, measuring adjacent points (~30cm apart) successively will likely have no 'cross-contamination' effects. If care is taken to plan out the order of measurements to avoid successive measurements closer than 60cm then cross-contamination can certainly be neglected.

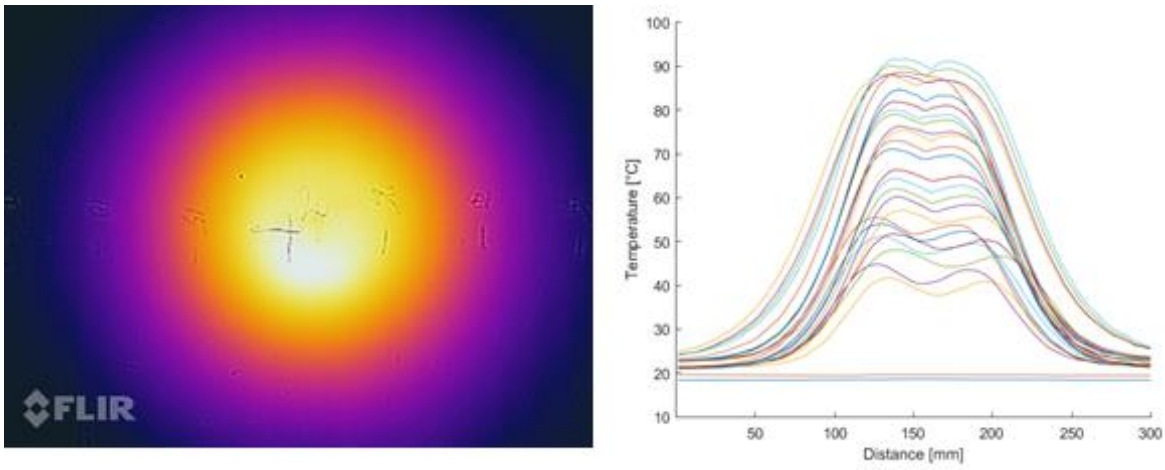

Figure 33 - Spatial temperature profile. (a) Typical thermal image. (b) Development of temperature profiles (across the centre of thermal image) over time

Another important aspect of the singe-ply results is the shape of the results distributions. Figure 34 shows a comparison of both 12 and 15mm plate results compared to the normal distribution. As can be seen from the plot, both sets of results are approximately linear, indicating normality in the underlying population. However the different gradients of the two data sets indicate that they have different spreads, with the 15mm results having a greater sample standard deviation. This could be due to greater variation in steel or paint thickness, greater variation in the heating/measurement set-up, or most likely, an insufficient number of sample data points. Figure 34 also indicates a significant outlier in the 12mm data set, for which the underlying data has been inspected. There are no obvious abnormalities in the data, which indicates that this hot spot may be a structural abnormality (causing very thin wall thickness), or a measurement defect (in heating device or thermal camera).

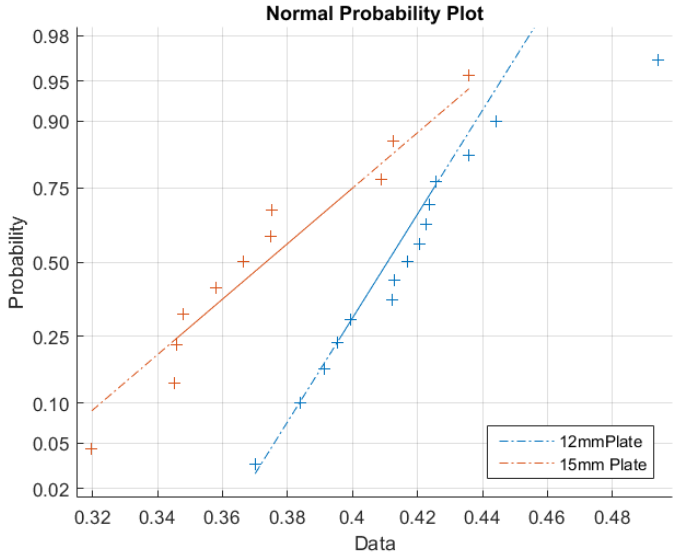

Figure 34 - QQ plot of 12mm and 15mm plate thermal measurements

4.2.3 Conclusion

There are several key inputs drawn from single-ply testing, both in terms of method validation and in providing input for two-ply measurement parameters. Firstly, it is clear the method can distinguish between 12mm and 15mm plates, which, while expected given the results of small plate measurements, reaffirms the sensitivity of the method. The change in thermal resistance between a 12mm and 15mm plate is roughly equivalent to difference in thermal resistance between two air gaps varying by less than $1/100^{th}$ of a millimetre. While this is based solely on conduction heat transfer, at low gap sizes radiation heat transfer is negligible, so this gives an idea of the sensitivity of the method at very small gap sizes.

The sensitivity of the method must be considered in conjunction with the precision of the method to gain a full understanding of the expected measurement error. Analysis of the variation in single-ply measurements shows that the precision of the measurement method is approximately ±13%. This assumes that there is minimal location based variation in the single-ply measurements and that the variation in the measurements is entirely measurement imprecision.

Thirdly, single-ply tests provide a good upper limit for testing time to avoid damaging the paint on the slip-joint. A maximum time of 180s would keep the joint surface temperature below 150°C, with ample safety margin for turning the heater off and any locational variation in temperature. The exact maximum test time cannot be evaluated directly because of unknown thermal conductivity of the paint layers and locational variation in the paint and steel properties. Therefore using a large safety margin with an estimated maximum heating time is the best approach.

Finally, single-ply measurements give strong evidence that successive measurements at adjacent points will not contaminate each other through diffusive heat transfer. The temperature increase from the measurement method is largely limited to within a 15cm radius from the measurement point. This could likely be reduced by using a more tightly would coil with a smaller radius, although if measurement points are carefully selected to avoid adjacent, subsequent measurements then this issue can safely be neglected.

4.3 Finite Element Models

4.3.1 Purpose and Setup

The heating process has been simulated using a finite element (FE) COMSOL model for both single-ply and multi-ply heating cases. The purpose of the single-ply model was to calibrate the unknown heating parameters (using data from real single-ply tests) to increase the accuracy of the two-ply model. In addition the single-ply models confirmed that the heating behaviour observed in real single-ply testing was consistent with theoretical models. Following on from this, the purpose of the two-ply model was to investigate the theoretical correlation between contact pressure/gap size and heat transfer. The two-ply model was also intended to provide an indication of the sensitivity of the measurement process to variables such as material thickness, induction coil power, coil geometry and input frequency.

The model (for the single-ply case) is pictured in Figure 35, showing the 2D axisymmetric, flat-plate geometry of the model. The induction coil was modelled as seven concentric rings with a diameter of 6mm, centre-centre spacing of 9mm and centre-plate surface spacing of 6mm. Adding a layer of silicone between the coil and the plate surface was found to have little effect on temperatures, so this was not included in the final models. The steel plate was modelled using COMSOL's in-built structural steel material because the exact material properties of the steel in the sample slip-joint are unknown. The steel plate was modelled in both 12mm and 15mm thickness for the single-ply case to offer comparison with single-ply measurements, although in the two-ply case two 12mm plates were modelled. The plate is a circular disc of 0.5m radius in the centre of a cubic air-filled domain of 1m side lengths. Both the plate radius and domain size were tested for influence on the solution and found to be sufficiently large.

The meshing strategy used in both models is a hybrid mesh of triangular and quadrilateral elements. Triangular elements were used for the entire model except for the steel plate(s) and air gap between the plates in applicable models. The steel plates were modelled with quadrilateral elements to increase accuracy, allow better control of size transition and allow better control of mesh density in

key regions. Care was taken to check element aspect ratio, element size transition and ensure that at least 3 elements were present across the air gap (in the two-ply case). The number 3 was chosen with consideration that, placing a larger number of elements across the gap minimises numerical inaccuracy but requires a significant increase in total element count due to smooth transition and aspect ratio requirements.

The final model parameters were set based on comparison with real life single-ply testing. The induction coil frequency was set at 30.4kHz to match the measured frequency in the iDuctor at full power. The current in the coil was then adjusted in conduction with the coil resistance to achieve the coil voltage and heating rate measured during single-ply tests.

In setting up both the single-ply and two-ply models a number of assumptions have been made. Firstly, the geometry of the steel plate(s) has been simplified from a portion of a cylinder wall to a flat disc. This assumption allows the use of an axisymmetric model which greatly reduces simulation time. This assumption is appropriate in this case as the slip-joint diameter is very large and only a small section of the wall is being simulated, meaning that the wall section is very similar to a flat plate. Another assumption is the simplification of the model through the elimination of paint layers, material around the induction coil. Comparative models with and without these features were used to confirm the minimal impact on the solution by such features and therefore justify their exclusion.

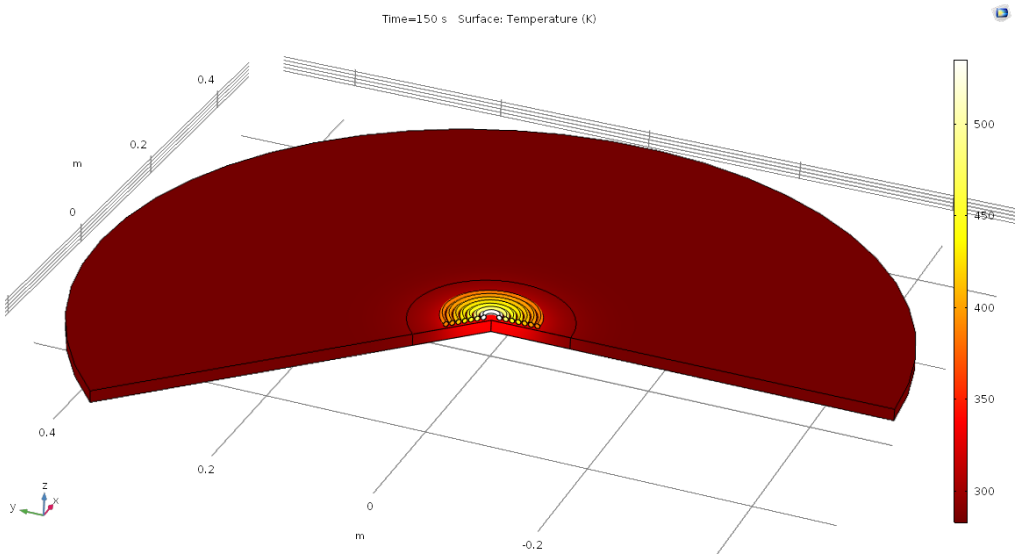

Figure 35 - Simulation of single-ply measurement using COMSOL

4.3.2 Results

Testing of varied coil geometry, coil frequency, coil current and steel properties revealed issues in mimicking the single-ply heating process with the finite element model. Specifically, if parameters were set such that the heating results in the 12mm single-ply model matched the 12mm single-ply measurement results, then the finite element model of the 15mm plate consistently under-predicted the temperatures from actual measurements. This may be attributed to difficulty in setting up the model correctly, as well as attempting to tune the model to an 'incorrect' measurement result. The reason single-ply measurements may have been inaccurate is that the

mean of all 15mm measurements was used to attempt to tune the finite element model. If the 15mm measurements were not distributed evenly about the real mean temperature, then the predicted mean temperature would not be correct. The same applies for 12mm measurement results, making it challenging to tune the heater parameters so that finite element results matched real measurements. To solve this issue, the heater parameters were tuned to match the 12mm plate results, as this is the thickness of the plates in the two-ply region. The final induction coil parameters used in two-ply simulations are presented below (as determined by single-ply simulations).

Parameter	Value	Units
Voltage	5.8	V
Current	200	A
Power	1160	W
Efficiency	97	%
Wire strands	70	-
Wire Diameter	0.1	mm
Geometry	As per section 4.3.1	-

Following single-ply modelling to parameterise the model, 4 gap sizes and 4 contact pressures were investigated in the two-ply model to investigate their correlation with measured surface temperatures (see Figure 36). Figure 36 shows the temperature at t4 after 150s of heating has been applied to the plates. The point name 't4' is consistent with Figure 12, where t4 is the name for the hottest point on the surface on the opposite side of the slip-joint to where the heat is applied (ie. the hottest point on the measurement surface). All points in Figure 36 began at 283.15K, therefore, instead of the figure presenting their final temperature, they could also be represented as a deltaT or temperature gradient over the 150s heating time (as per section 4.2). The horizontal axis of the figure is an amalgamation of contact pressure (for value less than zero) and gap size (for values greater than zero). In this way, one can see that as two plates are brought closer and closer together, the heat transfer moves along the orange plot from right to left. Then as the plates begin to touch the heat transfer begins to follows the blue line from right to left. The inverse is true if the plates are firstly clamped tightly together and then slowly separated.

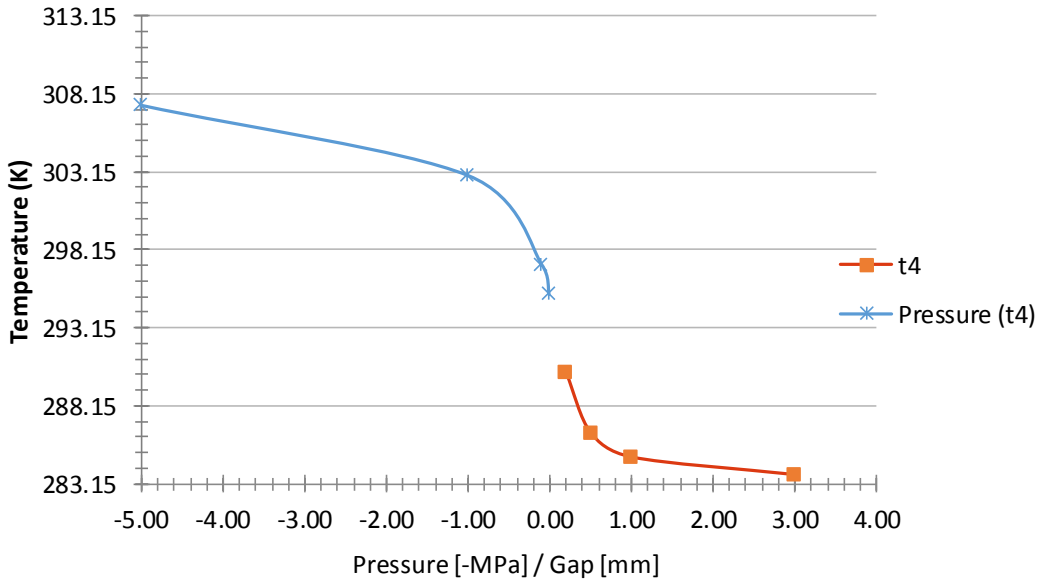

Figure 36 - Far-side temperature vs contact pressure/gap size

Figure 36 - Far-side temperature vs contact pressure/gap size shows that heat transfer has a non-linear correlation with both contact pressure and gap size. This is important as the literature covered in chapter 2 is largely focused on measuring this correlation for very thin materials, whereas this result shows that the correlation still holds for thicker plates with longer heating times and higher diffusion. The pressure correlation is particularly important as, there is currently no experimental way to measure the contact pressure in the slip-joint for comparison with thermal measurements. Therefore, if the accuracy of the measurement method is assumed to stay consistent between in-contact and non-contact regions, finite element results suggest that the thermography results can provide information on the contact pressure distribution. The lack of correlation between the exact temperature values in the FE model and real slip-joint means that an exact numerical correlation between contact pressure and thermographic measurements cannot be determined from the FE model. However, given that the model is very close to the real measurement process, the qualitative correlation may be applied to the real measurements.

A final observation, from the two-ply FE model, is that the measurement method is most sensitive in the transition region between contact and non-contact. This indicates that it may be difficult to accurately resolve regions with high pressures or large gap sizes, but also that the method should be able to clearly resolve variations around the contact transition.

4.3.3 Conclusion

From the single-ply simulations it was determined that it was not possible to create an induction heating model that matches both 12mm single-ply measurement and 15mm single-ply measurements. This may be due to difficulties in modelling the exact physics on the heating process with multiple unknown parameters, such the exact number and width of conductor strands in the induction coil, the exact working current or the exact steel properties. Alternatively, it is more probable that due to the imprecision in the measurement method, the heat conduction values estimated from the real single-ply testing were not completely accurate. Despite this discrepancy the model parameters developed to match the real 12mm single-ply measurements could be used to simulate two-ply measurements (with care).

The two-ply simulation results show that the temperature on the far side of the slip-joint wall is well correlated with contact pressure and gap size (for 12mm steel walls and heating parameters similar to the iDuctor). The inability to exactly match the FE model to real experiments means that no quantitative correlation can be developed between temperatures and either gap size or contact pressure. However, the results show that the sensitivity of the method is inversely proportional to gap size, which agrees with the small plate measurements in section 4.1. The method shows a similar correlation with contact pressure.

5 Results

5.1 Preliminary Two-Ply Measurements

After initial single-ply measurements to determine the potential variation in temperature results, it was necessary to conduct preliminary tests on the two-ply region. These tests serve a number of purposes including;

- Providing a basis for comparison with later (duplicate) measurements in the same spots,
- Determining the appropriate time scale for the heat measurements,
- Providing an initial estimate for the expected variation in results,
- Potential measurement difficulties, such as location access, measurement speed and connectivity issues,
- Providing an initial estimate of the size and shape of low/no contact regions.

The experimental setup of these tests was as per the measurement process described in chapter 3.

5.1.1 Results and Analysis

As previously noted, the initial two-ply measurements were conducted in two rings of 23 points around the top and bottom of the slip-joint. The measurements locations were chosen so as to avoid measuring adjacent points in immediate succession. The results of these measurements are shown below in a radial plot of heat transfer rate (°C/s) by location. The blue region of the plot indicates regions that have not been measured due to their proximity to the ground (due to an inability to record the temperature on the outside of the slip-joint at these locations). In these plots a larger radius indicates a greater heat transfer rate and therefore a smaller gap (or greater contact pressure). The black dotted line is plotted at a radius equal to the mean heat transfer rate to provide a reference point. Finally, the areas in between measurement points have been linearly interpolated from the adjacent points. Clearly, linear interpolation does not realistically represent the heat transfer rate function around the circumference; however without further information no other interpolation scheme would provide increased accuracy.

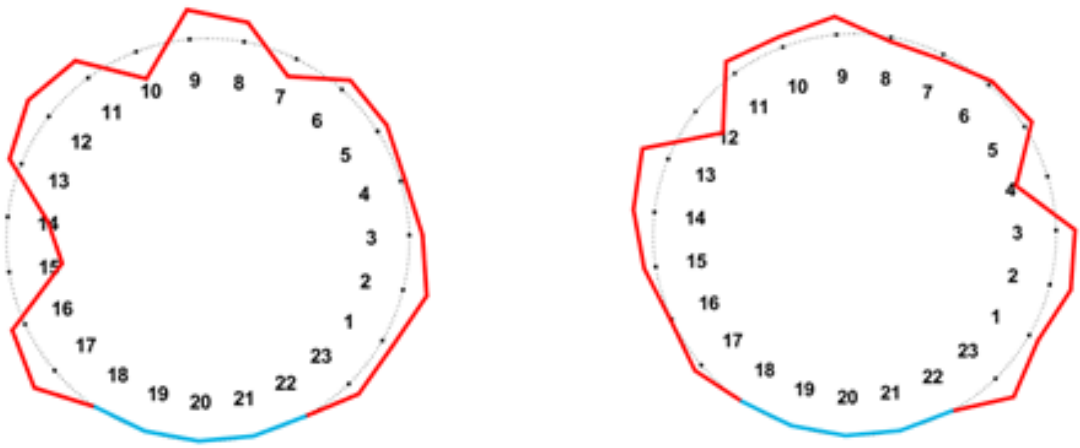

Figure 37 - Qualitative visualisation of initial two-ply measurement results. (Left) Ring 2. (Right) Ring 8.

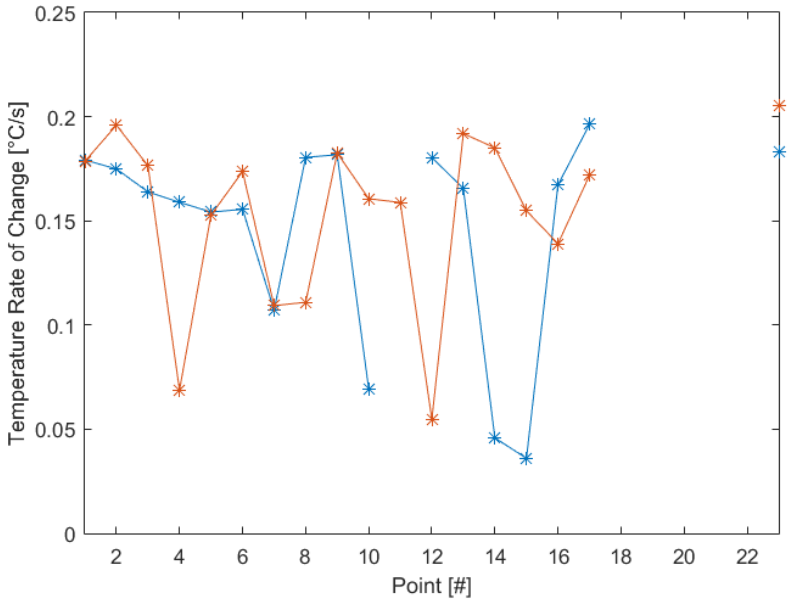

Figure 38 - Quantitative results of initial two-ply measurement results. (Blue) Ring 2. (Red) Ring 8.

From Figure 37 and Figure 38 it is clear that the same regions of low (or high) heat transfer are not always present in both rings. There are regions of high heat transfer (indicating high(er) pressure contact) around points 1-3, 5-6, 9 and 17 in both rings, although the general distribution of the measurements in both rings is mostly dissimilar. This indicates that either; the length of low-pressure (or no pressure) regions is limited to less than the length of the slip joint, or these regions are not running directly top-to-bottom in the joint.

These results also indicated the average width of 'low-pressure'/air-gapped regions in the joint (in the circumferential direction). As can be seen in both rings, such regions never extend across more than two adjacent points (such as ring 2, points 14-15) and are often only a single point (such as ring 8, point 12). This equates to a width of 0.3-1m for non-contact/low-pressure contact regions. The lower limit of 0.3m is arrived at from examination of curves such as Figure 33b, as any smaller regions would be revealed by rapid gradient changes in the plot. The upper limit is similarly derived as the maximum possible width 'defective' region, such that it would not impinge upon the

temperature curve of adjacent measurement points (which would otherwise create a non-symmetric temperature profile at those points).

It is of further interest to examine the spread of the initial two-ply measurements, which is presented in Figure 39. From this plot we can see that the data as a whole is likely not normally distributed (as the single-ply data is). This is likely due to the fact that the dataset is composed of two significantly different regimes (one in which contact occurs and one in which there is a gap). Additionally, we know from section 2.3 that heat transfer does not vary linearly with contact pressure. Similarly, while heat transfer varies pseudo-linearly with gap size, the variation is much more significant than that due to small variations in contact pressure. This can be seen in the variation in gradient between the left half (assumed no contact) and right half (assumed contact) of the plot below.

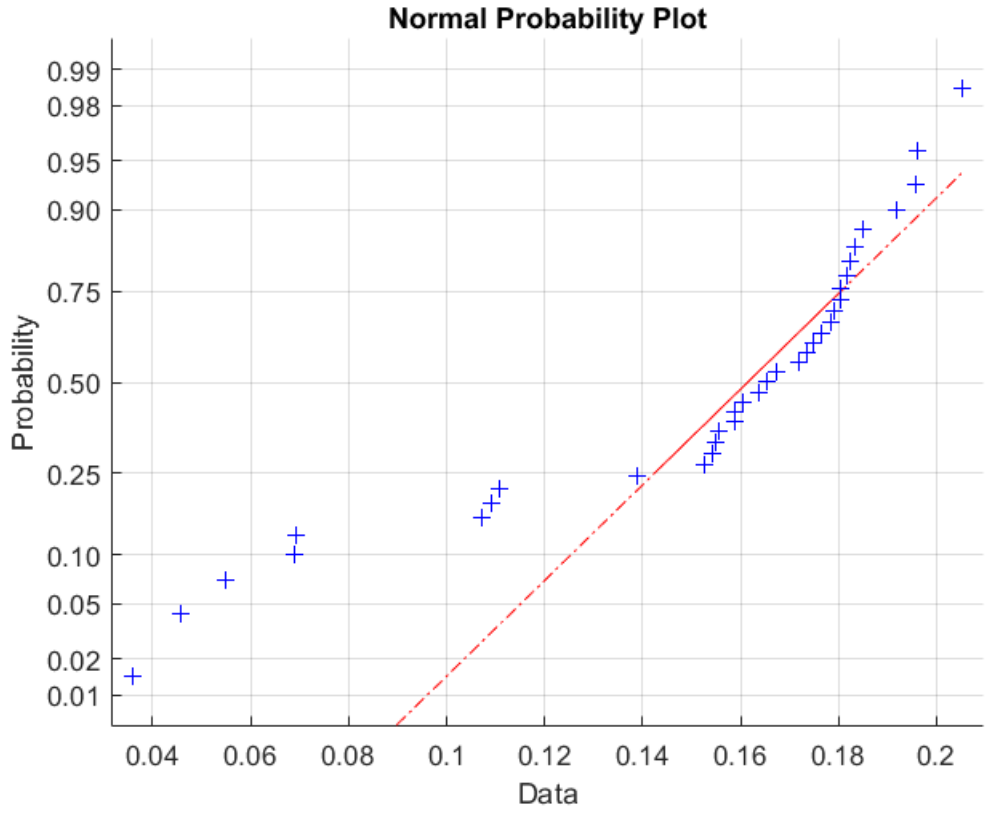

Figure 39 - QQ plot of initial two-ply measurements

5.1.2 Measurement Process-related Results

As previously stated, the initial two-ply measurements provided information on a number of measurement process-related factors. Firstly, it is necessary to determine the minimum amount of time required to achieve a measureable temperature rise at all points. This is necessary, as if the measurement (and heating) time is too short, then the low temperature rise in the measurement region will produce a low signal/noise ratio. Furthermore, if the temperature rise is too small the thermal camera may not be able to measure it at all, resulting in an inability to differentiate the heat transfer rates in areas with low heat transfer. Considering this, the results indicate that the minimum rate of temperature increase may be as low as 0.02°C/s (1.2°C/min), which would necessitate a

heating time of at least 2mins to ensure a clearly distinguishable temperature rise. This may be increase to 150s to ensure that even the regions with the largest gap between plates are measureable. On the other hand, the maximum heating time (to avoid damaging paint) must be derived from the earlier single plate measurements, as the greatest temperature is located at the surface closest to the heat source.

Further advantages of an initial testing run include the ability to identify and correct measurement issues to minimise errors in future measurements. For example, it was noted early on that the thermal camera could be set to manual calibration mode to avoid any re-calibration during measurements. Additionally, the frame for the heater element was magnetised to allow simpler, rapid placement and reshaped to smaller dimensions to minimise physical obstructions. Despite the change in size, obstructions within the slip-joint still prevented measurements at five locations (format: 'ring number'_'point number'); 1_13, 5_11, 5_14, 5_20 and 7_14. These locations are shown in red in subsequent plots.

5.1.3 Conclusion

Initial two-ply measurements show a wide range of thermal conductance, indicating significant variations in contact pressure and gap size within the sample joint. Low pressure regions are no more than 90cm in width (along the circumference), and do not extend the whole length of the slip-joint (from one ring to another). In more practical terms, at least 120s of heating will be required to heat regions with a large gap size and some points of the slip-joint may not be measured due to secondary steel obstructing the heater location. To increase measurement speed, ease of operation and accuracy, the full measurement grid should be drawn out on the joint prior to any measurements. Additionally, the heating coil should be placed in a frame to control its distance to the slip-joint wall and allow hands free operation. Finally, the slip joint must be raised onto support blocks and scaffolding erected to allow measurement access to the highest and lowest points on the joint.

5.2 Full Joint Measurements

5.2.1 Results and Analysis

As outlined previously, measurement of the full slip-joint was undertaken after preliminary measurements of single-ply and two-ply regions. The full slip joint region is divided into 9 rings of 23 points, with a grid spacing of 0.3-0.4m (see section 3.3.2 for full diagram). As mentioned in the previous section there were six points not measured due to physical obstructions. The remaining 201 points were measured over a three day period with an ambient temperature of 8-12°C. This small change in ambient temperature is negated by calibration of the thermal camera, the (relatively) large magnitude of joint heating during testing and the gradient-based heat transfer analysis.

Utilising the results processing method described in section 3, the heat transfer of the entire slip joint is presented in Figure 40. The real data points are located at the black circles on the plot and

indicate the temperature gradient of the slip-joint outer surface during the measurement period. As previously detailed in section 2 and 3, an increased temperature gradient is due to higher heat transfer through the slip joint which is related to the variation in pressure (and air gap size) over the slip-joint. From visual inspection, it is known that there is a gap in at least some areas of the joint, therefore it may be said that in Figure 40, the darkest blue regions indicate areas with the largest gap and the brightest yellow regions are areas with the highest contact pressure.

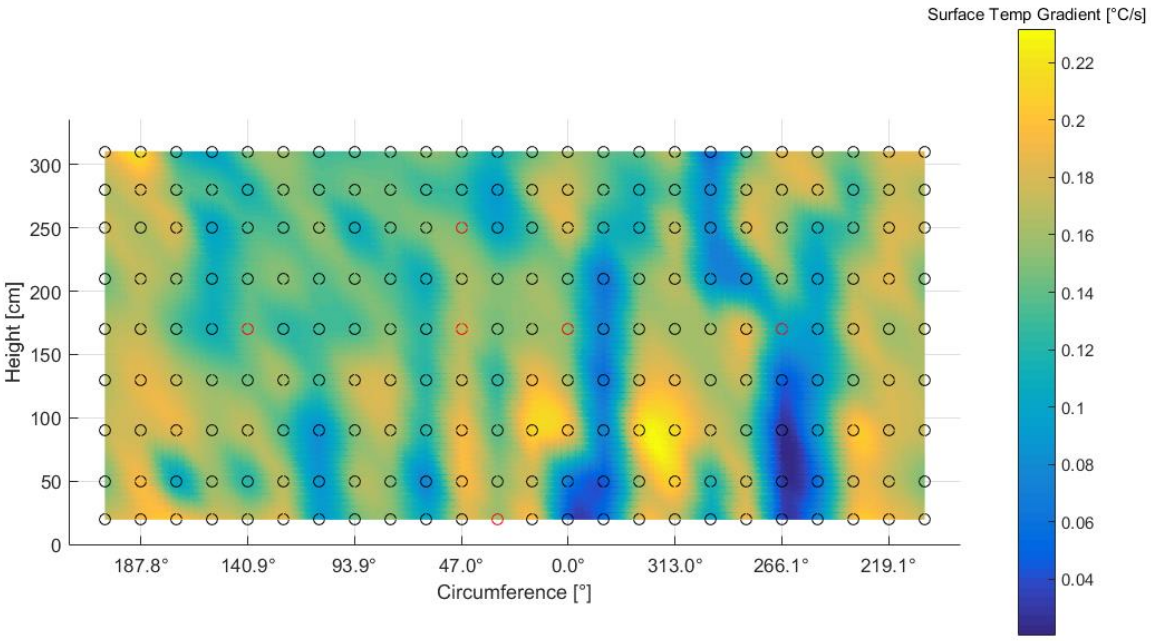

Figure 40 - Temperature gradient (thermal conductance) results for full slip-joint

Figure 40 has been made using cubic interpolation between the collected data set, with missing points in the data set manually esitmated. As noted in section 3 the slip-joint is 3.33m in height however the above plot only covers from 0.2m-3.1m of the joint. This is because measurements too close to the edge of the joint will suffer from overheating, as heat will not be able to diffuse within the joint as effectively. On the vertical edges of the plot there are no such issues with discontinuities as the physical measurement surface is continuous. In order to present the full measurement region the points on the far right edge have been replicated on the far left edge. Given the cylindrical nature of the joint, the measurement points on the right and left edges of the plot are (accurately) coincident with each other.

The shape of the contact distribution is discussed in chapter 6, however the are a few initial values to note from the plot above. Firstly, the point of highest heat transfer in the sample slip-joint was at (313°, 90cm) with a value of 0.232°C/s. The point of lowest heat transfer was at (266.1°C, 50cm) with a value of 0.024°C/s. Over 150s this translates to temperature increases of 34.8°C and 3.6°C respectively. Clearly this variation far exceeds the quoted precision of the thermal camera (5%), therefore it is highly likely that the variationin results is (at least partially) due to variations in the joint. This is also supported by the non-random nature of the results (ie. the formation of coherent low-pressure regions), although this will be discussed further in chapter 6. The results are presented in cyclindrical view in Figure 41 for clarity.

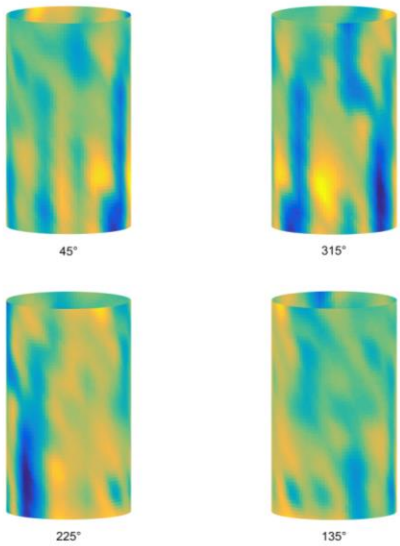

Figure 41 - 3D Representation of Slip-joint Measurement Results

5.2.1.1 Comparison with Initial Two-Ply Measurements

Comparison of the final joint measurements with initial two-ply measurements provides an idea of the error margin of the method itself. This is because it eliminates uncertainty caused by factors that may vary across the slip joint such as steel or paint thickness. As noted previously, the initial two-ply tests covered rings 2 and 8, located approximately 0.5m and 2.8m along the joint, although they did not include points between 18 and 22. The measurement results obtained from these tests, as compared to the latter full joint measurements are shown in Figure 42 below.

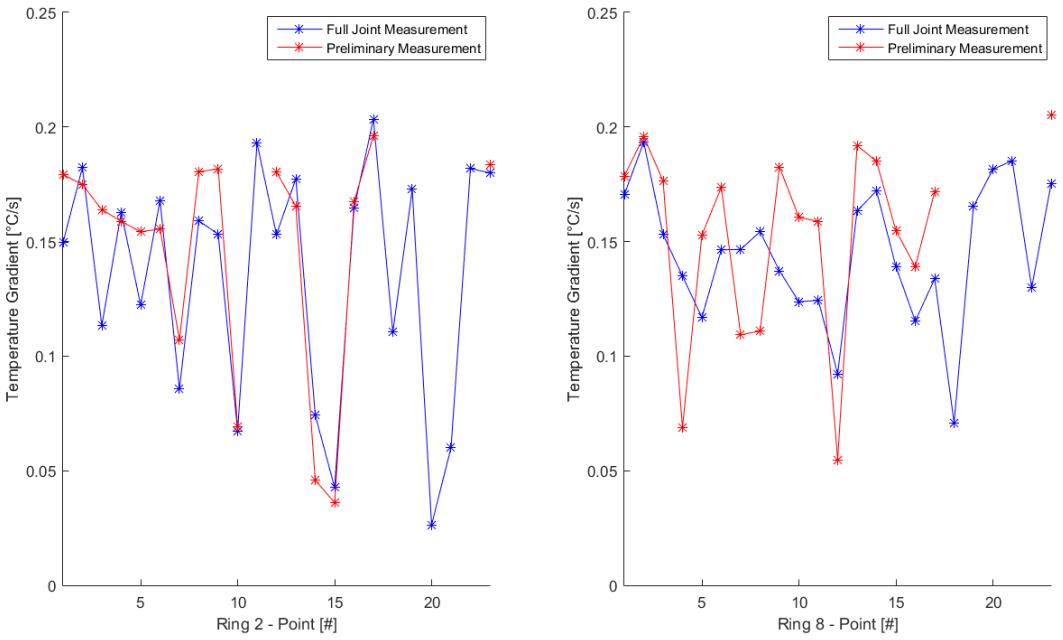

Figure 42 - Differences in preliminary and full joint measurements

As can be seen in the figure above, there is significantly more imprecision in the measurements on ring 8 than ring 2. This may be partially explained by the random nature of measurement imprecision, although a significant factor may also be the changes in the measurement grid and measurement device between measurements. The preliminary single-ply and two-ply measurements where obtained using an initial grid, marked out less methodically than for the full joint measurement. This has led to deviations in measurement location of up to 10cm (though typically closer to 5cm), which may cause variations in gap size/contact pressure between measurement rounds. A potential reason for the greater variation in ring 8 measurements is therefore, that the ring 8 measurement positions deviated further between measurement rounds, causing greater difference in the results.

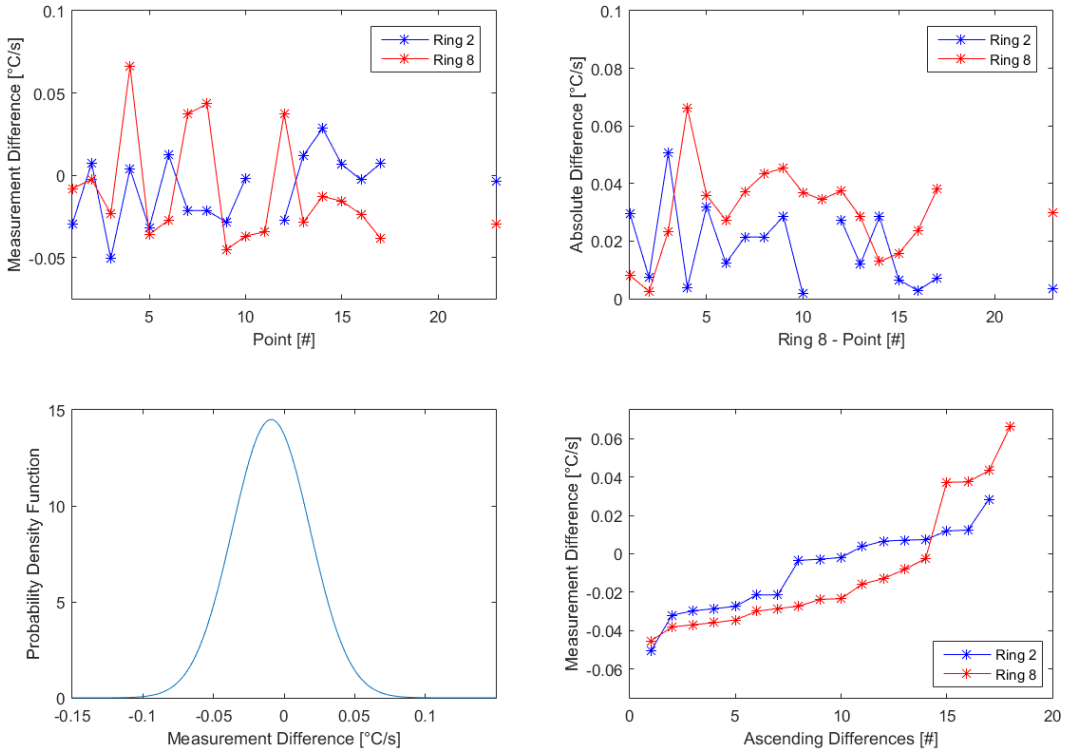

Figure 43 - Measurement precision in two-ply measurements

Figure 43 shows greater detail on the value and distribution of the differences between each measurement round. The top left figure shows the full joint results minus the initial results for both measurement rings. This shows that the variation is seemingly random, although the top right image confirms that there is a greater overall difference in ring 8 measurements. The upper right image also shows that the magnitude of the differences vary between near zero and 0.07°C/s, with an average of around 0.025°C/s. The bottom left figure shows the distribution of the variation (assuming a normal distribution) and indicates that if two successive measurements are taken, one may expect (with 90% confidence), that the second measurement to be within +0.036°C/s and -0.054°C/s of the first measurement. This is a significant measurement uncertainty, as the range is greater than 50% of the mean measurement value.

From Figure 43 it is therefore evident that the precision of the measurement method may impact its ability to perform as required. This can be improved in future in a number of ways, but firstly it must be noted that the sample data above may exaggerate the imprecision of the measurement technique. This is not only due to the changing of measurement positions between measurements but also changes in the heating coil and recording device. Since the varaition between the two rounds of measurement is not systematic, it is unlikely that something such as an extra coil winding during initial measurements is the issue, as this would cause consistently higher temperatures. It is possible however, that poor fastening of the heating coil during initial measurements led to greater variation in the wall to heater distance which has a great impact on heating. Having noted this, the method may be improved by taking an average over many readings to eliminate random variations, or by improving the precision of the measurement equipment, both of which are discussed further in chapter 6.

5.2.2 Conclusion

The measurement method was able to successfully measure 201 grid points covering the entire sample slip-joint over a period of 3 days. Using a cubic interpolation method the results have been interpolated from the measurement points to cover the entire joint. These results show clear pressure structures formed across the joint indicating that results are not completely random. Temperature gradient results vary by a factor of 10, which is far outside the uncertainty of the thermal camera, indicating that the results are at least partially reflective of actual underlying variations in the slip-joint.

The meaning of the observed pressure distribution is discussed in chapter 6, although further insight into the precision of the method is generated here through comparison between intial and final two-ply measurements. This comparison shows an imprecision of ±25% in the measurement method, although this is not entirely trustworthy due to small changes in measurement setup and location between these measurement rounds.

5.3 Feeler Gauge Testing

5.3.1 Purpose and Setup

A number of methods can be used to cross-compare and validate the results of the heat-based measurements, but the most certain way to verify results is to physically measure the gap size or contact pressure in the slip joint. As there is no clear way to accurately and directly measure the contact pressure in the joint, methods for measuring the gap size at various points on the slip-joint were investigated. The clearest method to achieve this is to cut open the slip-joint at selected measurement points and physically measure the gap size (or lack of gap). The method used to cut the slip-joint open and the method for measuring the gap size must be chosen together as they are somewhat co-dependent. For example, the slip-joint may be cut completely in half, allowing feeler gauges, Vernier callipers or laser measurement tools to measure the gap size at any point on the cut cross-section. However, such dramatic damage to the joint would likely alter the geometry of

the joint and would also inhibit future experiments on the joint. An alternative to this is to cut smaller holes in the joint at selected locations, which would limit the chances of geometric changes of the joint.

There are a few methods that could be used to cut such holes, including drilling and plasma cutting, although plasma cutting would likely melt a large amount of material into the gap, preventing measurements. Therefore, the only viable method is drilling and the only viable drilling method for large holes in thick steel is using an annular cutting bit. These come is sizes up to 100mm, however for the small magnetic-base drill available at DOT, 40mm diameter is the largest feasible drill bit. A 40mm hole eliminates the possibility of using anything other than feeler gauges to measure the gap size, as the gap between the two plates is not easily accessible by callipers or a laser tool.

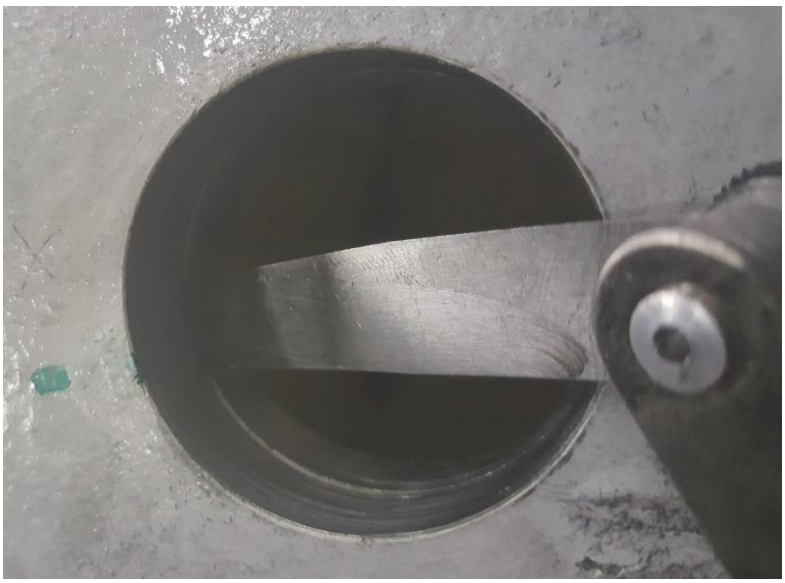

Figure 44 - Feeler gauge testing in sample slip-joint

Therefore using the aforementioned method a number of holes were drilled in the joint to facilitate physical gap size measurements (as per Figure 44). The location of these holes was chosen to provide a spread of points covering the suspected 'detachment value' and in doing so, give an estimate of which temperature gradient values correspond to contact and non-contact regions. A second, potentially more important aim was to provide an estimated function of measured temperature gradient vs gap size, which is why a wide range of points was selected and not just those close to the suspected contact/no-contact point. The measured values of the Points selected are shown in Figure 45.

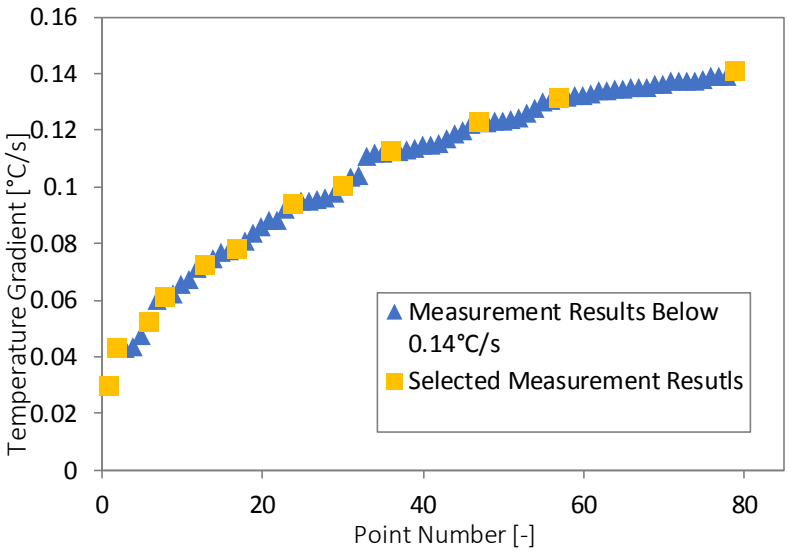

Figure 45 - Selection of feeler gauge test locations

5.3.2 Results

The results of the feeler gauge test are shown in Figure 46 as a comparison between the measured gap size and the expected results (based on heat measurements). The heat results have been normalised to allow for comparison with the results of the validation tests in section 4.1. When considering the results it should be noted that;

- The two points in dark orange have been excluded as outliers, using MAD method (as per section 3.4)[45].
- There is an additional feeler gauge point located at [0, 1] that cannot be seen because a yellow point is plotted over the top of it.
- The gap size of the furthest right is an estimate, as feeler gauges higher than 100μm were not available. Therefore, two stacked gauges (100μm and 35μm) were used and it is likely that a slightly larger gap (at least 140μm) could be measured using a single gauge.
- A large portion of the gap in each hole was blocked by swarf, making it challenging to find a place to insert the gauge. This creates the issue that only one or two locations within each hole were measured for gap size, necessitating the assumption that gap size is even across the perimeter of the hole. The swarf also creates the issue that it may have blocked the insertion of larger gauges, leading to an underestimation of gap size. This was checked to the greatest degree possible by visual inspection; however the possibility cannot be entirely discounted.

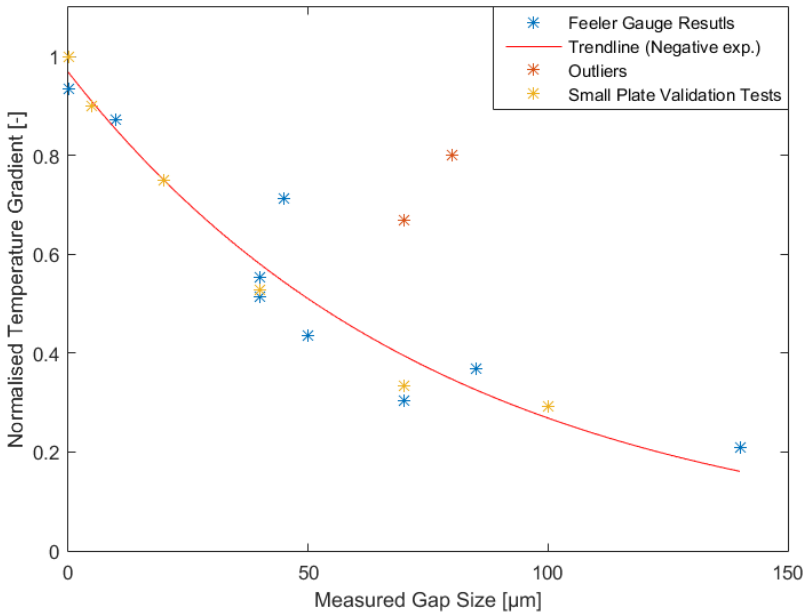

Figure 46 - Feeler gauge test results

As shown in Figure 46, the results indicate that the actual gap size is proportional to the results of heat-based measurements. This (normalised) relationship was fitted with the exponential trend line;

$$f(x) = 0.9685\, e^{-0.0128x}$$

The shape of this trendline is supported through comparison to the results of small scale plate testing (in section 4.1). To facilitate this comparison, the results had to be normalised against an assumed Y intercept value in each case, as the steel in both cases was not the same thickness. This trendline may then be used to convert the heat-based measurements of the slip joint to a gap size distribution, although clearly this gives no information about the pressure in contact regions. As noted from Figure 46, the measured temperature gradients at the chosen locations varied from ~0.14°C/s to ~0.03°C/s, with a predicted y-intercept value of 0.1359°C/s. Given the error present in the results, the 95% confidence interval for the y-intercept is [0.1197 0.1520] °C/s, which encompasses the results of both points where there was no gap present. The index coefficient and 95% confidence interval for the non-normalised trendline is [-0.01282 (-0.01644, -0.0092)] °C/s.

5.3.3 Conclusion

Feeler gauges offer a conclusive way to verify thermal measurement accuracy and establish a correlation between thermal measurements and gap size. This is valuable to establish what percentage of the joint is in contact, determine thermal measurement accuracy and allow comparison with small plate test results. The results of 12 feeler gauge test locations showed that thermal measurement results have an error of ±12% (with 95% confidence). The results also demonstrate that thermal test results are clearly correlated with actual gap size and that this correlation is similar to the correlation observed during small scale validation tests (section 4.1).

Two of the points measured with feeler gauges showed no contact gap, which is in line with the predicted gap/contact transition temperature gradient of 0.1359°C/s. This value may then be

combined with two-ply test results to determine what percentage of the slip-joint is in contact overall. Feeler gauge testing also showed that the region, predicted by thermal results, to have the largest contact gap had a gap of at least 140μm. This is relevant for future design consideration, but also for the accuracy of the method as the sensitivity of thermal measurements is inversely proportional to gap size.

6 Discussion

6.1 Contact Distribution Pattern

As noted previously, the heat measurements themselves cannot directly resolve the gap size and contact pressures in the slip joint. They can however give a good idea of the relative contact pressure in various regions and highlight the regions in which there may be non-contact. Seeing as contact/non-contact cannot be established directly from the heat measurements, regions with the lowest temperature gradient will be referred to as low-pressure regions (despite the fact that there may be a gap, i.e. no pressure).

6.1.1 Identifying Distribution Features

Knowing the distribution of the contact areas and identifying any patterns in this distribution is useful to aid in developing FE modelling strategies and in determining the cause of non-contact regions.

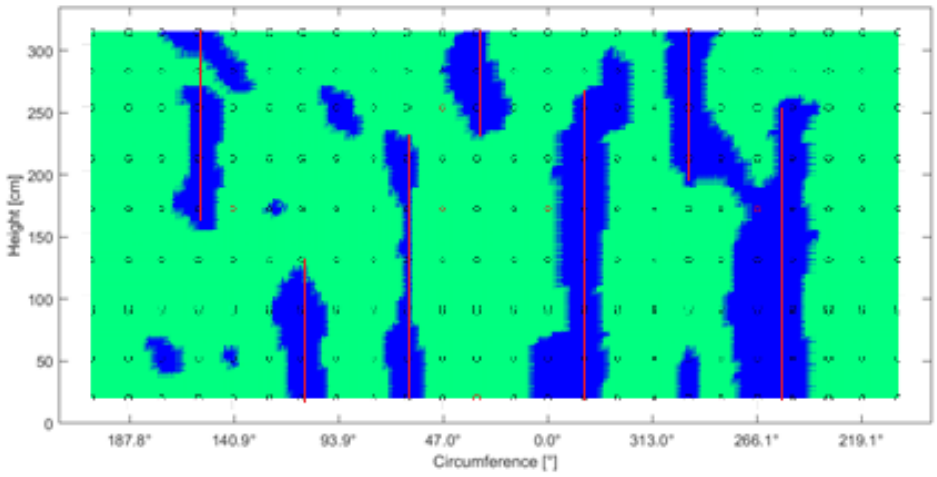

Figure 47 - Binary Plot of Temperature Gradient (Green/Blue = above/below 0.125°C/s)

The shape of low-pressure regions is most evident when looking at a binary plot (split at temperature gradient of 0.125°C/s), as shown in Figure 47. There are a number of interesting features, such as;

1. The low-pressure regions appear to be vertically oriented (as shown by red lines),
2. The low-pressure regions do not extend the full height of the joint,
3. The low-pressure regions seem to alternate in originating from the top or bottom of the joint (with exception of a 'missing' region around 94° circumference.
4. The low-pressure regions cover the entire circumference of the joint and are not distributed entirely on one side of the joint,
5. While considering the above statement, the low-pressure regions are more significant between 360° and 240°,
6. The regions of low pressure originating from the bottom of the joint are longer than those originating from the top of the joint,
7. Regions of low-pressure are typically no more than 60-70cm in width.

To further corroborate point 1 above, we can conduct a simple regression test, using the average result of the two adjacent points to predict the result at any random point on the slip-joint. This can be done using the points vertically adjacent or using the points horizontally adjacent, which is presented in Figure 48. This figure shows that there is a much clearer relationship between points vertically/longitudinally adjacent, thereby objectively demonstrating the vertical nature of the low-pressure regions. Another important conclusion from this relationship is that the cubic interpolation used to produce Figure 40 and Figure 41 in section 5.2, overestimates the influence of circumferentially adjacent points. This may mean, for example, that the connection between the two low pressure regions at around (270°, 200cm) does not exist and is simply an artefact of the low pressure regions to the left and right.

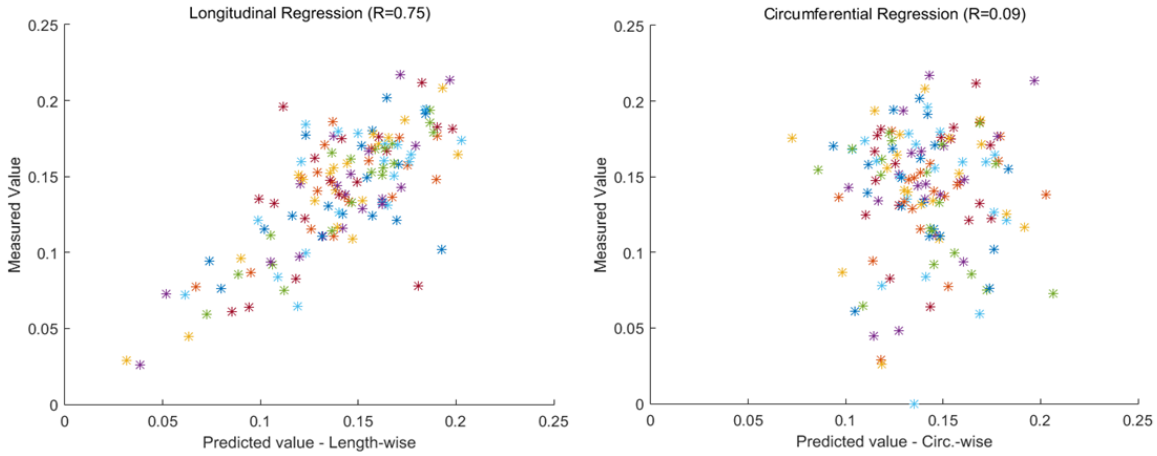

Figure 48 - Relationship between circumferentially and longitudinally adjacent measurement points

The identification of vertical low-pressure regions is supported by the work of Segeren [46], who found that for a slip-joint subjected to a static shear force and bending moment, vertical non-contact regions develop. The work was conducted on a loaded FE model meaning that the non-contact regions are due to elastic deformation (and therefore only present under load). Furthermore, the slip joint had greater wall thickness than that used in this paper and found that the non-contact regions developed on opposite sides of the slip joint (both vertically and circumferentially). However, it is feasible that a repeated elastic load in such a manner may cause plastic deformation over time leading to low-contact regions.

This deformation/pressure distribution is in contrast to the results of van de Bosch et al. [47] who found that due to the geometric tolerances in the DOT500 slip-joint, high/low-pressure regions will

run in circumferential bands. It should be noted that the result is due to the specific geometry of the slip joint used, which may explain why the results of this paper vary. However, [47] did find that ovality in the upper half of the joint and/or misaligned installation leads to vertical high/low-pressure regions in the joint. It should be noted that like [46] these regions appear vertically opposite each other.

6.1.2 Causes of Identified Distribution Features

The low-pressure regions seen in the slip-joint could have been introduced at any point in the life of the joint, from manufacturing to decommissioning. It also possible that various features of the pressure distribution were introduced by multiple sources, possibly at different stages in the tower's lifecycle. These potential causes are outlined below, sorted by lifecycle stage.

6.1.2.1 Manufacturing

The process of producing a monopile and turbine tower (or in this case, two tower sections) is a multi-step endeavour. Firstly, sections of steel plate must be rolled flat, after which these plates are cold rolled into cylindrical cans. The seam on each individual can is then welded together, followed by the circumferential welding of all the cans into one long tube (see Figure 49). Residual stresses can be introduced at any point in this process, which may later create high and low-pressure regions in the slip-joint. However, stresses induced during circumferential welding and during initial hot-rolling of the plate are typically longitudinal in the plate [48] (and thus circumferential in the slip-joint), which conflicts with the observed pressure pattern. Additionally, the longitudinal welds on each joint can do not line up on the actual slip-joint (which consists of 3 cans). Therefore the residual stress from each of these welds will not be aligned and the spread of low-pressure regions across multiple cans cannot be explained.

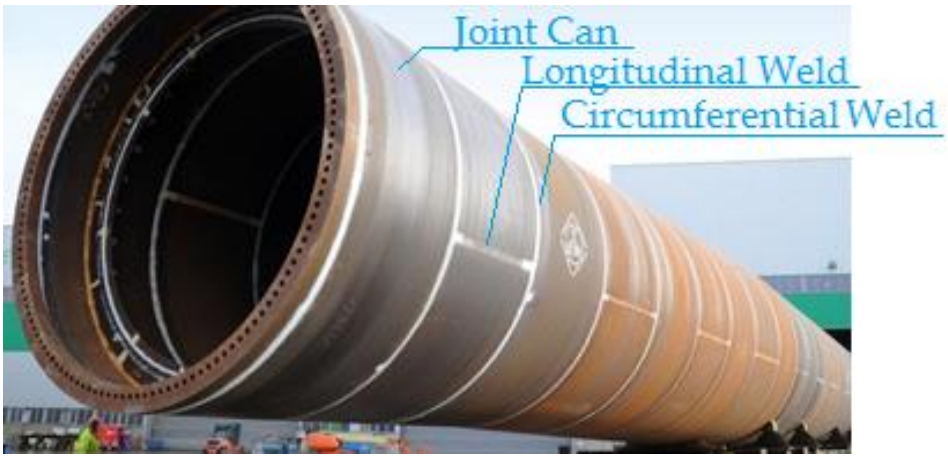

Figure 49 - Tower assembly and weld types

It is possible that residual stress induced in the can sections during the bending process could cause each individual can to tend towards out-of-roundness over time, although like the seam welds, it is unlikely that these regions are aligned across multiple cans. While it is likely that some out-of-

roundness and waviness were induced in each of the cans during bending, once again this is likely to be can-specific. It is possible however, that strong residual stress or out-of-roundness in one can may impart the same 'defect' into the adjacent can, although such large defects in any one can should be detected during production.

6.1.2.2 Transport and Installation

There is a great possibility for damage to the tubular structure during transport and installation, especially given the low wall thickness of the tower section studied. Given that the top and bottom halves of the tower are in complete pieces during transport and installation, any damage sustained could easily span across multiple cans, as seen from measurement results. Damage that may be sustained during transport includes plastic deformation of the underside of a cylindrical component due to its own weight, especially if dropped. If this occurred multiple times between manufacturing and installation in multiple orientations, then conceivably several 'flat' areas could be imparted onto the tower structure. 'Flat' sections developed in the outer cone of the joint would be expected to show a high-pressure region in heat testing, with two low pressure regions either side, while 'flat' sections on the inner cone of the joint would produce the opposite (as per Figure 50).

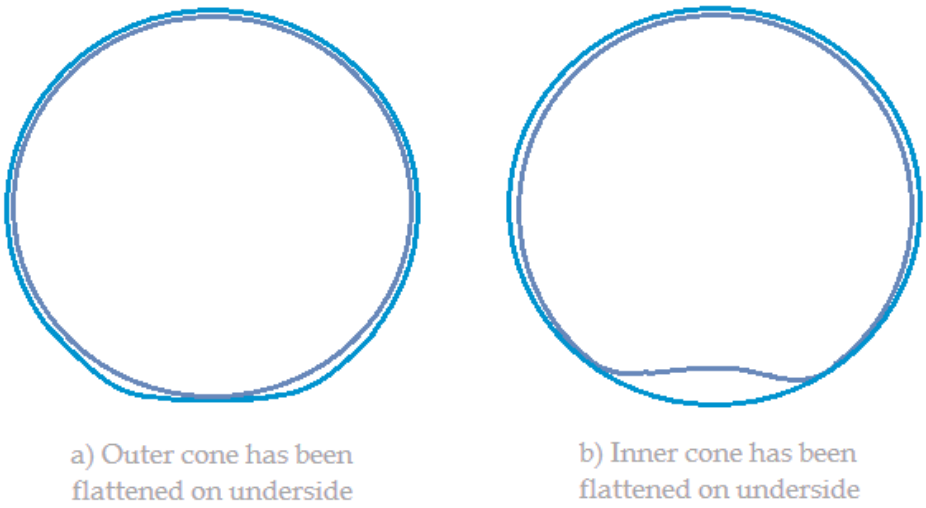

Figure 50 - Theoretical 'Flattened' (Damaged) regions in the slip-joint

Given the lower stiffness closer to the free end of each cone, it would seem unlikely that a region of the cone may be flattened that did not extend to the free edge. Additionally, due to the lower stiffness of the free end of each cone, one would expect more damage to occur close to the free end during transport and installation. It then follows that if the contact distribution were caused by such damage, that the low-pressure areas at the top of the cone were caused by upper sections of the inner cone being bent inwards. Conversely, the low-pressure regions in the lower half of the joint are more likely to have been caused by the bottom half of the outer cone being bent inwards (as per Figure 50a). While it is quite possible that the low-pressure regions in the upper half of the slip-joint were caused by such damage, the low-pressure regions in the bottom half of the joint do not come in 'pairs', as would be expected (per Figure 50a).

While it is improbable that damage to the lower half of the inner cone would be caused without also damaging the upper half of the cone (due to lower stiffness at the top), this situation is varied once the turbine was decommissioned. As seen in Figure 51, the slip-joint has been cut from the tower,

giving added flexibility to the lower end of the joint (left in image). With this added flexibility, it is possible that if the joint was impacted at the support location, by dropping onto supports or otherwise that the inner cone of the slip joint could deform as in Figure 50b. Given that the low-pressure region around 250° is located underneath the slip-joint (during current and previous joint storage), it is possible that the low-pressure result in that location was caused through this mechanism.

Figure 51 - Decommissioned Slip-joint

While the aforementioned physical damage to the joint may have caused some of the distribution features, other (low and high pressure areas) remain unaccounted for. It is possible that misalignment during installation caused some of these non-uniformities. Misalignment (as noted by [47]) during installation causes the formation of low-pressure regions on opposite sides of the joint. This could be the case with the low-pressure region pairs 155° and 345° or 110° and 295°, although clearly misalignment could only cause one of these pairs of low-pressure regions to form. Of the two mentioned pairs of low pressure regions it is more likely that the latter was caused by misalignment due to the relatively even length and gap size of the low pressure regions. However, one would expect in the case of misalignment that any gap created would increase linearly in magnitude from the middle of the slip-joint towards the top or bottom, which is not observed in either of the cases above. This makes it unlikely that misalignment has contributed to the observed pressure distribution.

Figure 52 - Shrink buckling in pipe liner

An alternative explanation for any low-pressure regions may be shrink buckling induced in the inner cone during installation (seen in Figure 52). However for this to occur, there has to be a relatively

large initial defect in the inner cone, otherwise the pressure from the outer cone will provide a corrective force. Additionally, typical cases of shrink buckling occur when a relatively flexible tube is inserted into a rigid cavity. As the two halves of the joint have the same wall thickness and diameter, it is more likely that the outer cone would stretch to accommodate the inner cone than initiate buckling. Therefore shrink buckling, while possible, is not a likely cause of the observed distribution pattern.

6.1.2.3 Operations

The final lifecycle phase where the observed pressure distribution may have developed is during turbine operation. Given the non-random nature of the wind direction it is likely that the turbine was repetitively loaded from only a few directions. Figure 53 shows that the wind direction for the turbine site is primarily unidirectional. It would therefore be expected that the overturning moment produced by such a wind rose would create an effect similar to misalignment of the upper cone, leading to low-pressure regions on diagonally opposite sides of the joint. It is possible that the regions seen at around 345° and 155° were caused by such loading, although the high pressure regions at around 100cm height either side of the 345° low-pressure region are then unable to be explained.

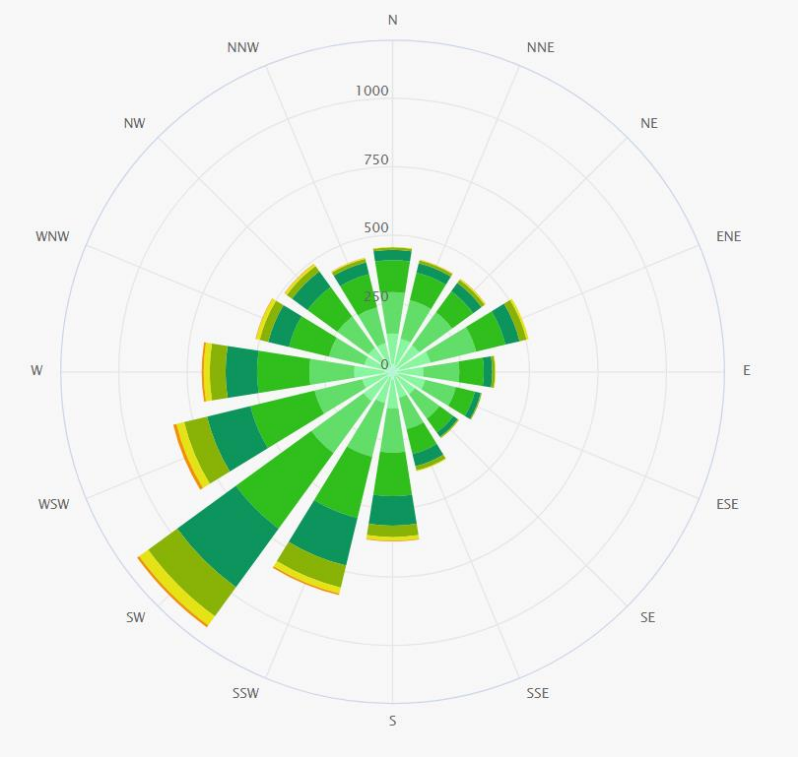

Figure 53 - Scheveningen, NH wind rose [49]

6.1.3 Conclusion

Without yet determining which regions of the slip-joint are in contact and which are not, the shape of the low-pressure regions provides a significant amount of information. These low-pressure

regions are thin vertical strips, originating from the top or bottom of the joint (in alternating sequence). The 'wavelength' of this corrugated pattern is approximately 60-70cm and the length of these strips is approximately 1-2.5m. Given the potential causes of low-pressure investigated, it is unlikely that a single factor caused all of the low-pressure regions observed in the sample joint. It is difficult to assess whether residual stress from manufacturing plays a role and further investigation should be undertaken. Other causes such as misalignment, ovality and operating loads would be expected to cause vertically opposite damage regions (causing vertically opposite pressure regions). It is therefore possible that one or two of the vertically opposite low-pressure regions were caused through these mechanisms, however the only remaining explanation for the others is impact damage when the joint was laying on its side during transport (pre or post operation).

6.2 Contact Percentage

Following analysis of the qualitative aspects of the heat-transfer distribution in the slip-joint it is necessary to address the quantitative aspects, in particular, the correlation between heat transfer rate and gap size/contact pressure. A clear idea of this correlation would allow a full finite element model of the slip joint to be created and ultimately load case simulations to be evaluated. On a slightly less complex note, it also allows one to establish a heating rate at which the contact/non-contact transition occurs and therefore establish what percentage of the joint is in contact. This could be useful as it establishes a boundary point between the correlations of gap size/heat conduction and contact pressure/heat conduction.

6.2.1 Statistical Methods

As noted in section 2 (Figure 16), thermal contact conductance (TCC) is a monomial function of contact pressure. If we assume contact pressure is normally distributed within the slip-joint, then the distribution of contact conductance within the joint should be a monomial function of the normally distributed pressure values. The cumulative density function (CDF) of such a distribution is shown in Figure 54a using varying coefficients. Given that contact pressure cannot become negative; the thermal contact conductance for the entire joint must be thought of as a piecewise function, where TCC is monomial function of contact pressure for pressures greater than zero (L(x)) and some function of gap size for pressures below zero (G(x)). Therefore, the CDF of all heat measurements (Figure 54b) should also be piecewise; with some portion in the left of the CDF resembling the CDF of G(x) and the right half resembling the CDF of L(x).

If the point at which these two different CDF functions meet can be determined, then this would be the TCC value at which the contact/non-contact transition occurs. However, in this case the CDF of all measurements (Figure 54b) resembles the CDF of L(x) (Figure 54a) in its entirety, making it impossible to determine the TCC at the contact/non-contact transition using this method. In other words, the CDF of the slip-joint measurements looks indistinguishably similar to the theoretical CDF if the slip-joint was 100% in contact (with normally distributed contact pressure). Therefore, for this sample slip-joint this method cannot be used to determine the contact/non-contact transition from thermal results.

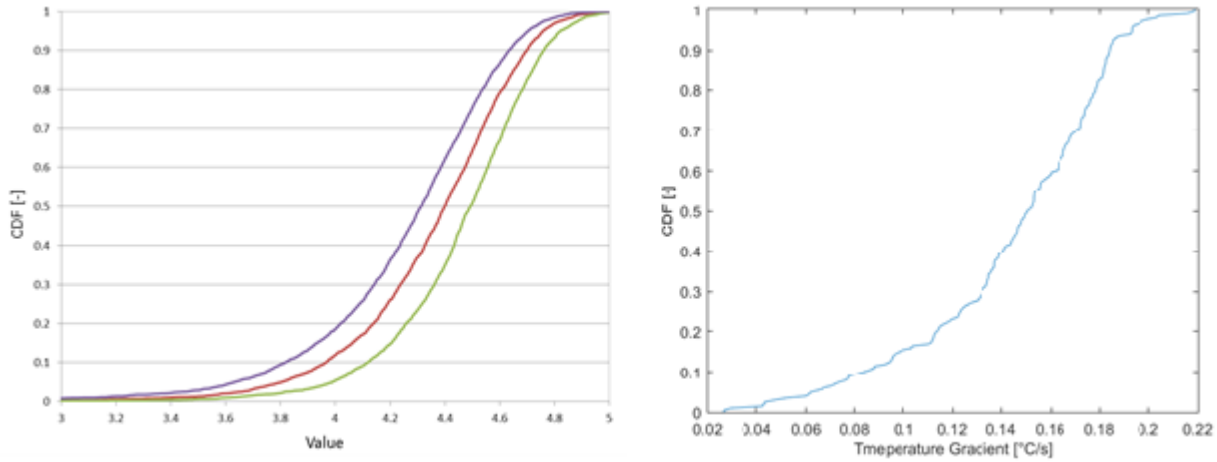

Figure 54 - (a) CDF of monomialy transformed normal distribution, (b) CDF of all slip-joint measurements

6.2.2 Experimental Methods

Given that statistical analysis of the distribution of results cannot yield any information about the transition point between contact/non-contact, it is necessary to turn to the feeler gauge results for this information. As noted in chapter 5, the following relationship between gap size and temperature gradient was observed;

$$Temperature\ Gradient\ \left[\frac{°C}{s}\right] = 0.1359e^{-0.01282*GapSize[\mu m]}$$

From this relation it can be deduced that the expected transition point between contact/non-contact occurs at a heat transfer of 0.1359°C/s, with a roughly 12% error margin either side. If this correlation is applied to the measurement results we obtain Figure 55, which shows contours of the regions of non-contact for the expected range of transition values.

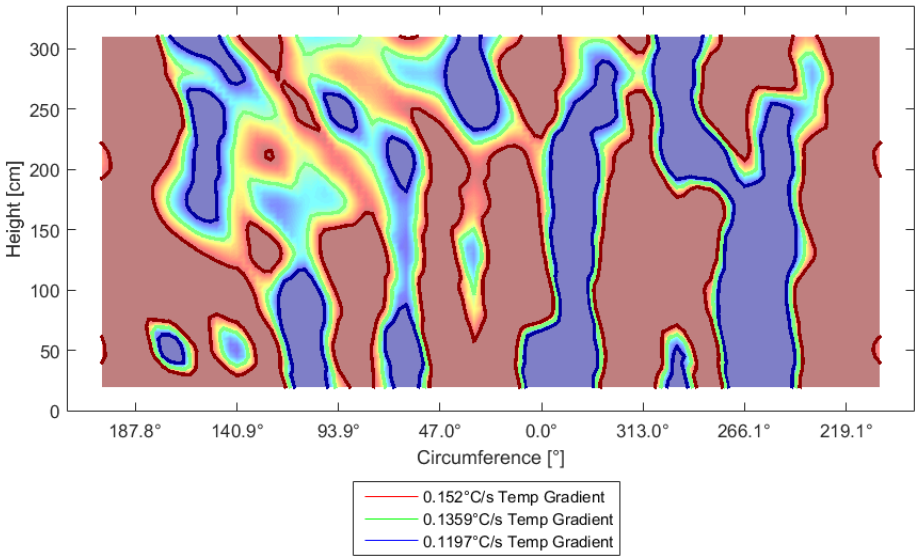

Figure 55 - Non-contact contour plot for varying transition values

For the expected contact/non-contact transition of 0.1359°C/s, approximately 34% of the slip-joint would not be in contact, with 95% confidence interval of [22.9% 50.7%]. This large confidence highlights the fact that ever though the confidence interval for the transition value itself is ~±12%, a large number of measured points are in this region, meaning that a small deviation in the transition value leads to a large change in contact percentage. It is however, important to note that the change in contact in Figure 55 does not significantly change the conclusions drawn in section 6.1 about the shape of the contact regions.

6.2.3 Pressure Correlation

It is very difficult to say anything quantitative about the correlation between contact pressure and measured temperature gradient, insofar as putting specific values to the relationship. This is primarily because the contact pressure in the contacting regions is challenging to measure directly using any known method. The heat measurements provide the *relative* distribution of the thermal conductance (temperature gradient), but further information is required to develop a numerical relationship between temperature gradient and pressure.

If a maximum contact pressure is assumed (~99^{th} percentile value), from mechanical analysis or otherwise, then based on the contact percentage found above and assuming pressures are normally distributed, the mean and standard deviation of the pressure distribution can be solved simultaneously.

$$0\ [\text{MPa}] = \mu - 0.433\sigma$$

$$99^{th}\ \text{Percentile Pressure} = \mu + 2.33\sigma$$

For investigative purposes, an arbitrary maximum contact pressure of 10MPa is used to generate a theoretical pressure distribution (mean ~3MPa, sigma ~3MPa). Figure 56 shows a comparison between the heat measurements taken from the slip-joint and the pressures in the joint from this theoretical pressure distribution. As indicated in the figure, the relationship between the two is far better captured with a parabolic function, or even linear function, than a monomial function, which shows that either;

- The relationship between pressure and temperature gradient is not monomial,
- Or, the pressure in the slip-joint is not normally distributed (in the contact regions),
- Or, the thermal measurements are very inaccurate.

Given the body of previous research into contact conductance and given the measurement error discussed previously, the first and third points are unlikely. Therefore, it can be concluded that the pressure distribution is likely not normally distributed. If the pressure distribution was right skewed the monomial relation would likely have a better fit. Of final note, is that this conclusion further eliminates the possibility of using the presented statistical methods to determine the temperature gradient at zero contact pressure (as per section 6.2.1), as the described method relies on assuming the type of pressure distribution.

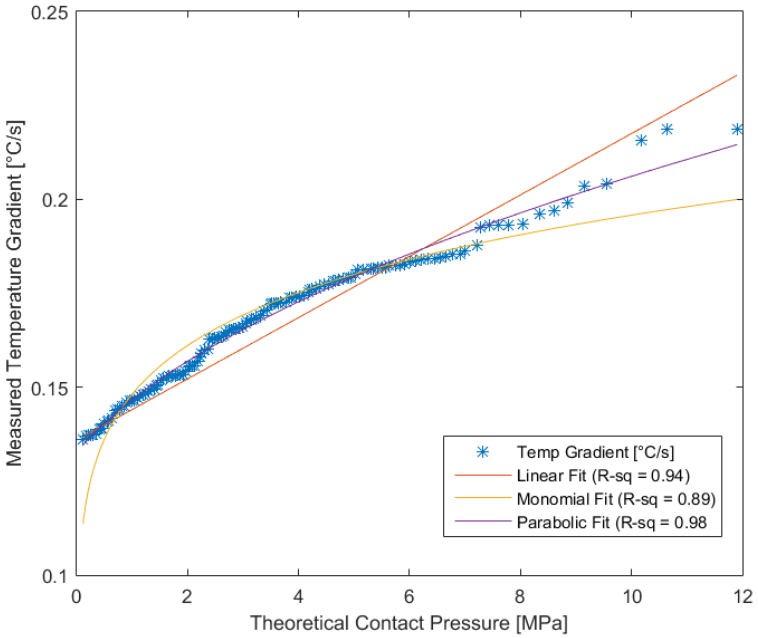

Figure 56 - Measured temperature gradient vs theoretical contact pressure in the slip-joint

6.2.4 Conclusion

The attempted use of a cumulative density based statistical method to correlated contact pressure and thermal measurements was not successful for the sample slip-joint. In an attempt to utilise non-destructive methods, the contact pressure was also analysed statically, showing that the pressure distribution in the joint is likely not normally distributed. This is relevent because it precludes the use of some statistical methods and provides further information for future finite element modelling of slip-joints.

Comparison of two-ply measurement results and feeler gauge tests indicates that 34% of the sample slip-joint is expected to not be in contact. Taking a 95% confidence interval, this value may be as high as 50.7% or as low as 22.9%. Figure 55 clearly shows that the observed shape of the pressure distribution (thin, vertical strips) remains no matter which contact percentage is correct. This result also indicates that future attempts to mechanically analyse or model slip-joints should investigate non-contact of up to 50% unless further information is obtained.

6.3 Improvements

6.3.1 Improvements to Equipment

There are a number of improvements that could be made to the test equipment to facilitate faster and more accurate measurements. These can be broadly divided into improvements to the heating side of the test equipment and improvements to the measurement/sensing side of the test equipment.

6.3.1.1 Heating Equipment

The two main ways the current heating equipment could be improved include increasing the speed at which the joint can be measured and increasing the consistency of heating. The speed at which points are measured can either be improved by decreasing the time taken to measure each individual point or by measuring a greater number of points at once (or a combination of these). To increase the speed of measurement a higher power output from the heating device is required. The current induction unit provided a maximum power of 1200W, however it is expected that for larger structures with thicker walls, this level of power will become inadequate. The use of an industrial size induction heater (eg. 3kW+) with infrared monitoring of the surface under the heater would provide both the ability to increase the heating power and the ability to monitor the heating surface to ensure that the temperature remains below acceptable levels (for the paint).

Even if the above methods were implemented the amount of man hours required to measure an entire slip joint would be at least 20, which is an expensive endeavour offshore. Therefore, in future it would be ideal to automate the process, with a magnetically mounted robotic vehicle moving the heating apparatus around the inside of the vehicle. However, prior to looking into such complex engineering problems, it may be of benefit to expand the measurements from point measurements to a ring measurement. This would require heating an entire ring of the slip-joint at once and measuring the temperature response of the opposing side of the joint using a ring of sensors. The heating could be achieved by mounting a flexible induction cable around the inside of the slip-joint and the measurement could be achieved by using many thermal cameras or a large array of thermocouples. The downfalls of this method are the increased investment in a much more powerful heating unit and the increased number of sensors. Additionally the slip joint would experience a lot more global heating from the increased rate of power input. However, this would greatly increase the speed of measurement (if the heater and sensors could be applied efficiently). Measuring in a line also avoids the issue encountered when attempting to heat and measure a surface, where the heat diffuses at different rates across the heated area (ie. higher diffusion near the edges).

6.3.1.2 Sensing Equipment

As discussed previously the type of temperature measurement sensor is based on a number of factors including accuracy, resolution, material surface finish, temperature range and the presence of electro-magnetic fields. In the current experimental set-up the presence of large electro-magnetic fields limits the use of thermocouples as induced current may affect the measurements. While it is possible to obtain shield thermocouples, the price notably increases. Noting this, as well as the movement flexibility of thermal imaging cameras, the sensing set-up may be improved by obtaining a more sensitive and more rigorously calibrated thermal camera. The camera used in testing has an advertised sensitivity of 3% or 1°C (whichever is greater), compared to a potential sensitivity of <0.2° for class leading cameras. A mechanical ring to hold the thermal camera in a fixed position relative to the surface, as well as a direct computer connection to automate the collection of data would also increase reliability and minimise measurement errors.

6.3.2 Improvements to Method

The measurement method could be improved in two ways; by minimising the measurement error and by better allowing the quantification of measurement errors. The measurement error can be minimised by removing as many human factors as possible, such as the placement of the heating device. This was countered to a degree by marking a measurement grid on the slip-joint, although this could be taken further by utilising some sort of positional monitoring system to achieve more precise positioning. Another human factor could be removed through the synchronisation of the heating device being turned on and the recording of temperature data. This would allow an in-depth analysis of the transient temperature development at each point rather than a more simplified gradient-based quantification of the heating rate.

The main improvements to the current method could be realised from better quantification of the measurement error. This could be achieved by taking a large number of repeated measurements at a single location (to quantify precision) and by taking a larger number of measurements in single ply regions (to quantify location-dependent material variations). Firstly, for multiple measurements taken at a single two-ply location, the variation in results can be attributed to imprecision of the measurement method (rather than changes in the expected output value). When a number of measurements are taken at varying single-ply locations the varying is due both to location based parameters, such as material thickness, paint thickness, etc., as well as imprecision in the measurement method. The measurement imprecision is already known from the multiple measurement at a single location and therefore the location-based variation in material properties may be estimated. This knowledge may then be applied to two ply measurements to estimate the expected error based on both locational variations and measurement imprecision. In the current testing obtaining a significant number of measurements in this style was limited by both time and the malfunction of the only available induction heater towards the end of the project.

6.3.3 Alternative Methods for Comparative Analysis

A possible way to validate the heat-based measurements and to obtain further information about the joint is through comparison with the results of alternative measurement methods. Two distinct possibilities for future investigation are outlined below.

6.3.3.1 Residual Stress Methods

Measuring residual stress may be a method to confirm the possibility that the observed contact distribution is caused by residual stresses from manufacturing processes. Residual stresses formed during circumferential or longitudinal welding, or bending of plates into cans can leave certain regions of the tower weak under stress, possibly causing deformations. It would be useful to measure the residual stress to confirm a number of issues including, the magnitude, the orientation, the location of the largest stresses in the joint and finally, if the residual stress pattern matches the thermal conductance distribution.

This measurement can be achieved through several methods, of which the most pertinent non-destructive techniques are x-ray diffraction and Barkhausen Noise methods. X-ray methods are fairly commonly used, measuring the diffraction of a target x-ray beam to determine the surface lattice

spacing in the target material [50]. While the common usage means that portable industrial machines exist that can be used in an industrial environment, x-ray methods measure only the outer 0.001-0.01mm of the surface (in steel). This means that the residual stress cannot be measured deeper in the material, although it would be expected that the residual stresses from welding or bending are at the surface anyway. A slight downfall of this method is that the measurement surface must be adequately prepared (such as removing paint and oxidation), although this can be done by commercially available devices. This requirement does mean that this could not be used to measure residual stress in an offshore slip-joint, although the stress in the individual halves of the joint could be measured prior to painting (immediately after assembling the cans).

An alternative method for measuring residual stress is the measurement of magnetic Barkhausen noise. This method is now well documented for use in a wide range of steel structures, both in research and commercially [51]. This method relies on measuring the change in magnetic properties of the target material caused by a change in orientation of internal magnetic domains under a varying applied magnetic field. The stress state of the material affects the preferred orientation and movement of magnetic domains in the target material which subsequently affect Barkhausen noise emissions. One benefit of this method are that the device can be set to target certain measurement depths (up to 3+mm), eliminating the need for paint removal. Additionally, compact measurement devices have been developed for industrial use, where complex calibration and measurement methods are not always possible. Due to the ability to measure painted parts and less bulky measurement sensor, this method is preferred over x-ray methods for slip-joint measurement.

6.3.3.2 Acoustic/Vibration Based Methods

Acoustic methods, as a tool to assess slip-joint contact and pressure, have been outlined in section 2.2.6. It should be noted that common acoustic methods (such as 'coin-tap' testing), differ significantly from modal analysis method, despite both tests involving the measurement of structural vibration following a brief impact. Model updating, which utilises modal analysis testing, is discussed in section 2.2.1, although the modal data collection procedure is not addressed. It is therefore necessary to address modal testing to examine how it differs from acoustic methods and which is more appropriate.

Firstly, modal analysis testing involves the measurement of accelerations at various points on a structure when a known load is applied. Knowing the response of the structure allows the user to determine the mode shapes and frequencies of the structure. The load can be either continuous (cyclic) or impulsive, which both have slight differences, although impulsive loading will be addressed here. When using an impulsive load, the load is typically applied with an instrumented impact hammer, while the response is measured with accelerometers attached to the structure. If only one hammer and one accelerometer are used to save cost, then it is the possible to choose from two configurations. The hammer may be moved to impact every chosen point on the structure while measuring accelerations in one location, or alternatively the accelerometer can be moved to the chosen points around the structure while the impacts are all at one location. In order to construct complete modes for the structure the response (or impact) on the x, y and z axes must be known for all point. Due to the fact that it is difficult to impact a plate in any orientation other than normal to the surface, it is easiest to impact a single location and measure the tri-axial acceleration at various points around the structure [52].

Data from the aforementioned modal testing then provides the frequency response function for all chosen points on the structure which can then be transformed into global mode shapes and frequencies. A significant issue with this method is that the mode shapes of the slip-joint do not tell us anything about the contact areas when examined in isolation. There needs to be some benchmark for comparison of the measured mode shapes to determine the physical differences between the measured slip-joint and the 'benchmark' slip-joint. The issue in this case arises in determining the benchmark case, as making an appropriate finite element model, or finding a perfect sample slip-joint to measure is difficult. It may be possible to forego any comparison and examine the frequency response functions directly to find response peaks unexplained by global modes. These localised vibration response peaks may indicate the presence of a non-contact region in the vicinity of the accelerometer, as the unsupported region can vibrate like the skin of a drum. However, even using this analysis method, a high density grid of accelerometer measurements is needed for spatial accuracy and properly characterising the size and depth of any gaps from the frequency response peak is likely very challenging.

Alternatively, acoustic methods, such as the coin-tap test rely on moving the accelerometer together with the impact hammer to chosen sites around the joint. For this reason however, it is not possible to locate the accelerometer on the surface, as there would be undesirable interactions between the closely spaced accelerometer and impact site. Therefore other measurement methods such as measurement of the acoustic emission or hammer acceleration must be used. The disadvantage of not being able to use an accelerometer on the surface, is however offset by the fact that impacting the structure at varying locations makes it much easier to excite the local resonance frequency of unsupported regions under the impact site. Additionally, measuring the response directly at the impact site allows the variation between sites to be more easily quantified.

As addressed in section 2.2.6, there are a number of methods for measuring the impact response including measuring the acoustic response with a microphone in the impact hammer, or measuring hammer acceleration. Based on further research in the field [16], each of these measurements individually provide similar levels of accuracy and could have difficulty in determining contact vs non-contact in such a large specimen as the slip-joint in question. Alternatively, resolution can be increased by utilised acceleration data to determine the free-vibration portion of the acoustic data, which can then provide much better distinction between regions of varying stiffness. There are some further issues to address if this method is to be applied to the slip-joint, including that the method likely does not have the resolution to distinguish well between areas with varying contact pressure, because the local stiffness of such regions likely does not vary significantly. Additionally, it is likely that the stiffness of a particular also does not vary significantly with gap size (beyond a certain gap size). Therefore the main objective of this method would be to determine where non-contact regions existed and the extent of such regions around the surface of the joint.

Some issues to note when design such testing include that the depth resolution of such tests may be increased through utilising a lower hammer mass [19], although it should be ensured that sufficient energy is input to excite the local resonant frequencies. Additionally, variation from the average response will be seen towards the ends of the joint and should be accounted for (due to the lower stiffness in such regions). Furthermore, near surface defects such as paint delamination could significantly affect the results as it can dampen the impact, therefore care should be taken to check for any such areas with alternative methods, such as ultrasonics. One final consideration is resonant frequency range of any non-contact regions and whether this will be significantly differentiable from global modal frequencies. The work of Segeren et al. [46] found that the natural frequencies for a slip -joint vary from 10-30Hz (for the first 6 frequencies). For a rough estimation we may assume that

non-contact regions in the slip joint are circular in shape and therefore treated as a circular membrane with fixed collar. Then, according to [53] the frequency of vibration is;

$$n = \frac{hc}{r^2}$$

Where;

n = natural frequency [Hz]
h = membrane thickness [m]
r = membrane radius [m]
c = speed of sound in membrane material [m/s]

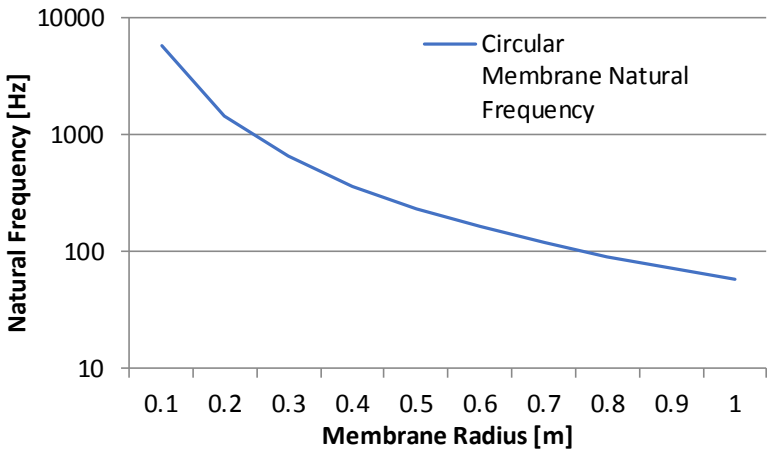

Figure 57 - Fixed collar circular membrane resonant frequency

As shown in Figure 57, the resonant frequency of such a circular membrane may venture into the range of global natural frequencies of the joint, which may make larger non-contact regions harder to detect. This may prove less of a problem in reality, as the curvature of the slip-joint surface likely makes any non-contact regions stiffer than in the above figure (which is for flat membranes). Overall, acoustic methods provide a possible method for comparison with available measurements, as they can rapidly determine regions of non-contact with reasonable accuracy, although investigation is needed into factors such as impact hammer mass and stiffness to obtain best results.

7 Conclusion

7.1 Method

A continuous-heating, thermographic test method can be used to qualitatively determine the contact and pressure distribution within the slip-joint connection. This method is preferred over alternative methods, as heat transfer through the joint wall is correlated with both contact pressure and gap size, allowing measurement of all areas of the joint. Additionally, the method is most sensitive to contact pressure (or gap size) variations in regions where the contact pressure is near zero, making this method a good tool to investigate the contact percentage in the slip-joint. Furthermore, the spatial resolution and heating power of the method may be increased as need to investigate larger slip-joints. The key downside of the method is that measurements are relative and no non-destructive method has been found to establish a direct quantitative correlation between thermal measurements and exact contact pressure or gap size values. A destructive method was therefore evaluated for this purpose and will be addressed later.

The most appropriate measurement configuration is a transmission mode measurement, using a continuously applied induction heater as a heat source and a thermal camera to measure heat variations. This measurement method is accessible, easy to setup and has been shown to be appropriate for pressure and gap size measurements. Induction heating is the best heating option because it provides a large (scalable) amount of heat, with excellent control and low peak temperatures (to avoid paint damage). Thermal cameras should be utilized because they allow a large area to be recorded at once and are immune to any electromagnetic fields generated by the induction heater.

7.2 Validation

The thermographic method developed has been tested and validated for use in measuring the contact and pressure distribution in a sample slip-joint structure. From validation testing in section 4.1 and 4.3 it is evident that measurement results are directly correlated to contact gap size and that the thermographic method can resolve gap sizes from 0.05mm up to greater than 1mm. Finite element validation testing shows that measurement results are non-linearly correlated with contact pressure. A direct quantitative correlation has not been established; however the observed qualitative correlation indicates that measurement results may be used to establish the relative distribution of contact pressure within the measured slip-joint. This information may be used to

determine if some (high contact pressure) regions may suffer from fatigue or have lower limit strength.

Apart from establishing the qualitative correlation between measurement results and joint contact, validation measurements show that the method has adequate accuracy and precision to assess contact distribution. Single-ply measurements show that the precision of the measurement method, using the current experimental setup, is ~±13%. This value was not supported by comparison between initial and final two-ply measurements, which showed ~±25% precision, although this result is unreliable due to changes in the experimental setup between measurement rounds.

7.3 Results

Following validation, the sample slip-joint was measured at 201 grid points to evaluate contact pressure across the entire joint. The sample joint exhibits clear (non-random) pressure variations, in the form of thin, vertical low-pressure regions. These low-pressure regions alternate in origin between the top and bottom of the joint and extend towards the centre of the joint, but do not extend the full height of the joint. These regions, typically 0.2-0.6m in width and 1-2m in length, show that future 'partial contact' computer models of the slip-joint should consider vertical contact strips as opposed to horizontal rings. It is important to consider that these results are likely not representative of other slip joints as the sample joint has identical wall thickness, while a typical slip-joint has a thicker inner wall.

Feeler gauges have confirmed the accuracy of the measurement results through (destructive) physical inspection of the joint. Feeler gauge measurements show that measurement results have a ±12% error and provide a quantitative correlation between measurements and gap size that matches small-scale validation testing results. Using this correlation, it is estimated that 34% of the sample slip-joint is not in contact with a 95% confidence interval of [22.9% 50.7%]. This means that it is not sufficient for design engineers to assume full contact within the slip-joint, and calculations must be performed assuming up to 50% non-contact unless further investigation is undertaken.

The observed pressure and gap distribution in the sample joint was likely not caused by a single factor. It is likely that at least one low-pressure region on the underside of the slip-joint was caused by localized impact damage during transport and handling. The other low-pressure regions may have been caused by operating loads, manufacturing defects or high residual stresses arising from manufacturing processes. Considering that typical slip-joints have a much stiffer inner cone, it is unlikely that they would suffer the same degree of impact damage and therefore such a slip-joint would have fewer low-pressure regions.

7.4 Recommendations

It is recommended that the residual stress in the sample joint be investigated to determine if there is a correlation between residual stress and contact distribution. This would be best carried out using Magnetic Barkhausen Noise methods, as the high penetration depth and lack of required surface preparation are both advantageous to slip-joint measurement. This measurement should be augmented by acoustic localized stiffness measurements to provide a comparison for thermographic measurements. This method is more appropriate than other investigated methods as it is accessible, theoretically able to resolve both contact pressure and gap size variations and non-destructive.

It is also recommended that the accuracy and precision of the method are more clearly defined through further single-ply and two-ply measurements. As outlined in section 6.3.2, many measurements should be taken in a single (two-ply or single-ply) location to better establish the measurement precision. This should be subtracted from the variation in measurements collected from a series of single-ply locations to provide an estimate for the location-based variation in measurement values. It is expected the precise manufacturing specifications of offshore structures will result in minimal variation in measurement results due to location based variations (such as wall thickness, paint thickness). Instead, it is expected that a majority of the variation in single-ply results is due to measurement imprecision, therefore several unique measurements should be taken at each location (and averaged) to minimise imprecision and provide better results.

Results may also be improved by utilising a more sensitive, well calibrated thermal camera and more reliable frame to hold the induction coil and camera during measurement. Despite this improving accuracy and precision it should not be prioritised, as the method will still provide relative results and no way to directly identify the contact pressure or gap size at a particular point on the slip-joint. Instead the method should be scaled for used with larger monopiles and tested using an induction heater to heat an entire ring of the slip-joint at once (to improve measurement speed). Based on contract distribution results, a measurement grid with up to 80cm spacing between rings should adequately characterise contact regions. Combined with measurement of an entire ring of the slip-joint, greater measurement spacing could bring the total measurement duration closer to that required for offshore use.

8 References

1. Wind Europe, *The European Offshore Wind Industry: Key Trends and Statistics 2016*. 2017: Brussels.
2. Wind Europe, *Wind in Power: 2016 Annual Statistics*. 2017, Wind Europe.
3. Lotsberg, I., *Structural mechanics for design of grouted connections in monopile wind turbine structures.* Marine Structures, 2013. **32**(Supplement C): p. 113-135.
4. Diepeveen, N.F.B., *On the application of fluid power transmission in offshore wind turbines*. 2013.
5. Van der Tempel, J. and B. Lutje Schipholt, *The Slip-Joint Connection, Alternative connection between pile and tower.* DOWEC report-F1W2-JvdT-03-093/01-P, Dutch Offshore Wind Energy Converter project, 2003.
6. Kamphuis, T., *Design, testing and verification of the DOT-500 slip-joint support structure*. 2016, TU Delft: Delft.
7. Friswell, M. and J.E. Mottershead, *Finite element model updating in structural dynamics*. Vol. 38. 2013: Springer Science & Business Media.
8. Haritos, N. and J. Owen, *The use of vibration data for damage detection in bridges: a comparison of system identification and pattern recognition approaches.* Structural Health Monitoring, 2004. **3**(2): p. 141-163.
9. Totten, G.E., *Steel heat treatment: equipment and process design*. 2006: CRC Press.
10. Park, K.-H., et al., *Laminated magnetic flux sensor for thick-steel-plate control.* IEEE Transactions on Industrial Electronics, 2003. **50**(2): p. 379-384.
11. Kamphuis, T., *Acoustic Measurement Report*. 2016, DOT B.V.: Delft.
12. Ping-jie Huang and Z.-t. Wu, *Inversion of thicknesses of multi-layered structures from eddy current testing measurements.* Journal of Zhejiang University-SCIENCE A, 2004. **5**(1): p. 86-91.
13. Online, K.N. *US$1M container scanner now fully operational*. 2011 [cited 2017 2 May]; Available from: https://www.kaieteurnewsonline.com/2011/06/01/us1m-container-scanner-now-fully-operational/.

14. Zentai, G., *X-ray imaging for homeland security.* International Journal of Signal and Imaging Systems Engineering, 2010. **3**(1): p. 13-20.

15. Cawley, P. and R. Adams, *The mechanics of the coin-tap method of non-destructive testing.* Journal of Sound and Vibration, 1988. **122**(2): p. 299-316.

16. Wu, H. and M. Siegel, *Correlation of accelerometer and microphone data in the" coin tap test".* IEEE Transactions on Instrumentation and Measurement, 2000. **49**(3): p. 493-497.

17. Georgeson, G., S. Lea, and J. Hansen, *Electronic tap hammer for composite damage assessment.* Nondestructive Evaluation of Aging Aircraft, Airports, and Aerospace Hardware, SPIE, 1996. **2945**: p. 3-5.

18. Jüngert, A., C. Große, and M. Krüger, *Local Acoustic Resonance Spectroscopy (LARS) for Glass Fiber-Reinforced Polymer Applications.* Journal of Nondestructive Evaluation, 2014. **33**(1): p. 23-33.

19. Esola, S., et al., *Defect Detection via Instrumented Impact in Thick-Sectioned Laminate Composites.* Journal of Nondestructive Evaluation, 2017. **36**(3): p. 47.

20. Division, M.E.S.C.L.A.M.a.S., *Mitsui Woodpecker*. 1993.

21. Pfund, B., *Portable Test Hammer Apparatus*. 1996: USA.

22. Ibrahim, M., *Nondestructive evaluation of thick-section composites and sandwich structures: A review*. Composites Part A: Applied Science and Manufacturing, 2014. **64**: p. 36-48.

23. Engineering, M.D.o.N., *Radiation Interactions: Neutrons*, in *Principles of Radiation Interactions*. 2004, MIT: Massachusetts, USA.

24. Hobbs, C.W., D. Kenway-Jackson, and J.M. Milne. *Quantitative measurement of thermal parameters over large areas using pulse-video thermography*. in *Thermosense XIII*. 1991. International Society for Optics and Photonics.

25. Authority, U.A.E., *Transient Thermography using Pulsed Radiant Energy Source Provides Nondestructive Testing Technique for Detecting Internal Defects in Body.* European Patent Number 0-089-760-A, Published November, 1983.

26. Cawley, P., *Inspection of composites–current status and challenges.* proceedings of 9th ECNDT, Berlin, 2006.

27. Shepard, S., B. Rubadeux, and T. Ahmed. *Automated thermographic defect recognition and measurement*. in *AIP Conference Proceedings*. 1999. AIP.

28. Shepard, S., et al., *Synthetic processing of pulsed thermographic data for inspection of turbine components.* Insight, 2001. **43**(9): p. 587-589.

29. Almond, D.P., et al. *Round Robin comparison II of the capabilities of various thermographic techniques in the detection of defects in carbon fibre composites*. in *Quantitative Infrared Thermography (QIRT2000) Eurotherm Seminar 64*. 2000. University of Bath.

30. Bergman, T.L. and F.P. Incropera, *Fundamentals of heat and mass transfer*. 2011: John Wiley & Sons.

31. Cengel, Y.A., et al., *Fundamentals of thermal-fluid sciences*. 2008: McGraw-Hill New York, NY.

32. Kaminski, D.A. and M.K. Jensen, *Introduction to Thermal and Fluids Engineering*. 2011: Wiley.

33. MacGregor, R. and J. Emery, *Heat Transfer*. 1969.

34. Catton, I. *Natural convection in enclosures*. in *Proceedings of the sixth international heat transfer conference*. 1978.

35. Dassault Systèmes. *Thermal Contact Resistance*. 2017 [cited 2017 10 May]; Available from: http://help.solidworks.com/2017/English/SolidWorks/cworks/c_thermal_contact_resistance_contact_analysis.htm.

36. Yovanovich, M.M., *Four decades of research on thermal contact, gap, and joint resistance in microelectronics.* IEEE transactions on components and packaging technologies, 2005. **28**(2): p. 182-206.

37. Cooper, M., B. Mikic, and M. Yovanovich, *Thermal contact conductance.* International Journal of heat and mass transfer, 1969. **12**(3): p. 279-300.

38. Thermopedia. *Thermal Contact Resistance*. 2011 [cited 2017 15 May]; Available from: http://www.thermopedia.com/content/1188/.

39. Peterson, G.P. *Thermal Contact Resistance in Waste Heat Recovery Systems*. in *Proceedings of the 18th ASME/ETCE Hydrocarbon Processing Symposium*. 1987. Dallas, TX: ASME International.

40. Stewart, W.E.J., *Determination of thermal contact resistance between metals using a pulse technique*, in *Mechanical and Aerospace Engineering*. 1972, Missouri University of Science and Technology: Missouri.

41. SML Marine Paints. *Epoxy Paints and Coatings*. 2017 10/6/2017]; Available from: https://www.smlmarinepaints.co.uk/epoxy.

42. Harvey, P., *EXIFTOOL by Phil Harvey*. 2017, Queen's University: Ontario, Canada.

43. Usamentiaga, R., et al., *Infrared Thermography for Temperature Measurement and Non-Destructive Testing.* Sensors (Basel, Switzerland), 2014. **14**(7): p. 12305-12348.

44. FLIR Systems AB, *FLIR AX5 GenICam ICD Guide*. 2013.

45. Various. *Average Absolute Deviation*. 2018 [cited 2017 July 25]; Available from: https://en.wikipedia.org/wiki/Average_absolute_deviation#Mean_absolute_deviation_around_the_mean.

46. Segeren, M.L.A., et al., *Investigation of a slip joint connection between the monopile and the tower of an offshore wind turbine.* IET Renewable Power Generation, 2014. **8**(4): p. 422-432.

47. van de Bosch, J., E. Descourtieux, and M.L.A. Segeren, *DOT500 SLJ Project: TU Delft FEM Analysis Report*. 2017, Technische Universiteit Delft: Delft.

48. Wang, X., et al., *FEM analysis for residual stress prediction in hot rolled steel strip during the run-out table cooling.* Applied Mathematical Modelling, 2013. **37**(1): p. 586-609.

49. MeteoBlue, *The Hague Wind Rose*. 2017, MeteoBlue.

50. Fitzpatrick, M., et al., *Determination of residual stresses by X-ray diffraction.* 2005.

51. Žerovnik, P. and J. Grum. *Determination of residual stresses from the Barkhausen noise voltage signal*. in *International Conference of the Slovenian Society for Non-Destructive Testing Application of Contemporary Non-Destructive Testing in Engineering*. 2009.

52. Siemens AG. *Modal Tips: Roving Hammer versus Roving Accelerometer*. 2018 [cited 2017 19 December]; Available from: https://community.plm.automation.siemens.com/t5/Testing-Knowledge-Base/Modal-Tips-Roving-Hammer-versus-Roving-Accelerometer/ta-p/378619.

53. Powell, J. and J. Roberts, *On the frequency of vibration of circular diaphragms.* Proceedings of the physical society of London, 1922. **35**(1): p. 170.